The Development of a Time-Resolved, Vesicle-Based, Fluorescence Assay for the Activity of the Lipid Kinase Pik1

Kailey Meehan, BSc

A thesis submitted to the Department of Chemistry
Centre for Biotechnology
In partial fulfillment for the requirements for the
degree of Master of Science

Faculty of Mathematics and Sciences
Brock University, St. Catharines, Ontario

Abstract

Pik1 is a yeast phosphatidylinositol-4 kinase that is critical for vesicular traffic to the plasma membrane and endosomes from the trans-Golgi (1, 2). Pik1 is a soluble enzyme, and the small myristoylated, Ca^{2+} binding, EF hand protein, Frequenin (Frq1) facilitates its membrane localization (3). It has been suggested that Pik1 finds its substrate, phosphatidylinositol (PI), within phospholipid bilayers with assistance from the PI/PC transfer protein Sec14 (4). It is proposed that Sec14 stimulates the activity of Pik1 by partially removing PI from the bilayer and presenting it to the kinase as a more suitable substrate (4). In order to test this hypothesis, the Bellbrook Labs Transcreener ADP^2 FI Assay kit, a fluorescence-based enzyme assay kit that reports the production of ADP, was adapted to create a time-resolved, vesicle-based assay. The assay was developed and validated with the catalytic subunit of Protein Kinase A (PKA) and the commercial human PI kinase PIK3C3. An expression system for Pik1 was created in yeast. To preserve the stability of the 125 kDa enzyme it was co-expressed with both Frq1 and the heat shock protein, Cdc37, producing the Pik1-Frq1 complex with a removable 10xhistidine tag on Pik1. The growth of the yeast transformants was investigated using different culture conditions, media, and methods of inducing protein expression. The expression of the Pik1-Frq1 complex was confirmed on a Western blot that showed a band corresponding to the molecular weight of the complex. Next steps will involve optimizing the purification of the Pik1-Frq1 complex on a metal affinity resin, with the ultimate goal being to test the Sec14 presentation mechanism by measuring the kinase activity of Pik1 from purified fractions in the presence and absence of Sec14.

Keywords: Phosphatidylinositol, Pik1, Sec14, Fluorescence, Lipid Kinase Assay

Acknowledgements

I would like to express my sincere gratitude to my supervisor, Dr. Jeffrey Atkinson. I consider myself blessed to have had the opportunity to work as a member of his research team for the past 3 years. He is a fantastic mentor and teacher, and I am grateful for his time, patience, guidance, and his aptitude at sharing a wealth of information.

I acknowledge the valuable work of Dr. Candace Panagabko that was included in this thesis. I am also very grateful for her assistance, mentorship, and willingness to answer all of my questions for the past 3 years. Many thanks to Shraddha Khirwadkar and Alexandra Bernekier for their assistance with some of the growth curve experiments. Special thanks to Shannon Jewel for her support and valuable discussions. Thank you to all the members of the Atkinson research group for contributing so positively to my time as a MSc student.

A note of thanks to Dr. Paul Zelisko and Dr. Aleksander Necakov for being on my committee and providing valuable input on my thesis. I would also like to thank Dr. Julie Brill for taking on the role of external examiner.

I wish to thank my family, my friends, and all those whom have been praying for me. I am thankful for the dance breaks, prayers, support, and encouragement. I also wish to thank God; this work is the fruit of the gifts He has given me.

I will praise you, Lord, with all my heart;
I will declare all your wonderous deeds. – Psalm 9: 2

Table of Contents

List of Tables

List of Figures

List of Abbreviations

10NE: transformed BJ2168 with clone 10 (pYEXC3H+PIK1) and clone N (pESC-Trp+FRQ1+CDC37) sequentially, colony E

ACBD3: acyl-CoA-binding domain containing protein 3

AdBR: N-terminal adaptor binding region

ADP: adenosine diphosphate

AP-1: clathrin adaptor protein complex 1

APS: ammonium persulfate

ARF1 and ARF1-GTP, Afr1: ADP-ribosylation factor 1

ATP: adenosine triphosphate

B8NA: transformed BJ2168 with clone 8 (pYEXC3H+PIK1) and clone N (pESC-Trp+FRQ1+CDC37) at the same time, colony A

B8ND: transformed BJ2168 with clone 8 (pYEXC3H+PIK1) and clone N (pESC-Trp+FRQ1+CDC37) at the same time, colony D

BJ2168: *Saccharomyces cerevisiae* strain that was cultured for protein expression

BSA: bovine serum albumin

CAT: chloramphenicol acetyltransferase

Cdc37: cell division cycle protein 37

CDC37: gene for cell division cycle protein 37

CDP-choline: cytidine 5'-phosphocholine

CDP-DG: cytidine diphosphate-diacylglycerol

CR: cysteine-rich

DAG: diacylglycerol

DEP: dishevelled, Egl-10 and Pleckstrin domain

DOPC: 1,2-dioleoyl-sn-glycero-3-phosphocholine

DTT: dithiothreitol

EDTA: ethylenediaminetetraacetic acid

EGTA: ethylene glycol-bis(β-aminoethyl ether)-N,N,N′,N′-tetraacetic acid

ER: endoplasmic reticulum

EtOH: ethanol

Fab1: forms aploid and binucleate cells, *Saccharomyces cerevisiae* type III PIPK

FAPP1 and FAPP2: Four-phosphate-adaptor protein 1 and 2

FI: fluorescence intensity

FPLC: fast protein liquid chromatography

FRQ1: frequenin gene

Frq1: frequenin protein

FYVE: a PI(3)P binding domain

GFP: green fluorescent protein

GPBP: goodpasture antigen-binding protein

GTPase: enzyme that hydrolyses guanosine triphosphate

HEPES: 4-(2-hydroxyethyl)-1-piperazineethanesulfonic acid

His: histidine

Hrs: hepatocyte growth factor-regulated tyrosine kinase substrate

HUGO: human genome organisation

IMAC: immobilized metal affinity chromatography

IN: induced

IP3: inositol 1,4,5-trisphosphate

Kes1: KrE11-1 suppressor, aka Osh4

LKU: lipid kinase unique domain

Lsb6: las seventeen binding protein, *Saccharomyces cerevisiae* type II PI4K

Max FI: maximum fluorescence intensity of assay window

Min FI: minimum fluorescence intensity of assay window

mQH2O: milli-Q H2O

Mss4: multicopy suppressor of Stt4 mutation, *Saccharomyces cerevisiae*
PIPK that is homologous to mammalian type I and type II PIPKs

MW: molecular weight

NCS-1: neuronal calcium sensor-1

NLS: nuclear localization sequence

NMR: nuclear magnetic resonance

OD: optical density

OSBP: oxysterol-binding protein 1

p85BR: p85 binding region

PA: phosphatidic acid

PBS: phosphate buffered saline

PC: phosphatidylcholine

PCR: polymerase chain reaction

PDB: protein data bank

PH: plekstrin homology

PI or PtdIns: phosphatidylinositol

PI(3,4,5)P_3: phosphatidylinositol 3,4,5-trisphosphate

PI(3,4)P_2: phosphatidylinositol 3,4-bisphosphate

PI(3,5)P_2: phosphatidylinositol 3,5-bisphosphate

PI(3)P: phosphatidylinositol 3-phosphate

PI(4,5)P_2: phosphatidylinositol 4,5-bisphosphate

PI(4)P: phosphatidylinositol 4-phosphate

PI(5)P: phosphatidylinositol 5-phosphate

PI3K: phosphatidylinositol 3-kinase

PI4K: phosphatidylinositol 4-kinase

***PI4KIIIβ*:** phosphatidylinositol 4-kinase type III beta gene

PI4KIIIβ: phosphatidylinositol 4-kinase type III beta protein

PIK1: *Saccharomyces cerevisiae* type III β PI4K gene

Pik1: *Saccharomyces cerevisiae* type III β PI4K protein

PIK3C3: HUGO gene name for the human phosphatidylinositol 3-kinase Class III gene

PIK3C3: human phosphatidylinositol 3-kinase Class III protein

PIPK: phosphoinositol phosphate kinase

PIPKc: phosphatidylinositol phosphate kinase central kinase core domain

PIPs: phosphatidylinositol phosphates

PITPs: phosphatidylinositol/phosphatidylcholine transfer proteins

PKA: protein kinase A

PLC: phospholipase C, and PLCδ1

PLD: phospholipase D

PM: plasma membrane

PMSF: phenylmethylsulfonyl fluoride

PR: proline rich domain

PS: L-α-Phosphatidylserine

PTEN: phosphatase and tensin homolog protein

pVEX: BJ2168 transformed with empty pYEXC3H and pESC-Trp vectors

PX: phox-homology domain

Ras-BD: Ras binding domains

RFU: relative fluorescence units

RO: Reverse osmosis

RPM: rotations per minute

SAC1: phosphoinositide phosphatase SAC1

SCAT: selective complete, adenine, tryptophan

SCUTA: selective complete, Ura-Trp- dropout powder, adenine

SCUTAD: selective complete, Ura-Trp- dropout powder, adenine, dextrose

SCUTAD*: selective complete, Ura-Trp- dropout powder, adenine, 0.2% dextrose

SCUTAGE: selective complete, Ura-Trp- dropout powder, adenine, glycerol, ethanol

SCUTAR: selective complete, Ura-Trp- dropout powder, adenine, raffinose

SDS-PAGE: sodium dodecyl sulfate - polyacrylamide gel electrophoresis

SDS: sodium dodecyl sulfate

Sec14: a *Saccharomyces cerevisiae* PITP

Ser: serine

Sfh: Sec14 homolog

START-like PITPs: steroidogenic acute response related transfer domain

STT4: Stauroporine and Temperature sensitive, *Saccharomyces cerevisiae* type III α PI4K gene

Stt4: Stauroporine and Temperature sensitive, *Saccharomyces cerevisiae* type III α PI4K protein

TCP-1: Cpn60/TCP-1 chaperonin family domain

TEMED: Tetramethylethylenediamine

TGN: trans golgi network

Thr: threonine

TLC: thin layer chromatography

Tris-HCl: trisaminomethane-hydrochloride

Trp: tryptophan

Ura: uracil

Vol: volume

***VPS15*:** vacuolar protein sorting mutant 15 gene

Vps15: vacuolar protein sorting mutant 15 protein

VPS34: vacuolar protein sorting mutant 34 gene

Vps34: vacuolar protein sorting mutant 34 protein, *Saccharomyces cerevisiae* class III PI3K

wt: wild type

YEPG: yeast extract, peptone, galactose

YPAD: yeast extract, peptone, adenine, dextrose

1 Introduction

1.1 Phosphatidylinositol (PI) and Phosphoinositides (PIPs)

1.1.1 PI

Phosphatidylinositol (PI) is a membrane phospholipid that is ubiquitous in eukaryotic cells (5), and constitutes approximately 5-7% of the total cellular phospholipids in mammalian cells (6). PI is a glycerophospholipid with two fatty acyl chains esterified to positions *sn*-1 and *sn*-2, and an inositol ring linked to position *sn*-3 by a phosphate group (5) (Figure 1). The fatty acid tail in the *sn*-1 position is typically saturated, and that in the *sn*-2 position is usually unsaturated (7). The most common fatty acids at position *sn*-1 of PI are stearic acid (18:0) in humans and palmitic acid (16:0) in yeast. Arachidonic acid (20:4) (in humans) and oleic (18:1) or palmitoleic acid (16:1) (in yeast) are the most common fatty acids in PI in the *sn*-2 position (5).

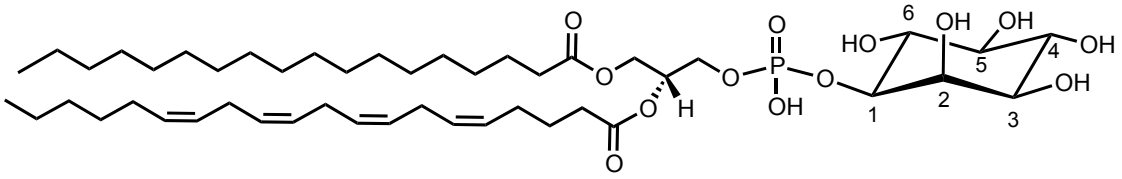

Figure 1: The structure of PI with stearic acid (18:0) and arachidonic acid (20:4) in positions *sn*-1 and *sn*-2 respectively.

PI is present in different proportions in living systems according to the type of membrane; in yeast, PI is present in two distinct compartments, the plasma membrane (PM) and the Golgi (5). *De novo* synthesis of PI occurs mainly at the endoplasmic reticulum (ER) from phosphatidic acid (PA) (6). In the final step of PI synthesis, cytidine diphosphate-diacylglycerol (CDP-DG) and *myo*-inositol are combined by PI synthase (Pis1 in yeast) mainly on the cytoplasmic face of the ER, but also on Golgi, mitochondria, and microsomes (5, 6). PI is then transported to the correct membrane via vesicular transport or phosphatidylinositol transfer proteins (PITPs) (6, 8). Loss-of-function mutants of the PI synthase gene are lethal in both *Drosophila melanogaster* and *Saccharomyces cerevisiae*, emphasizing the central role of PI signaling in eukaryotic cell biology (6, 9). PI participates in signaling mainly via phosphorylated derivatives called phosphatidylinositol phosphates (PIPs) (6).

1.1.2 PIPs

Phosphatidylinositol phosphates (PIPs) are a minor constituent of cellular membranes making up approximately 1% of total cellular phospholipids, with PI representing approximately 5-7% (5, 6). The inositol headgroup of PI can be phosphorylated at positions 3-, 4-, and/or 5- in different combinations to produce 7 different PIPs: PI(3)P, PI(4)P, PI(5)P, PI(3,4)P_2, PI(3,5)P_2, PI(4,5)P_2, PI(3,4,5)P_3 (5) (Figure 2). All 7 PIPs are essentially interconvertible; however, the organism must have the enzymes essential for the conversions (5). Mammals synthesize all seven; yet yeast synthesize all but PI(3,4)P_2 and PI(3,4,5)P_3 (10). PI(4)P and the enzyme that generates this species at the Golgi in yeast, Pik1, are two of the key players focused on in this thesis.

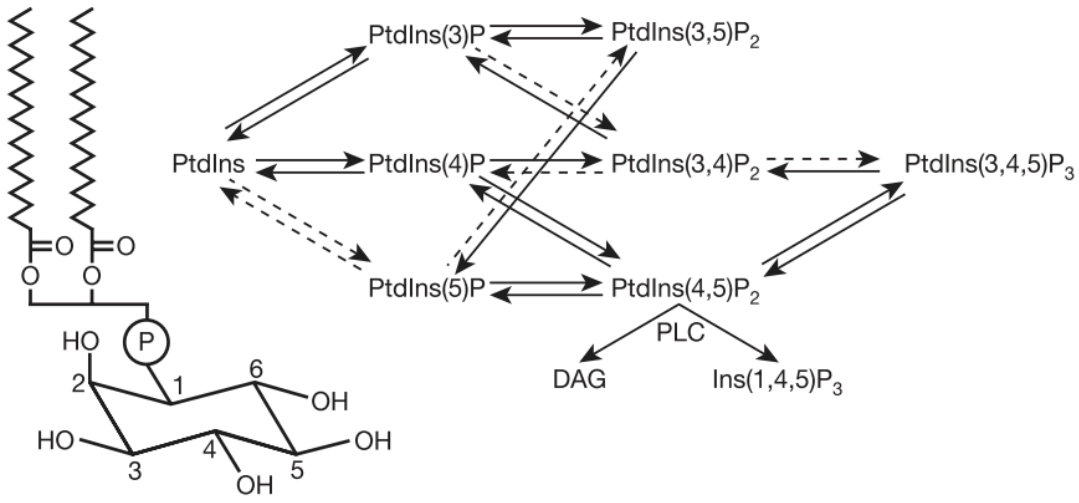

Figure 2: PI and the metabolic reactions that result in the seven PIP species. Dotted arrows indicate transitions that have been shown in vitro, but their biological relevance is still ambiguous. Figure used with permission from (8).

PIPs show continuous turnover (11), are low in abundance, and their local concentration can be extremely variable (5). PIPs are vital in regulating membrane-cytosol interfaces by mediating signal transduction, assisting in defining organelle identity, and regulating the cytoskeleton, membrane traffic, permeability, and transport (8). The seven different PIPs have distinct and essential regulatory functions that are executed via the recruitment and/or activation of effector proteins, and the creation of second messengers such as diacylglycerol (DAG) or inositol 1,4,5-trisphosphate (IP_3)

(Figure 2) (5, 6, 11). PIPs have properties that make them optimal mediators of signaling events; these include their differential intracellular distribution and their high turnover (8). PIP signaling is covered in greater detail in Section 1.1.5.

PIP signaling is highly related to the spatial distribution of PIPs among cellular compartments. The 7 different PIPs are not equally abundant; PI(4)P and PI(4,5)P_2 are the most abundant and PI(3)P, PI(3,4)P_2, and PI(3,4,5)P_3 have a much lower abundance (6). In addition, the 7 PIPs are present in most cell types in different levels and each intracellular compartment has a signature PIP composition; for example, the predominant PIP at the plasma membrane, the Golgi, and endosomes are PI(4,5)P_2, PI(4)P, and PI(3)P respectively (8) (Figure 3). Moreover, the PIP composition of a given intracellular membrane may not be homogeneous (8). The differential distribution assists in defining the membrane identity for different organelles and contributes to a powerful coincidence detection code for the regulation of membrane cytosol interactions (8) (covered in more detail in Section 1.1.3). The presence and abundance of a particular PIP on a certain membrane is determined by the interplay between lipid kinases and phosphatases on that membrane in response to stimuli, thus resulting in the spatial and temporal regulation of PIPs (5, 6). An overview of PI kinases is provided in Section 1.2. The correct activity of PIP metabolizing enzymes is essential for proper PIP signaling and homeostasis, and this is relevant to medicine as imbalances in PIP metabolism have been linked to a variety of human pathologies (5, 8).

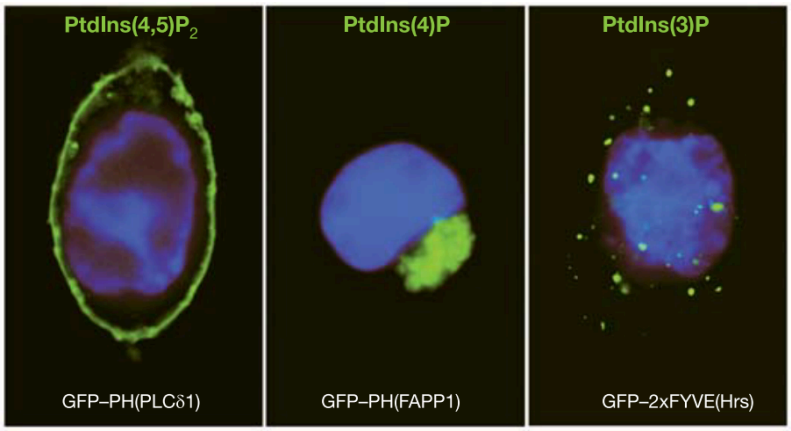

Figure 3: Fluorescence micrographs of Chinese hamster ovary cells showing the signature PIP compositions of the PM (PI(4,5)P_2), Golgi (PI(4)P), and endosomes (PI(3)P). The pleckstrin homology (PH) domains of PLCδ1 and FAPP1, and the tandem FYVE domain of hepatocyte growth factor-regulated tyrosine kinase substrate (Hrs) were fused to green fluorescent protein (GFP) to visualize PI(4,5)P_2, PI(4)P, and PI(3)P respectively. Image used with permission from (8).

1.1.3 PIP Signaling

The phospholipase C (PLC) signaling pathway is one of the well-studied PIP signaling pathways (7). In this pathway PI(4,5)P_2 is cleaved by PLC to give inositol 1,4,5-trisphosphate (IP_3) and diacylglycerol (DAG) (7). These products act as second messengers in signal transduction cascades that control important processes such as growth factor signaling and neurotransmitter release (7). (Figure 4)

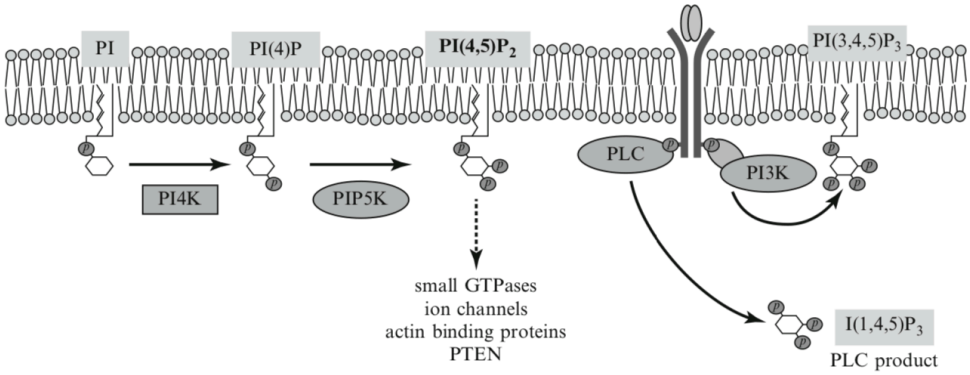

Figure 4: The PLC pathway up to the production of IP_3 and DAG. PI is sequentially phosphorylated to generate PI(4,5)P_2, which is then cleaved by PLC to yield inositol 1,4,5-trisphosphate (IP_3) and diacylglycerol (DAG). Image used with permission from (12).

There are multiple examples of PIPs acting as precursors to second messengers; however, PIPs have also been shown to act directly as signaling molecules. PIPs exert

their signaling effects via the binding of the effector protein to the PIP head group thereby recruiting the effector proteins to the phospholipid membrane or by mediating the functions of the effector proteins (8). Cytosolic proteins or the cytosolic domains of membrane proteins can bind the PIP head group via well-defined modular domains (11), such as the PH domain (13). These binding interactions are generally of low affinity, but when PIPs cooperate with other membrane components to bind multiple sites on the effector protein, higher affinity interactions occur (8) (Figure 5). Such multivalent interactions are the basis of the coincidence detection code. In essence, the specificity and strength of membrane binding of an effector protein is a combination of affinities for lipids and co-resident proteins that assure proper signal integration (8). For example, if it were a "two key mechanism" the two components (a GTPase and a PIP for example) can be independently regulated and the effector protein will only bind with high affinity and transduce a signal when both are correct. This helps to distinguish where and when the effector protein should bind (8). The specific intracellular distribution of PIPs and their co-receptors gives rise to the selective recruitment of effector proteins to particular compartments (11). The coincidence detection code allows for the fine control of PIP signaling in both space and time.

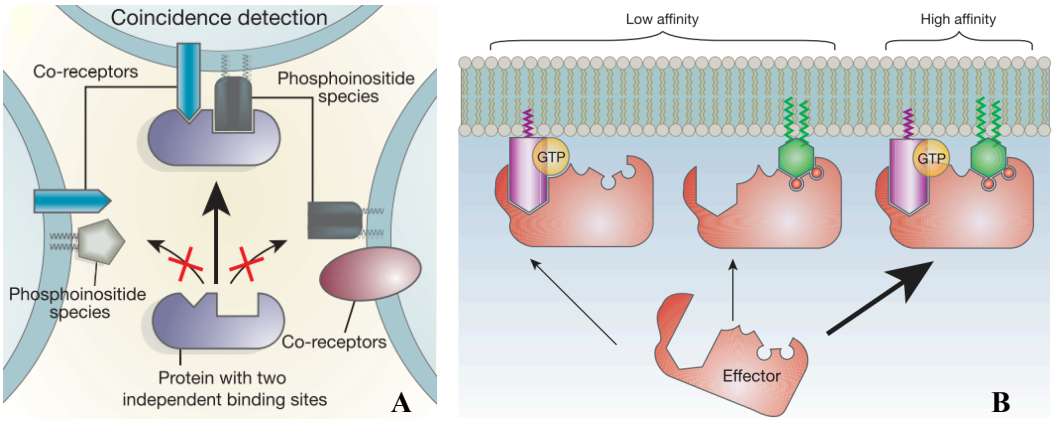

Figure 5: Coincidence detection between PIPs and effector proteins. High specificity and affinity are achieved when PIPs work in cooperation with co-receptors to bind effector proteins. This plays a key contribution in the spatial and temporal regulation of PIP signaling. **A.** A generic visualization of how coincidence detection is used to define organelle identity. **B.** A generic visualization of how binding affinity increases when an effector cooperatively binds two ligands. In this example the two ligands are a PIP_2 and a GTPase. Figures used with permission from (8)

1.1.4 PI(4)P, Signaling, and Membrane Traffic

PI(4)P accounts for approximately 30% and 45% of total PIPs in yeast and humans respectively (5). PI(4)P is enriched at the Golgi and is also found at the PM (5). PI(4)P is an intermediate in the production of $PI(4,5)P_2$ and $PI(3,4,5)P_3$, which are essential in receptor-activated phospholipase C (PLC) (Figure 4) and phosphoinositide 3-kinase signaling respectively (14). However, PI(4)P itself has also been established as essential for cell function independent of these two signaling pathways, although it was initially considered solely as an intermediate in the production of other PIP species (11).

PI(4)P is largely produced by the phosphorylation of PI by PI-4 kinases; however, it is also produced by the dephosphorylation of $PI(4,5)P_2$ and $PI(3,4)P_2$ (5). In yeast there are two type III PI-4 kinases and each carries out this function at their respective organelle membrane; Pik1 acts at the Golgi and Stt4 at the PM (5). Deletion of either *STT4* or *PIK1* is lethal and increased expression of either cannot compensate for the loss of the other, despite having the same biochemical activity; this is evidence that each enzyme produces functionally distinct pools of PI(4)P (15). Temperature-conditional mutants led to the discovery that Stt4 activity is necessary for proper vacuole morphology, cell wall integrity, and actin cytoskeleton organization, and that Pik1 activity is essential for normal secretion, Golgi and vacuole membrane dynamics, and endocytosis (2, 15).

Direct evidence linking PI(4)P and Golgi trafficking in yeast was initially observed when secretory defects were seen in PI-4 kinase mutants (1, 2). Since then multiple PI(4)P effectors have been identified through which PI(4)P spatially and temporally regulates a variety of functions on Golgi membranes. One such function is the regulation of vesicle budding. PIP composition is an important factor in vesicle budding and fusion and in the recruitment of the proteins required for these processes (Figure 6A). The following are mammalian examples of some of these proteins. PI(4)P cooperates with the small GTPase ADP-ribosylation factor 1 in its GTP bound state (ARF1-GTP) to recruit proteins that initiate vesicle formation, such as clathrin adaptor protein complex 1 (AP-1) (10, 16). Four-phosphate-adaptor protein 1 and 2 (FAPP1 and FAPP2) control membrane traffic between the Golgi and the cell surface. It is proposed

that FAPP1 and 2 do this by coordinating the budding and fission reactions that generate mature and properly tagged vesicles that are competent for fusion with the PM (17). FAPP1 and FAPP2 bind PI(4)P and ARF1 via their PH domain; these interactions recruit FAPP1 and FAPP2 to TGN exit sites (17, 18) (Figure 6B). PI(4)P and ARF1 provide an example of recruitment by PIP coincidence detection code and it highlights another way PI(4)P is required in the secretory pathway from Golgi to the PM. In addition, local concentrations of PI(4)P pools at different stages in vesicle maturity can lead to the activation of different effectors (19). Some PI(4)P effectors have been shown to transport lipids in association with PI(4)P (5, 8), and PI(4)P also functions in the maintenance of Golgi structure (18).

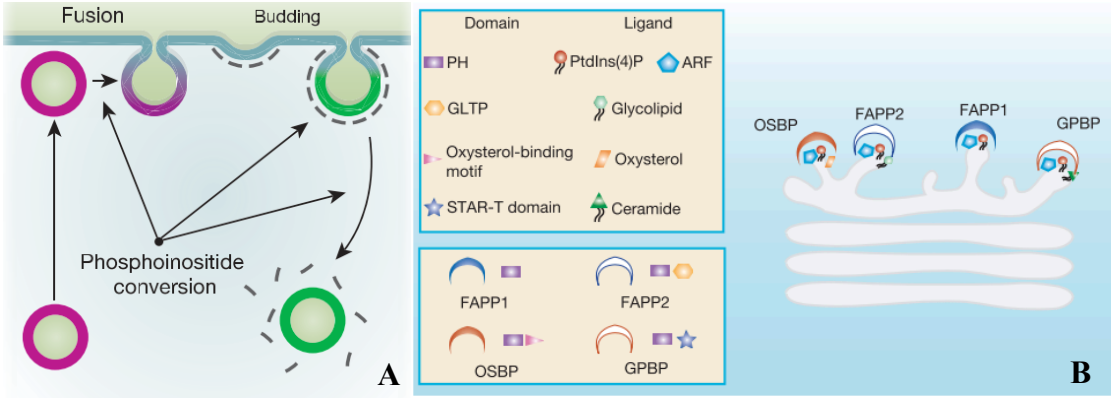

Figure 6: PIPs and membrane traffic. A. The PIP compositions of a vesicle, an acceptor membrane, and a budding membrane must be correct to recruit the correct factors required for fusion and budding. This ensures vectoral membrane traffic. Image used with permission from (8). **B.** The coincidence detection of PI(4)P, ARF1, and other membrane factors by OSBP, FAPP2, FAPP1, and goodpasture antigen-binding protein (GPBP) to coordinate budding and fission reactions to generate vesicles that are competent for fusion with the PM. Image used with permission from (17).

1.2 The Story of PI Kinases

PI(4)P and PI(4,5)P_2 were isolated in the 1940s by Folch (20). This began a search for the enzymes that phosphorylate the inositol head group. A PI kinase is an enzyme that uses PI or a PIP and ATP as its substrates, and which catalyzes the transfer of the gamma phosphate to position 3, 4, or 5 of the inositol ring. By 1969 it was suspected that more than one PI kinase existed based on the differential activation of PI kinases in liver plasma membranes and endoplasmic reticulum by a nonionic detergent (21). By 1984 different researchers had measured PI kinase activity in many different tissues and a connection had been made between the turnover of PI lipids and signal transduction (22). As PI kinases were isolated prior to 1988, they were distinguished from each other by their sensitivity to adenosine and to nonionic detergents, and their apparent molecular weight and intracellular location (21). Type I PI kinases were inhibited by detergent and were not inhibited by adenosine (21). Type II PI kinases were activated by detergent and inhibited by adenosine (21). Type III PI kinases were relatively resistant to inhibition by adenosine and were activated by detergents; they also had different apparent molecular weights, and were resistant to inhibition by a monoclonal antibody that caused greater than 90% inhibition of the Type II PI kinases (21). However, prior to 1988 it was thought that the PIP pathway was simple and only consisted of the sequential phosphorylation of PI at positions 4 then 5 to form PI(4,5)P_2, and the phospholipase C (PLC) signaling pathway (Figure 4) (21). Up until this point the enzymes and products of this restricted original view of the PIP pathway had been found in virtually every organism and tissue studied, and no other phosphorylated PI derivatives had been detected. Prior to 1988, the products of PI kinases were characterized using one and two dimensional thin layer chromatography (TLC), and since PI(3)P and PI(4)P appeared to co-migrate in these systems, all PI kinase enzymes were thought to be phosphatidylinositol-4 kinases (23). However, in 1988, it was discovered that Type I PI kinases actually phosphorylate position D3 on the inositol ring to produce PI(3)P (23). The perceived complexity of PIP metabolism greatly increased between 1988 and 1990 due to the discovery of PI-3 kinases and PI(3)P, the subsequent discovery of PI(3,4)P_2, PI(3,5)P_2, and PI(3,4,5)P_3, and the detection of PI-3 kinase activity and PI(3)P in *Saccharomyces cerevisiae* (21, 23, 24).

1.2.1 Notes About PI Kinase Nomenclature and Classification

PI kinase nomenclature and classification are valuable in denoting the characteristics of a PI kinase and how it is related to other PI kinases. Regrettably, a concern is that the nomenclature and classification has not always been consistent and there are multiple factors that complicate the process of trying to understand PI kinase nomenclature and classification. Figure 7 and Table 1 are helpful tools to understand the nomenclature and classification of PI kinases.

A PI kinase is denoted as a PI3K (phosphatidylinositol 3-kinase), PI4K (phosphatidylinositol 4-kinase), or PIPK (phosphatidylinositol phosphate kinase). The number in this short form (*e.g.,* PI**3**K) indicates the position onto which the enzyme adds a phosphate group. This is not an indication of substrate specificity; for example, a PI3K always adds the phosphate to position 3, but different PI3K enzymes use PI, PI(4)P, and/or PI(4,5)P_2 as substrates to produce PI(3)P, PI(3,4)P_2, and PI(3,4,5)P_3. However, the next step in classification, the type or class of the enzyme, is meant to categorize the structure, the substrate, how the enzyme is related to other PI kinases, and gives an indication of other properties that characterize that class. The PI3Ks are split into Classes IA, IB, II, and III, while the PI4Ks are split into Types II and III, and the PIPKs are split into Types I, II, and III (Figure 7). See Sections 1.2.2-1.2.4 for information on how each subgroup is characterized.

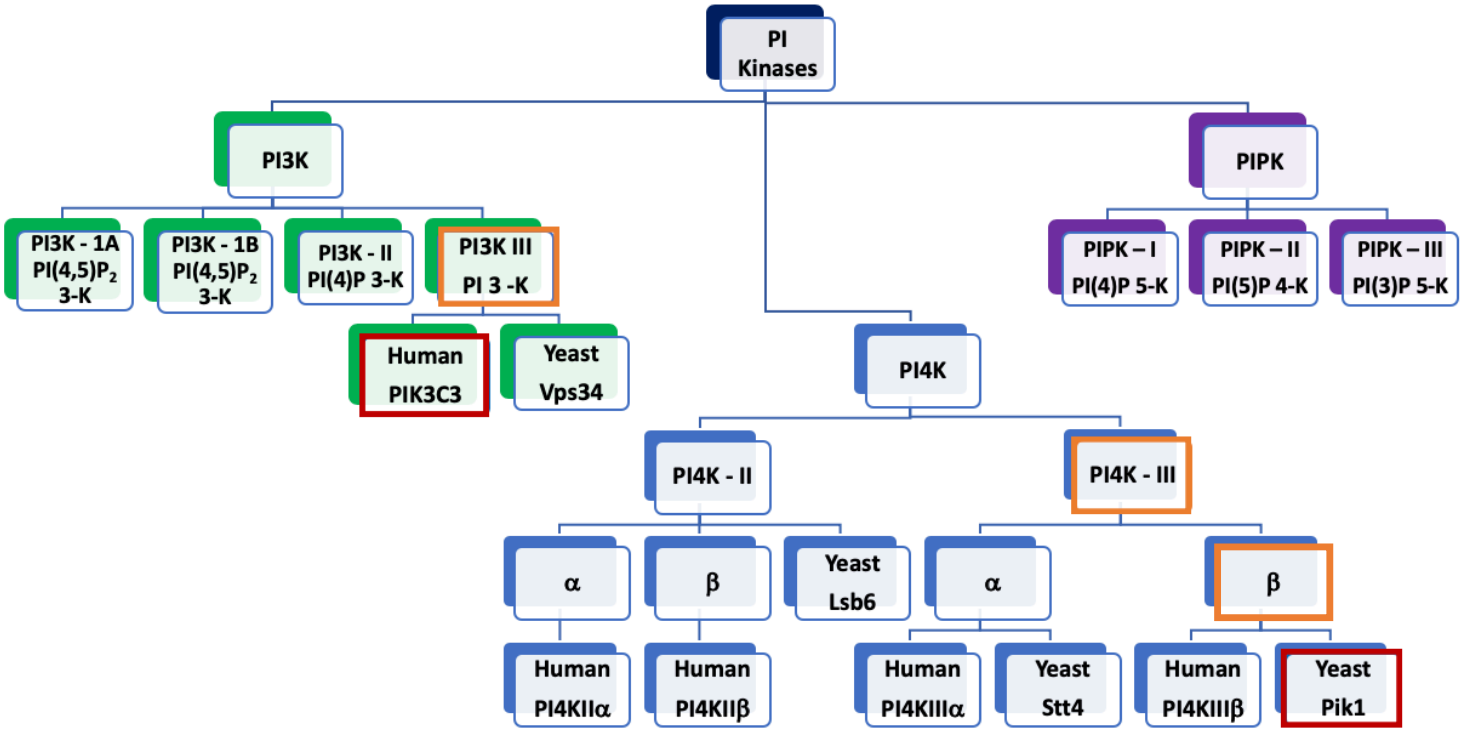

A

Figure 7A: Nomenclature and classification of PI Kinases. A. Standard nomenclature and classification of PI kinase enzymes based on substrate specificity and other enzyme characteristics. PI3Ks (green), PI4Ks (blue), and PIPKs (purple). The two proteins of interest in this thesis are boxed in red and their classifications are boxed in orange.

B

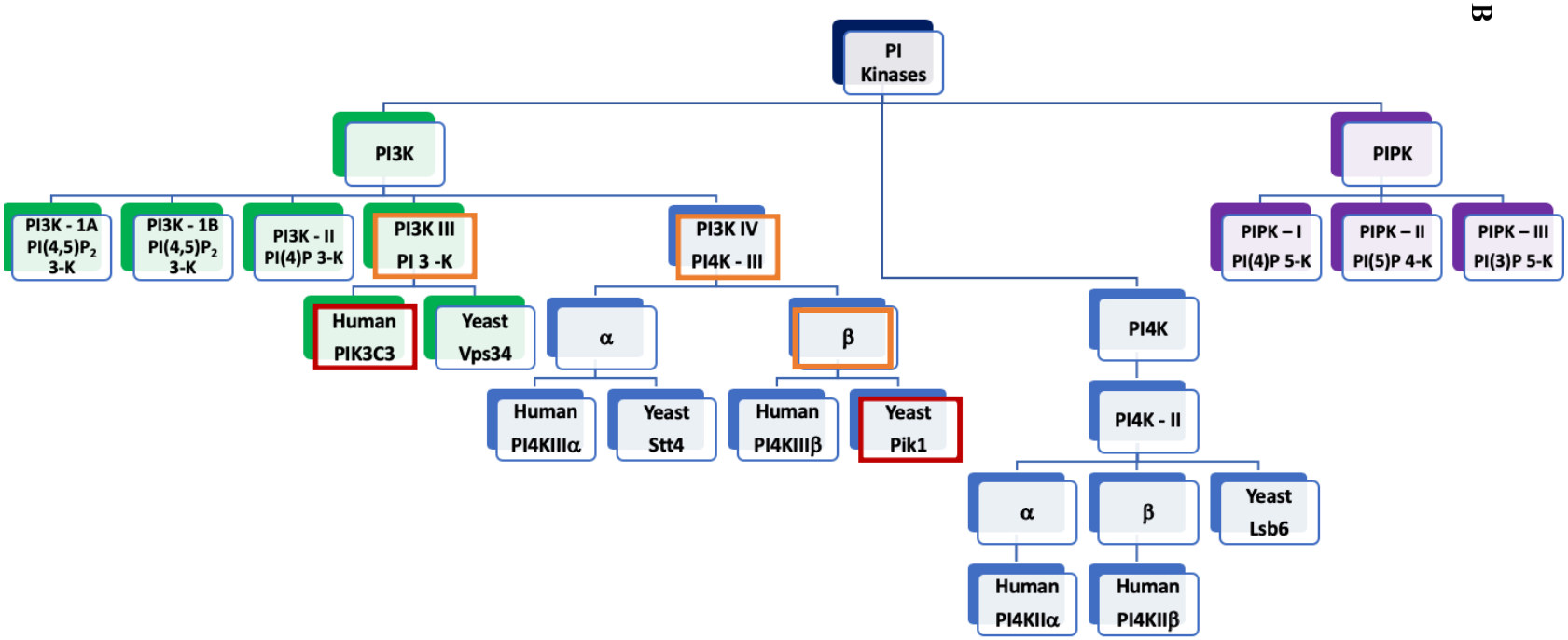

Figure 7B: Nomenclature and Classification of PI Kinases Based on Evolutionary Relationships. Classification of PI kinases based on phylogeny as proposed by Brown and Auger (25). PI3Ks (green), PI4Ks (blue), and PIPKs (purple). The two proteins of interest in this thesis are boxed in red and their classifications are boxed in orange.

This brings us to the first challenge, the fact that the two types of the PI4Ks are called Type II and Type III and that there is, in fact, no Type I. This challenge was unfortunately initiated when PI3 kinases were incorrectly first identified as Type I PI4Ks. When this mistake was rectified, the Type I enzymes were classified as PI3Ks instead, but the PI4Ks were, and still are, classified as Type II and III, and the designation of Type I PI4Ks has been dropped. It was not possible to devise a comprehensive and accurate classification system without more information about the enzymes. As such, the classification has been expanded and adapted over time as a greater understanding of PI kinase sequence, structure, homology, *etc*. was achieved. Another complicating factor was that the initial classifications were based on characteristics of the enzymes (phosphorylation position, inhibitors, molecular weight (MW), *etc*.) and were not based on sequence or phylogeny. Once more information about sequence homology and phylogeny was known, Brown & Auger classified Type III PI4Ks as Type IV PI3Ks, because even though Type III PI4Ks phosphorylate position 4, they are more closely related to the PI3Ks than the Type II PI4Ks (25) (Figure 7B). Nevertheless, this did not become standard, and they are still classified as Type III PI4Ks (Figure 7A). This is an example of how sequence homology and phylogeny complicated the classification, but it also allowed types or classes to be characterized by sequence homology and by the presence or absence of particular domains, which makes the classes/types reflect information about structure, and relatedness, at least for the PI3Ks and the PIPKs. It also makes the classification more robust; without phylogeny if a person just looked at substrate for example, one could look at Type IA PI3Ks, which mainly phosphorylate $PI(4,5)P_2$ to form $PI(3,4,5)P_3$, and think that these enzymes belong with the PIPKs. However, looking at the domains of the PI3Ks and the PIPKs, Type IA PI3Ks belong with the other PI3Ks. An overview of the classification of PI kinases can be found in Figure 7 and Table 1.

Table 1: Mammalian and yeast PI Kinase classification and nomenclature. Modified from Sasaki *et al.* (26)

Class/Type		Protein	Reaction	Gene (HUGO) (25, 26)	Alternative Names	Yeast Homolog
Phosphoinositide 3-kinases (PI3K)	Class IA PI3K	p110α	$PI(4,5)P_2 \rightarrow PI(3,4,5)P_3$ $PI \rightarrow PI(3)P$ $PI(4)P \rightarrow PI(3,4)P_2$	*PIK3CA*	PI3Kα PIK3CA	
		p110β	$PI(4,5)P_2 \rightarrow PI(3,4,5)P_3$ $PI \rightarrow PI(3)P$ $PI(4)P \rightarrow PI(3,4)P_2$	*PIK3CB*	PI3Kβ PIK3CB	
		p110δ	$PI(4,5)P_2 \rightarrow PI(3,4,5)P_3$ $PI \rightarrow PI(3)P$ $PI(4)P \rightarrow PI(3,4)P_2$	*PIK3CD*	PI3Kδ PIK3CD	
	Class IB PI3K	p110γ	$PI(4,5)P_2 \rightarrow PI(3,4,5)P_3$ $PI \rightarrow PI(3)P$ $PI(4)P \rightarrow PI(3,4)P_2$	*PIK3CG*	PI3Kγ PIK3CG	
	Class II PI3K	PI3K-C2α	$PI \rightarrow PI(3)P$ $PI(4)P \rightarrow PI(3,4)P_2$	*PIK3C2A*	PIK3C2α Cpk-m	
		PI3K-C2β	$PI \rightarrow PI(3)P$ $PI(4)P \rightarrow PI(3,4)P_2$	*PIK3C2B*	PIK3C2β	
		PI3K-C2γ	$PI \rightarrow PI(3)P$ $PI(4)P \rightarrow PI(3,4)P_2$	*PIK3C2G*	PIK3C2γ	
	Class III	Vps34	$PI \rightarrow PI(3)P$	*PIK3C3*	PIK3C3 PI3KC3	Vps34 (25)
Phosphatidylinositol 4-kinases (PI4K)	Type II PI4K	PI4K IIα	$PI \rightarrow PI(4)P$	*PI4K2A*	PI4K2A	Lsb6 (27)
		PI4K IIβ	$PI \rightarrow PI(4)P$	*PI4K2B*	PI4K2B	
	Type III PI4K	PI4K IIIα	$PI \rightarrow PI(4)P$	*PIK4CA*	PIK4CA PI4KA	Stt4 (27)
		PI4K IIIβ	$PI \rightarrow PI(4)P$	*PIK4CB*	PIK4CB PI4KB	Pik1 (27)
Phosphatidylinositol phosphate kinases (PIPK)	Type I PIPK	PIPK Iα	$PI(4)P \rightarrow PI(4,5)P_2$	*PIP5K1A*	PIP5KIα PIP5K1A Mouse: PIPKIβ PIP5K1B	Both Type I and Type II PIPks are homologs to yeast Mss4 (25)
		PIPK Iβ	$PI(4)P \rightarrow PI(4,5)P_2$	*PIP5K1B*	PIP5KIβ PIP5K1B Mouse: PIPKIα PIP5K1A	
		PIPK Iγ	$PI(4)P \rightarrow PI(4,5)P_2$	*PIP5K1C*	PIP5KIγ PIP5K1C	
	Type II PIPK	PIPK IIα	$PI(5)P \rightarrow PI(4,5)P_2$	*PIP4K2A*	PIP4K2A PIP5K2A PIP5IIα	
		PIPK IIβ	$PI(5)P \rightarrow PI(4,5)P_2$	*PIP4K2B*	PIP4K2B PIP5K2B PIP5KIIβ	
		PIPK IIγ	$PI(5)P \rightarrow PI(4,5)P_2$	*PIP4K2C*	PIP4K2C PIP5K2C PIP5KIIγ	
	Type III PIPK	PIPK III	$PI(3)P \rightarrow PI(3,5)P_2$ $PI \rightarrow PI(5)P$	*PIP5K3*	PIKFYVE p235 PIP5K3	Fab1 (25)

Another complicating factor is that the complexity of PI metabolism was not known at the outset, and so a naming system was not initially devised, and discovery was subject to chance timing. Some proteins were named based on how they were found by their cellular function (*e.g.*, Vsp34, and sorting vacuole proteins) before their molecular/enzymatic function (phosphorylation of PI to PI(3)P) was elucidated. In the late 1990s Gehrmann, Heilmeyer and colleagues tried a different approach to the nomenclature that used the PI3K or PI4K designation followed by the enzyme molecular weight. For example, they called the *S. cerevisiae* protein Pik1 PI4K120 (28). Some papers were published with this nomenclature (29–31) but mostly just from this group of researchers. The naming system that has survived includes the position the enzyme phosphorylates, the Class or Type, and the isoform (refer to Table 1). It is also common to use the Human Genome Organisation (HUGO) gene name, which follows this format (position, type, isoform); if italicized it refers to the gene and if it is not italicized, it refers to the protein. Despite this more standard naming system, it is still not perfectly consistent. For example, the Type II PI4Ks have the 4 before the K but the Type IIIs are written PIK4CB and the only indication that PIK4CB is a Type III PI4K is that it does not have a 2 in the name like the Type II enzymes do (*eg*. PI4K**2**B). However, Table 1 is very helpful in understanding the nomenclature of mammalian and yeast PI kinases.

Figure 7A is a visual organization of the classification of PI kinases. It is important to note again that the original classification is based on which position the PI kinases phosphorylate, what their substrate is, the effect of different inhibitors and other characteristics; therefore, Figure 7A is not based on or representative of relatedness or evolutionary relationships, or else the Type III PI4Ks would be classified with the PI3Ks next to the Type III PI3Ks (Figure 7B). For a more in depth look at the phylogenomics of PI kinases see the paper by Brown and Auger (25). The two PI kinases that were used and studied in this thesis are human PIK3C3 (a PI3K III) and yeast Pik1 (a PI4K III), therefore these and their respective yeast and human homologs (Vps34 and PI4KIIIβ) are the only PI kinases that will be discussed in detail in this document. See Table 2 (p.28) for a summary of the characteristics of these PI kinases.

1.2.2 Classification, Nomenclature, and Structure of PI3Ks

The Type I "PI4Ks" (*aka* PI3Ks) phosphorylate position D3, have molecular weights of approximately 100-200kDa, and are typically inhibited by non-ionic detergents but not by adenosine (21, 32). Wortmannin is a potent, specific, covalent inhibitor of PI3Ks (33). Wortmannin also has many other practical advantages such as being cell permeable, being commercially available, and having very little effect on other signaling molecules (33). Wortmannin was therefore used extensively to study PI3Ks and to explore the role(s) of PI3Ks in cell surface receptor-mediated signaling pathways, and growth factor and oncogenic signaling (32, 33). Research on PI3K contributed to the PI field in two significant ways: one was through its close association with cancer, and the second was evidence that the product PIP functions as a signaling entity in the membrane and not just as a precursor to other signaling molecules. Furthermore, later work found that proteins must exist that respond to these changes in lipid composition (32). Interest in the association between growth factor and oncogenic signaling and PI3K activity drove research on this class of enzymes and this effort resulted in the discovery of various subclasses of PI3Ks as well as the characterization of the primary structures of these enzymes and their adaptor proteins (32).

Type I "PI4Ks", also known as PI3Ks, began to be classified separately from the PI4Ks; however, they were still sometimes referred to as Type I enzymes and this type of PI kinases was further classified into different classes (Class IA, IB, II, and III). Note that some older publications refer to PI3Ks as Type I, Class IA, IB, II, and III; however, some newer publications use Type IA, IB, II, and III. The classes are characterized by enzyme structure, amino acid homology and regulatory domains (25), activation cascades (25), and by the preferred PI or PIP substrate.

Class I PI3Ks are heterodimeric (a catalytic subunit and a regulatory subunit), and preferentially phosphorylate PI(4,5)P_2 to generate PI(3,4,5)P_3. This class is further subdivided into Class IA and IB based on their associated regulatory proteins. Each catalytic subunit contains a regulatory protein binding domain, Ras-binding domain, a C2 domain, a helical domain (also known as the Lipid Kinase Unique (LKU) domain), and a lipid kinase domain (Figure 8). The Ras-binding domain is where GTP-bound Ras binds

to activate the catalytic subunit. The C2 domain is thought to participate in membrane interaction, and the LKU domain is important in interdomain packing (26).

Class II PI3Ks are monomeric and they typically phosphorylate PI to generate PI(3)P. Class II PI3Ks have structural similarity to Class I enzymes as seen by their common domains: the Ras-binding domain, the C2 domain, the LKU domain, and the lipid kinase domain. Class II enzymes also have a phox (PX) domain, and an additional C2 domain at their C-termini, as well as at least two proline rich (PR) regions (Figure 8). The phox homology domain is known to bind PI(3)P and other PIP species (26, 34).

Class III PI3Ks have a limited substrate specificity and only phosphorylate PI to form PI(3)P. These proteins have a C2 domain, a helical domain, and a lipid kinase domain, however, they lack the other domains common to Class I and Class II enzymes (Figure 8). Class III is further distinguished from Class I by their metal ion requirement; Class III enzymes have been demonstrated to have higher activity in the presence of Mn^{2+} than Mg^{2+}. The only PI3K found in *S. cerevisiae* is an enzyme called Vps34 (vacuolar protein sorting 34) and it is a Class III PI3K. This enzyme has been conserved from yeast to humans and, of the known members of the mammalian PI3K family, the mammalian homolog of Vps34 is the only one that is classified as a Class III PI3K. Vps34 and its homologs occur in all major taxonomic groups and it is the only PI3K in plant and fungus genomes (25). (As of 2011, PIK3C3 was the only class III known, and even in 2019 publications, PIK3C3 is the only one mentioned as a class III PI3K (35)). Sometimes this mammalian protein is referred to as Vps34 and sometimes it is referred to as PIK3C3 as its HUGO gene name is *PIK3C3*. To prevent this protein from getting confused with *S. cerevisiae* Vps34, PIK3C3 will be used in this document to denote the human Class III PI3K protein and Vps34 will be used to denote the *S. cerevisiae* homolog (26).

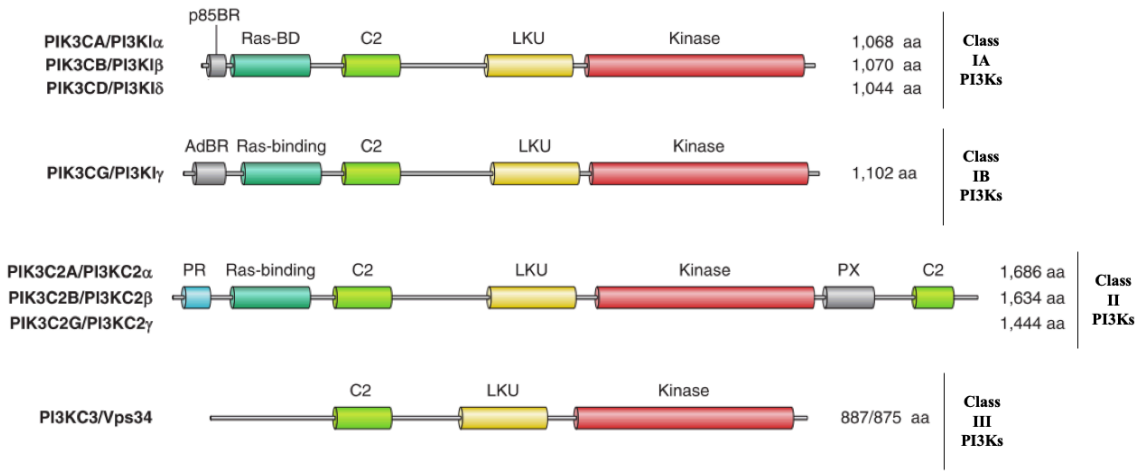

Figure 8: The vertebrate family of PI3Ks and the yeast homolog Vps34. The Class I PI3Ks are often called p110. Vps34 is the only PI3K in yeast. All PI3Ks have a conserved C-terminal catalytic domain (red) preceded by a lipid kinase unique (LKU) domain (yellow), and a C2 domain (bright green). Other domains include a p85 binding region (p85BR) where the regulatory subunits bind (grey), Ras binding domains (Ras-BD) (forest green), an N-terminal adaptor binding region (AdBR) (grey), a proline rich (PR) sequence (light blue), and a phox-homology (PX) domain (grey). Modified with permission from (32).

1.2.3 Classification, Nomenclature, and Structure of PI4Ks

All PI4Ks use PI as their substrate and phosphorylate position D4 of the inositol ring to produce PI(4)P (26). Type II PI4Ks are typically activated by detergent and inhibited by adenosine (21). Type III PI4Ks are also activated by detergents but are relatively resistant to inhibition by adenosine. They also are resistant to inhibition by a monoclonal antibody that caused greater than 90% inhibition of the Type II PI kinases (21). There are no Type I PI4Ks.

Type II PI4Ks are the most abundant subgroup of PI kinases in most animal cells and tissues. As a result of this, they were among the first PI kinases to be detected and characterized biochemically and were originally thought to be the only source of PI(4)P (27). Type II PI4Ks have an apparent MW of 45-55kDa, are stimulated by Triton X-100, and have a relatively low sensitivity to wortmannin (27). Type II PI4Ks are also inhibited by Ca^{2+}, a monoclonal antibody called mAb 4C5G, and by low concentrations of adenosine (27). Type II PI4K enzymes do not share sequence homology with any of

the PI3Ks or the Type III PI4Ks (25). The catalytic lipid kinase domain is split in two with a long insert between them (26, 27) (Figure 9). In mammalian isoforms the N-terminal half contains a cysteine-rich domain that is palmitoylated, which likely facilitates membrane targeting (26). It is possible that the yeast isoform may also require S-palmitoylation (27). There are two mammalian Type II PI4K isoforms, namely PI4KIIα and PI4KIIβ, and one yeast isoform Lsb6 (Table 1, Figure 9). However, these enzymes will not be covered in further detail in this thesis.

Type III PI4Ks generally have much greater apparent MWs than Type II PI4Ks (26, 27). Type III PI4Ks are stimulated by Triton X-100 and, like PI3Ks, are sensitive to inhibition by wortmannin (28, 36). Ca^{2+} has no direct effect on Type III PI4K activity, they are not inhibited by the monoclonal antibody mAb 4C5G, and they display little or no inhibition by adenosine (27, 36). Type III PI4Ks are structural relatives of PI3Ks and contain a C-terminal lipid kinase domain similar to the PI3K kinase domain, which explains the inhibition of Type III PI4Ks by wortmannin (25, 26, 36). The structure of the human PI4KIIIβ was close enough to the structure of the human PI3KIII (PIK3C3) that the structure could be solved by molecular replacement using the structure of PIK3C3 (37). Mammalian Type III PI4Ks also contain a proline rich N-terminal region, and a lipid kinase unique (LKU) domain that is predicted to be helical and homologous to the helical domain in the PI3Ks (26, 36). Type III PI4Ks are further classified into α and β isozymes based on their domains (26). The α-isozymes have a pleckstrin homology (PH) domain between the LKU and the catalytic domain that may be involved in the association with membranes. Mammalian α-isozymes also have a bipartite nuclear localization sequence (NLS) (26, 36). The β-isozymes can share three regions of varying degrees of homology between the LKU and the catalytic domain. In Pik1, the yeast PI4K IIIβ, immediately following the C-terminus of the LKU domain is the Frq-binding site and there is some level of conservation in this region in the vertebrate PI4KIIIβ. Following the Frq-binding site there is a serine rich region that contains multiple phosphorylation sites (not shown in Figure 9). Adjacent to this region is a third region of homology that was shown to be a Rab binding domain in the mammalian β-isozymes (36). Rab binding may regulate membrane transport from the Golgi to the PM (26).

There are two Type III PI4Ks in *S. cerevisiae* Stt4 (a PI4K IIIα isozyme) and Pik1 (a PI4K IIIβ isozyme) and these are homologous to the two Type III PI4Ks in mammals, PI4KIIIα (*aka* PIK4CA, a PI4K IIIα isozyme) and PI4KIIIβ (*aka* PIK4CB, a PI4K IIIβ isozyme) (26, 36). Pik1 and PI4KIIIβ are the only Type III PI4Ks that will continue to be discussed in this document. (Figure 9)

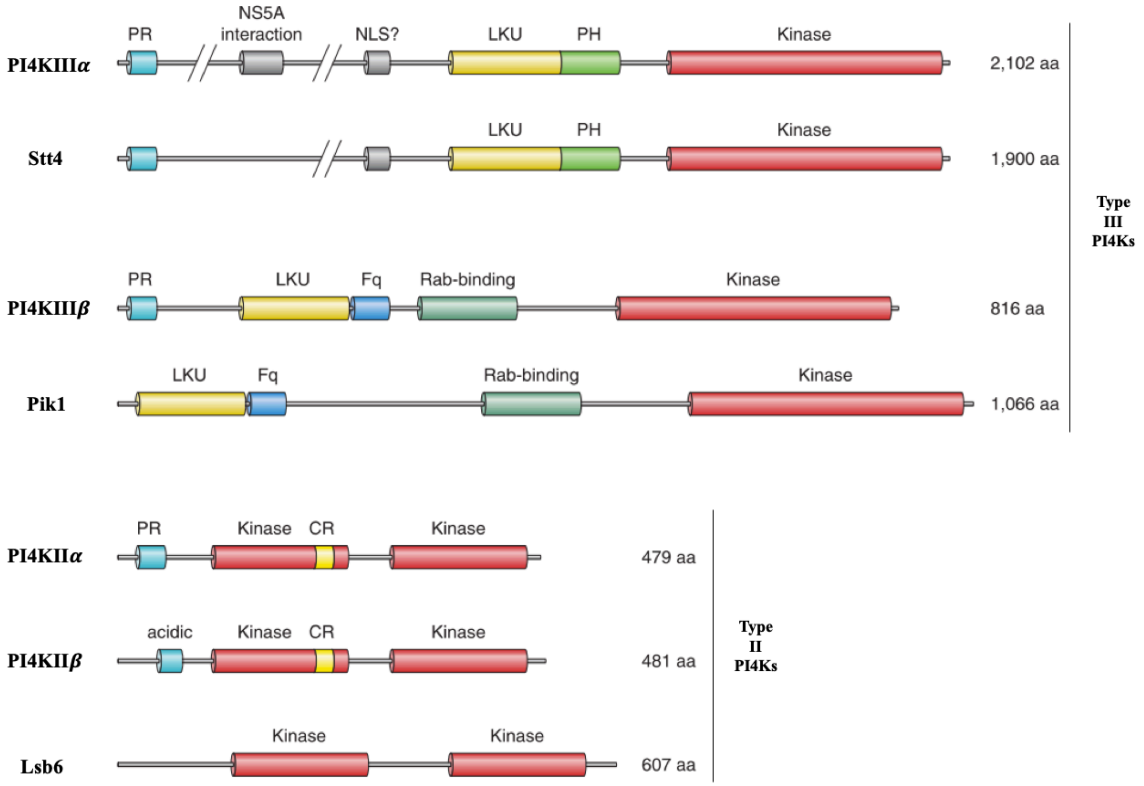

Figure 9: The vertebrate family of PI4K enzymes and the yeast homologs. The yeast proteins, Stt4, Pik1, and Lsb6, are depicted below their vertebrate homologs. The type III PI4K enzymes are comprised of two proteins PI4KIIIα (Stt4 in yeast) and PI4KIIIβ (Pik1 in yeast). They are related to the PI3Ks and they have some domains in common with the PI3Ks, including a highly conserved C-terminal catalytic domain (red) and a lipid kinase unique (LKU) domain (mustard yellow). Other domains include proline-rich (PR) sequences (light blue), the binding site for the viral protein NS5A (grey), a nuclear localization signal (NLS, grey), pleckstrin homology (PH) domains (bright green), frequenin-binding (Fq) domains (royal blue), and Rab binding domains (forest green). There are two forms of type II PI4Ks in vertebrates, PI4KIIα and PI4KIIβ, and one form in *S. cerevisiae* (Lsb6). There is a non-conserved insert between two halves of the lipid kinase domain and the vertebrate PI4Ks also have cysteine-rich (CR) sequences (yellow) that get palmitoylated. Figure modified with permission from (32).

1.2.4 Classification, Nomenclature, and Structure of PIPKs

The third group of PI kinases are called phosphatidylinositol phosphate kinases (PIPKs). These enzymes do not share significant sequence homology with any other known lipid or protein kinases, but all PIPKs share a central kinase core domain (PIPKc) that shows approximately 80% amino acid identity with other PIPK proteins (Figure 10). There are three types of PIPKs: Type I enzymes phosphorylate position D5 of PI(4)P, Type II enzymes phosphorylate position D4 of PI(5)P, and Type III enzymes phosphorylate PI and PI(3)P at position D5 to produce PI(5)P and PI(3,5)P (26).

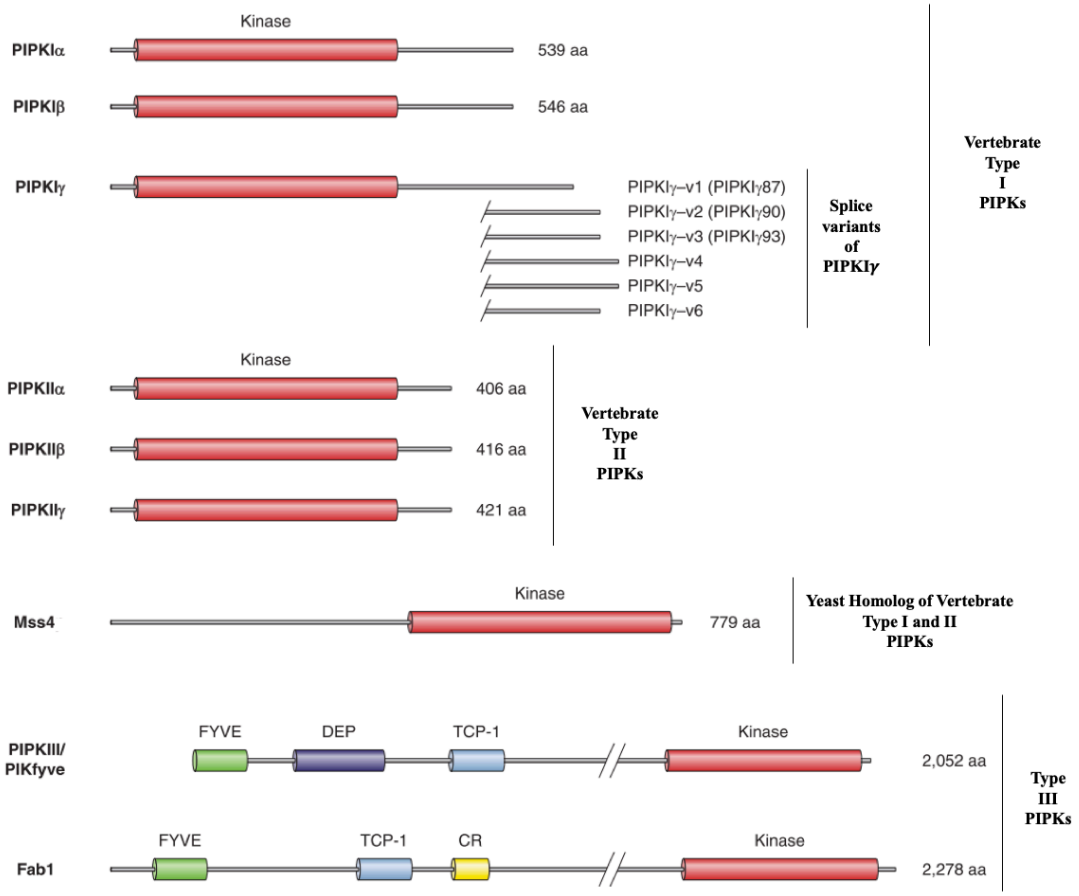

Figure 10: The vertebrate family of PIPK enzymes and the yeast homologs. Vertebrate Type I and Type II PIPKs generate PI(4,5)P2 from either PI(4)P (Type I) or PI(5)P (Type II) and there are six Type I and Type II PIPKs total. There is only one yeast enzyme that generates PI(4,5)P2; it is called Mss4 and it uses PI(4)P as its substrate. Type III PIPKs generate PI(3,5)P2 from PI(3)P and Fab1 is the yeast Type III PIPK. PIPKs do not share significant sequence homology with PI3Ks or PI4Ks, but all PIPKs share a central kinase core domain (red). Other domains include the PI(3)P binding domain FYVE (green), a dishevelled, Egl-10 and Pleckstrin domain (DEP) domain (navy blue), a Cpn60/TCP-1 chaperonin family domain (TCP-1) (light blue), and a cysteine-rich (CR) sequence (yellow). Figure modified with permission from (32).

1.2.5 Type III PI-3 Kinases: PIK3C3 and Vps34

PIK3C3 and Vps34 are homologous proteins from humans and *S. cerevisiae*, respectively, and they show a high degree of homology over their entire length: 37% identity and 58% similarity at the amino acid level (38). PIK3C3 and Vps34 are both Type III PI3Ks which specifically phosphorylate the D-3 position of PI to form PI(3)P (38–40). They both also require Mn^{2+} for their activity, but can be weakly active in the presence of Mg^{2+} (38, 40). PIK3C3 has a calculated MW of 101,549 Da (UniProtKb-Q8NEB9) (41), a specific activity between 78-216 nmol/min/mg (42), and it does not exhibit autophosphorylation (38). Vps34 has a calculated MW of 100,921 Da (UniProtKB- P22543) (43), and it does undergo autophosphorylation *in vivo* and *in vitro* (39, 40). See Table 2 (p.28) for an overview of the characteristics of the PI kinases focused on in this thesis.

The inhibitory or stimulatory effects of different entities on PI kinase activity have been explored to characterize their function. PI3Ks are typically inhibited by non-ionic detergents; this is consistent with PIK3C3 and Vps34, as both are inhibited by the non-ionic detergent NP40 with IC_{50} values of 0.01% and 1% for PIK3C3 and Vps34, respectively (38). However, low concentrations of NP40 (around 0.05%) stimulated the of activity of Vps34, but no stimulation of activity was observed for PIK3C3 at the tested concentrations (*i.e.,* NP40 was inhibitory at all concentrations tested for PIK3C3) (38). Adenosine sensitivity is another way of characterizing PI kinases; both PIK3C3 and Vps34 are insensitive to inhibition by adenosine up to 1mM (38). PIK3C3 and Vps34 differ in their sensitivity to wortmannin. PIK3C3 is inhibited by wortmannin at low nanomolar concentrations and has an IC_{50} value of 2.5nM (38). Vps34, however, is resistant to inhibition by wortmannin and has an IC_{50} value of 3μM (39, 40).

These proteins are the only Type III PI-3 kinases in both *S. cerevisiae* and mammals (25, 26). Yeast cells containing a null mutant form of Vps34 lack the PI3K activity that is seen in wild-type strains, thus indicating that Vps34 is the sole source of PI(3)P in *S. cerevisiae* (27). PIK3C3 is likely the primary but not the only kinase that produces PI(3)P in mammals. A reduction in PI(3)P levels in the quadriceps muscles of skeletal muscle specific PIK3C3 knockout verses wildtype mice supports this claim. It is

hypothesized that the other enzyme producing PI(3)P is the type II PI3K Pik3c2β based on gene expression data. However, the reduction of and not abolition of PI(3)P production may be caused by residual PIK3C3 expression in myofibers or PIK3C3 expression in non-muscle cell types that are present in total muscle extracts (44). Whole-animal gene knockout of PIK3C3 results in early embryonic lethality (44). *S. cerevisiae* with a Vps34 null allele are viable, but are compromised with respect to growth at 30°C and are inviable at 37°C (27).

1.2.5.1 Adaptor Proteins and Recruitment to the Membrane

Vps34 was identified during genetic studies focused on finding cellular components required for vacuolar protein localization (45). Many yeast mutants that were defective in vacuolar protein sorting (*vps* mutants) were identified, *vps34* and *vps15* being two of them. These two mutants were of particular interest because the phenotypes implied that they are specifically required for the sorting of soluble vacuolar proteins and that they act at the same step of the vacuolar protein sorting pathway (45, 46). Vps15 was found to be a 160kDa serine/threonine kinase that is myristoylated and is located on the cytoplasmic face of a late Golgi compartment or an intermediate membrane in the transport between the Golgi complex and the vacuole (38, 45). Vps15 and Vps34 physically and functionally interact; Vps15 is responsible for the membrane localization of Vps34 and Vps15 protein kinase activity is required for the stimulation of Vps34 PI kinase activity (27, 45, 46). Vps15 and Vps34 act in two different multi-subunit complexes to regulate two different pathways (27). Complex I comprises the proteins Vps15, Vps34, Vps30, and Atg14, and it regulates the autophagy/cytosol-to-vacuole transport pathway (27). Complex II is composed of Vps15, Vps34, Vps30, and Vps38 and it controls the Vps pathway (27).

In 1995 Volinia and coworkers identified and characterized a human phosphatidylinositol 3-kinase complex related to the yeast Vps34-Vps15 complex (38). The proteins of interest in this complex were later referred to as PIK3C3 and p150 (*aka* PIK3R4). After PIK3C3 was found, cloned, and characterized using degenerate primers based on amino acid sequences that are conserved among yeast Vps34 and bovine p110α,

immunoprecipitation of PIK3C3 from human Jurkat 6 cell lysates revealed three proteins that associated with PIK3C3 (38). The 150 kDa protein (p150), co-immunoprecipitated in an approximately equimolar ratio with PIK3C3 and further investigation revealed that p150 is homologous to Vps15 (38). The amino acid sequences of these proteins are 29.6% identical and 53% similar (47). A region with 100% identity between Vps15 and p150 is a typical signature of protein kinases (38). Details about the other proteins in this complex and the role of the complex in autophagy can be found in (48).

1.2.6 Type III PI-4 Kinases: PI4K IIIβ and Pik1

PI4K IIIβ and Pik1 are homologous proteins from human and *S. cerevisiae,* respectively, and they show a high degree of sequence homology, especially in particular domains. *PI4K IIIβ* and *PIK1* have 42% sequence identity in the catalytic domain and 17% in the lipid kinase unique domain (49). The Pik1 protein also shares sequence similarity with p110 (a Class I PI3K) and *S. cerevisiae* Vps34 in these two regions (9). The C-terminal region of homology is the catalytic domain and Pik1 shares 30% identity with Vps34 and 29% identity with p110 in this region (9). If conservative amino acid replacements are taken into account, the similarity of all three proteins exceeds 50% in this domain (9). The second main region of homology is near the N-terminus and Pik1 has 24% and 25% identity with Vps34 and p110 in this region (9). However, Vps34 has a large insert in this region, while p110 does not (9). This region is referred to as the LKU domain and this region is homologous to the helical domain (*aka* the LKU domain) in PI3Ks (26, 27, 32) (Figures 8 & 9). See Table 2 for an overview of the characteristics of the PI kinases focused on in this thesis.

PI4K IIIβ and Pik1 are both Type III PI4Ks and specifically phosphorylate the D-4 position of PI to form PI(4)P (49, 50). Both are typically assayed in the presence of Mg^{2+} (50–52). PI4K IIIβ has a calculated MW of 91,379 Da (UniProtKb- Q9UBF8) (53), and the specific activity of apo PI4K IIIβ was determined to be 0.8 (SD $\pm$ 0.11) or 1.71 (SD $\pm$ 0.05) nmol ADP/min/mg depending on the vesicle substrate using the Transcreener ADP^2 FI Assay (Bellbrook Labs) (see Section 1.4 for a description of the assay) (52). PI4K IIIβ is activated by the phosphorylation of Ser294 by protein kinase D; this phosphorylation mediates the recruitment of proteins that stabilize the lipid kinase

activity of PI4K IIIβ (54). Pik1 has a calculated MW of 119,923 Da (UniProtKB-P39104) (55), and the specific activity of a purified fraction of Pik1 was determined to be 4.3 μmol/min/mg protein on detergent lipid micelles using a PI kinase assay based on [γ-^{32}P]ATP (50).

The inhibitory or stimulatory effect of different entities on PI kinase activity also contributes to the characterization of PI4Ks. PI4K IIIβ is stimulated by non-ionic detergent, but not as much as Type II PI4Ks are (49). The activity of Pik1 is stimulated by the non-ionic detergent Triton X-100; when Triton X-100 was removed from the assay $\leq$50% of the activity of the standard conditions was observed (50). In general, Type III PI4Ks are inhibited by wortmannin but are not sensitive to adenosine (37). However, PI4K IIIβ and Pik1 differ in their sensitivity to wortmannin and to adenosine. PI4K IIIβ is strongly inhibited by wortmannin (IC_{50} = 120nM -140nM) and experiences modest inhibition by 500μM adenosine (49). Pik1 is unaffected by wortmannin and is insensitive to adenosine (27, 50). No inhibition of Pik1 is observed up to 1mM adenosine and only modest inhibition ($\leq$30%) is seen at very high concentrations of adenosine (10mM) (50).

There are four mammalian PI4K isozymes: PI4KIIα, PI4KIIβ, PI4KIIIα, and PI4KIIIβ; each localizes to a specific cellular compartment, indicating that each produces a pool of PI(4)P required for a different function (26). PI4KIIIβ was found to be ubiquitously expressed in rat tissues and it localized to either early Golgi compartments or the nucleus depending on the phosphorylation state of the PI4KIIIβ protein. Phosphorylation on Ser294 targeted the enzyme exclusively to the Golgi, whereas phosphorylation on Ser496 or Thr504 results in its detection in the nucleus (26). In yeast, there are also two Type III PI4K isozymes: Type IIIα Stt4, and Type IIIβ Pik1 (27). Both are essential for yeast cell viability and the overexpression of one cannot make up for the knockout of the other (27). This is evidence that Pik1 and Stt4 generate discrete pools of PI(4)P that regulate different essential physiological processes (27). Pik1 generates PI(4)P at the Golgi and Stt4 generates PI(4)P at the plasma membrane (5).

1.2.6.1 Adaptor Proteins and Recruitment to the Membrane

Frequenin (Frq1) is the 22kDa adaptor protein for Pik1. Pik1 is the only essential target of Frq1, which is required for the optimal activity of Pik1 (3). Frq1 is essential for the growth of budding yeast and it belongs to the recoverin/frequenin branch of the EF-hand superfamily (56). Proteins in this superfamily detect changes in intracellular Ca^{2+} levels and transduce the signal via conformational changes upon Ca^{2+}-binding to control many important physiological processes (56). *N*-Myristoylation and the Ca^{2+}-binding contribute to the ability of Frq1 to associate with membranes *in vivo* (56). However, the *N*-myristoylation is important but not essential for the recruitment and stimulation of the catalytic activity, and there is evidence that Frq1 does not contain a functional Ca^{2+} -myristoyl switch (3, 57). After Pik1 was initially characterized, further investigation lead to the discovery that the purified Pik1 was actually a tightly bound complex of Pik1 and Frq1, with the two proteins being present in a 1:1 ratio (3). The binding energetics for the complex were determined by isothermal titration calorimetry and the dissociation constant and binding enthalpy were determined to be ~100nM and +7kcal/mol (57, 58). The NMR structure of Ca^{2+}-bound Frq1 complexed to an *N*-terminal Pik1 fragment (residues 121-174) was determined (PDB code 2JU0) (57). Frq1 forms a groove with two hydrophobic pockets, while the Pik1 fragment forms two helices connected by a 20-residue loop such that each helix contacts a pocket in the groove of Frq1 (57). This can be seen in Figure 11.

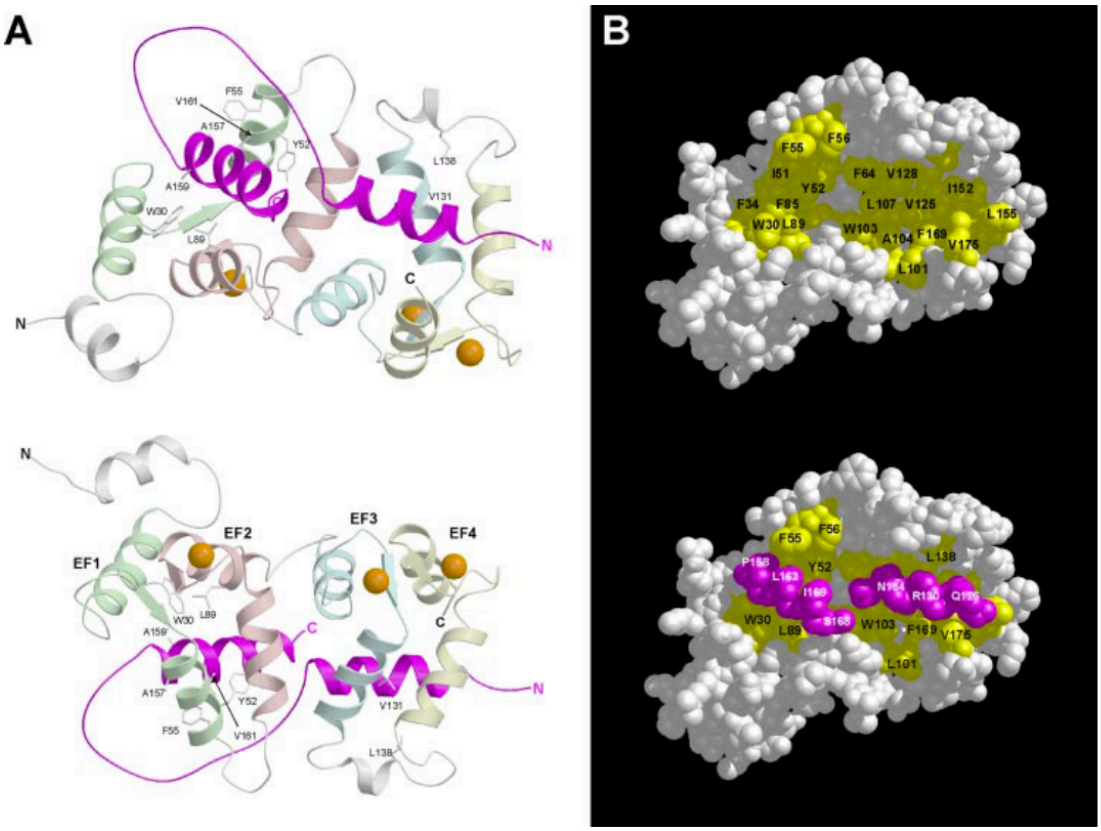

Figure 11: Solved NMR-derived structures of a fragment of Pik1 (residues 121-174) with Frq1 (PDB code 2JU0). A. Ribbon diagram of the average main chain structure of 20 NMR-derived structures of the complex, viewed from the binding surface and rotated 180°. Ca^{2+} ions are shown in orange and Pik1 residues are in magenta. **B.** Space-filling model of the average main chain of 20 NMR-derived structures of the complex. The two hydrophobic patches in the groove of Frq1 are shown in yellow and the Pik1 residues are in magenta. This figure was reproduced with permission from Strahl *et al.* (57).

Frq1 has been shown to facilitate the membrane targeting of Pik1 and to stimulate its activity (3, 56, 57). Measuring the catalytic activity of Pik1 mutants showed that activation of Pik1 by Frq1 does not involve relief of an autoinhibitory constraint; instead the Pik1 catalytic domain by itself is inactive and requires interaction and stabilization by an auxiliary domain at the *N*-terminus (57). The necessary auxiliary domain was determined to be the LKU domain (57). The binding of Ca^{2+}-bound Frq1 to Pik1 imposes a U-turn in the Pik1 chain that may modulate the interaction between the LKU and catalytic domains (57). This is the proposed model of the activation of Pik1 by Frq1 and this model is depicted in Figure 12.

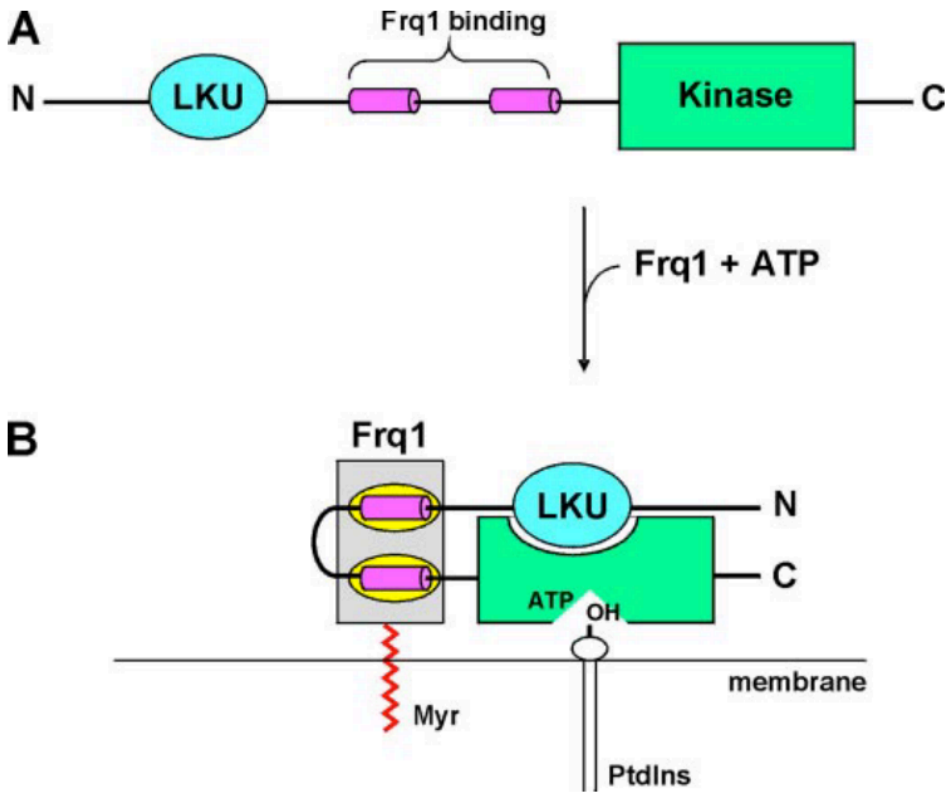

Figure 12: Cartoon diagram of how Frq1 is proposed to stimulate Pik1 activity. Figure reproduced with permission from Strahl *et al.* (57).

The human orthologue of frequenin is neuronal calcium sensor-1 (NCS-1); however, the roles of NCS-1 and of Frq1 are likely to be different. A helix that is involved in the binding of Frq1 with Pik1 is not conserved in PI4KIIIβ and although NCS-1 binds PI4KIIIβ and enhances its activity, it does not localize PI4KIIIβ to the Golgi (54). However, three different proteins, the GTPase ADP-ribosylation factor 1 (Arf1), the small GTPase Rab11, and the Acyl-CoA-binding domain containing protein 3 (ACBD3), have been shown to recruit PI4KIIIβ to the Golgi. The interaction between PI4KIIIβ and each of these proteins have been shown to be important in PI(4)P production at the Golgi and ultimately for efficient transport from the Golgi to the plasma membrane (26, 54). PI4KIIIβ is also localized to the nucleus and localization is associated with phosphorylation at different protein sites. For example, PI4KIIIβ phosphorylated on Ser-294 is only found at the Golgi, while PI4KIIIβ phosphorylated on Ser-496 and Thr-504 is found in nuclear speckles (59). Phosphorylation at Ser-294 increases the lipid kinase activity (59).

Table 2: Summary of the characteristics of the PI kinases PIK3C3, Vps34, PI4KIIIβ, and Pik1.

Enzyme	PIK3C3	Vps34	PI4K IIIβ	Pik1
Type	PI 3-kinase: Type III	PI 3-kinase: Type III	PI 4-kinase: Type III	PI 4-kinase: Type III
Organism	Human	Yeast	Human	Yeast
MW	101,549 Da (UniProtKb-Q8NEB9)	100,921 Da (UniProtKB-P22543)	91,379 Da (UniProtKB-Q9UBF8)	119,923 Da (UniProtKB-P39104)
Adaptor Molecule	p150 (38) (*aka* PIK3R4)	Vps15 (38, 39)	ACBD3, Rab11, Arf1 (26, 51, 52, 54, 60, 61)	Frq1 (3)
Substrate Specificity	PI (38)	PI (39, 40)	PI (49)	PI (50)
Phosphorylates position:	D3 (38)	D3 (39, 40)	D4 (49)	D4 (50)
Product	PI(3)P (38)	PI(3)P (39, 40)	PI(4)P (49)	PI(4)P (50)
Null allele/ knockout lethal	Yes (44)	Yes at 37°C but viable 30°C (27)	No (62)	Yes (15)
Cation Dependence	Mn^{2+} dependent, weakly active with Mg^{2+} (38)	Mn^{2+} dependent, weakly active with Mg^{2+} (40)	Activity assayed with Mg^{2+} (51, 52)	Activity assayed with Mg^{2+} (50)
Effect of low [non-ionic detergent NP40] / effect of Triton	Inhibition (IC_{50} = 0.01%) at low [NP40] (38)	Inhibition (IC_{50} = 1%), but stimulation at very low [NP40] (38)	Modestly affected by non-ionic detergent (49)	Stimulated by Triton X-100. (50)
IC_{50} for Wortmannin	IC_{50} = 2.5nM Inhibited at low nanomolar range (38)	IC_{50} = 3μM (39) Highly resistant to wortmannin (40)	IC_{50} = 120nM - 140nM Strongly inhibited by wortmannin (49)	Unaffected by wortmannin (27)
Adenosine Sensitivity	Insensitive No inhibition up to 1mM (38)	Insensitive No inhibition up to 1mM (38)	Modest inhibition by 500μM (49)	Insensitive (50) No inhibition up to 1mM (50)
Sequence Homology	Extensive sequence homology to yeast Vps34, 37% identity, 58% similarity at amino acid level (38)	Extensive sequence homology to PIK3C3, 37% identity, 58% similarity at amino acid level (38)	Shares sequence homology with yeast *PIK1*, 42% identity in the catalytic domain and 17% in the LKU domain at the gene level (49)	Shares sequence homology with yeast Vps34, 30% identity in the catalytic domain, and 24% identity in the LKU domain at the amino acid level (9)

1.3 Lipid Transfer Proteins, Sec14, and the Regulation of Pik1

1.3.1 The Structure of Sec14 and the Sec14 Superfamily

Sec14 is the archetypal member of the Sec14 superfamily. This family is composed of phosphatidylinositol (PI)/phosphatidylcholine (PC) transfer proteins (PITPs), which are ancient, eukaryotic, non-enzymatic proteins that bind PI and mediate the transfer of PI between membrane bilayers *in vitro* in an energy independent manner. PITPs exhibit similar *in vitro* biochemical activities; however, they are categorized into two groups based on their structure and their primary sequence homology. The two groups are not structurally related and do not share primary sequence similarity. These two groups are the Sec14-like PITPs and the START-like PITPs (steroidogenic acute response related transfer domain). Only Sec14-like PITPs will be covered further within this thesis (4).

The Sec14 fold is composed of 12 α-helices, 6 β-strands, and 8 3_{10} helices (Figure 13) (4). The 6 β-strands and 3 of the α-helices form a hydrophobic pocket that is gated by a A_{10}/T_4 helix gating module; the phospholipid binds in this hydrophobic pocket. The A_{10}/T_4 helix gating module is mobile and is in different conformations based on the presence or absence of bound hydrophobic ligand, or if the protein is bound to a membrane or not (shown in red in Figure 13). Sec14 likely associates with a membrane and inserts the gating module into the hydrophobic core as it transitions to the open state (63). The A_1-A_4 α-helices at the N-terminus form a tripod like motif and this structural segment is responsible for the targeting of Sec14 to Golgi membranes. The crystal structure of apo-Sec14 (1AUA – open, crystalized with bound detergent) and of holo-Sfh1 (3B7N - closed and containing PI in the hydrophobic pocket) are shown in Figure 13. The detergent β-octylglucoside was required for the crystallization of Sec14, therefore the crystal structure represents the open conformation with the detergent in the lipid binding site. However, the crystal structure of the closest Sec14 homolog, Sfh1 (62.3% identity with Sec14), was achieved without detergent and with physiologically relevant phospholipid ligands. Therefore the structure of Sfh1 could be used to infer how Sec14 binds its physiological ligands (4, 64).

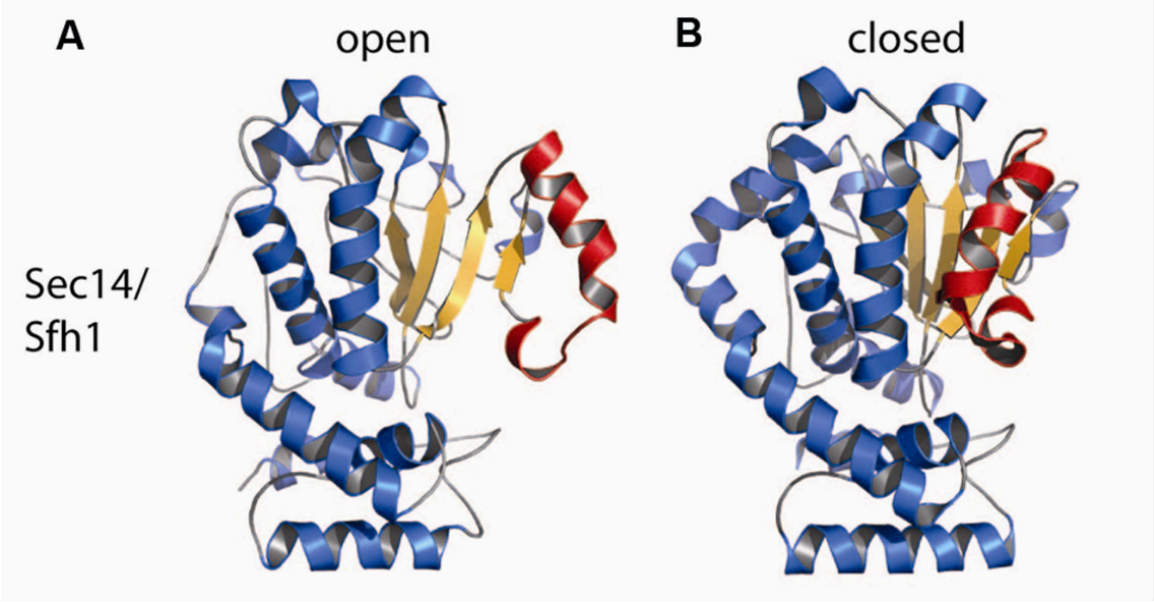

Figure 13: Ribbon diagram of (A) Apo-Sec14 (1AUA) and (B) Holo-Sfh1bound to PI (3B7N). α-Helices are in blue, β-strands are in yellow, and the A10/T4 helix gating module is in red. Image reproduced with permission from (65).

The classical functional description of Sec14 involves its action as a lipid ligand transfer agent between membranes (63). In this model, Sec14 in its closed, ligand-bound state associates with a membrane and inserts the A10/T4 helix gating module into the bilayer as it transitions to the open state (63). In the open state, the bound phospholipid is released into the membrane and a different phospholipid can bind in the hydrophobic pocket (63). Multiple exchange cycles may occur but ultimately the helix gating module closes and Sec14 dissociates from the membrane (63). Sec14 then shuttles its phospholipid ligand to a different membrane and the processes repeats. This is visualized in Figure 14 (63). However, genetic studies and the analysis of the structure of wild type Sec14 suggest that the function of Sec14 is more complicated than membrane-to-membrane phospholipid exchange (66). Sec14 has been shown to act as a signal integrator between lipid metabolism and PIP signaling (4) and it stimulates the kinase activity of Pik1 *in vivo* (1, 64, 67–70). This led to a presentation model of Sec14 mediated Pik1 activation.

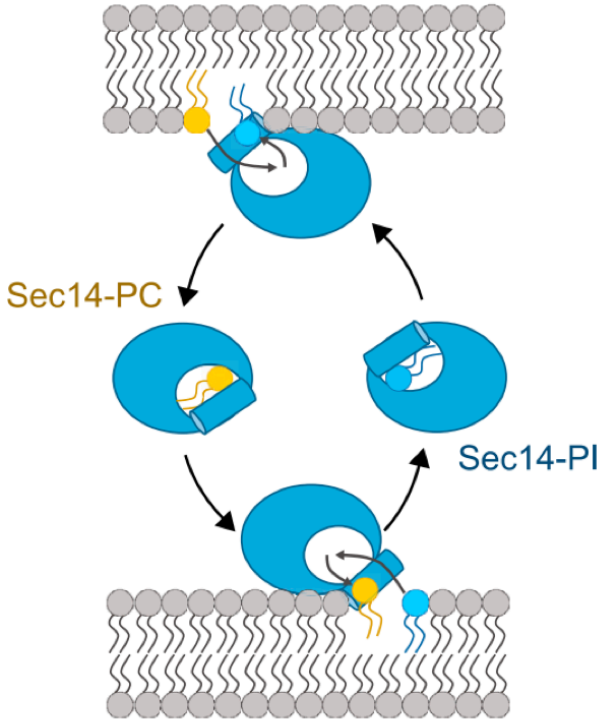

Figure 14: Classical lipid transfer model of Sec14 activity. Helix gating module shown as a cylinder, PI shown in blue, and PC shown in yellow. Image used with permission from (63).

1.3.2 Presentation Model of Sec14-Mediated Pik1 Stimulation

Bankaitis and colleagues proposed a lipid presentation model to describe the stimulation of Pik1 by Sec14 (Figure 15). In this model, Sec14 is proposed to mediate heterotypic exchange, binding both PI and PC, and during this exchange PI is presented to Pik1 making it a better substrate for phosphorylation. In this model, the *in vitro* PITP ligand transfer activity of Sec14 does not describe the *in vivo* activity; the essential activity of Sec14 is not to transport a phospholipid between lipid layers, rather it is to undergo heterotypic exchange at the membrane. Any cytosolic Sec14 bound to PI or PC would therefore be non-functional artefacts instead of active components or intermediate stages of the essential activity. There are two hypotheses for how the presentation of PI occurs during the heterotypic exchange; however, these hypotheses are not mutually exclusive (64). The exchange may occur through different portals so that as PC is entering the Sec14 ligand binding site via one portal, PI is ejected from the hydrophobic binding pocket through an exit portal. As PI is ejected, it transiently exists as an exposed intermediate and the inositol head group is susceptible to phosphorylation by Pik1.

Under the second hypothesis, the exchange occurs via overlapping entry and exit portals. The headgroup of PC is bound deep within the hydrophobic binding pocket (Figure 16) and PC will therefore slowly egress from the binding pocket. The headgroup of PI, however, is bound with a higher affinity than PC by a network of residues nearby but below the surface of the protein. Sec14 has a ~16-fold preference for PI over PC. Therefore, PI will ultimately displace bound PC from Sec14 but during the process there may be multiple unsuccessful attempts of PI to bind. During these attempts, PI would exist as an exposed intermediate susceptible to Pik1. See Figure 15 for a diagram of this presentation model (10, 64).

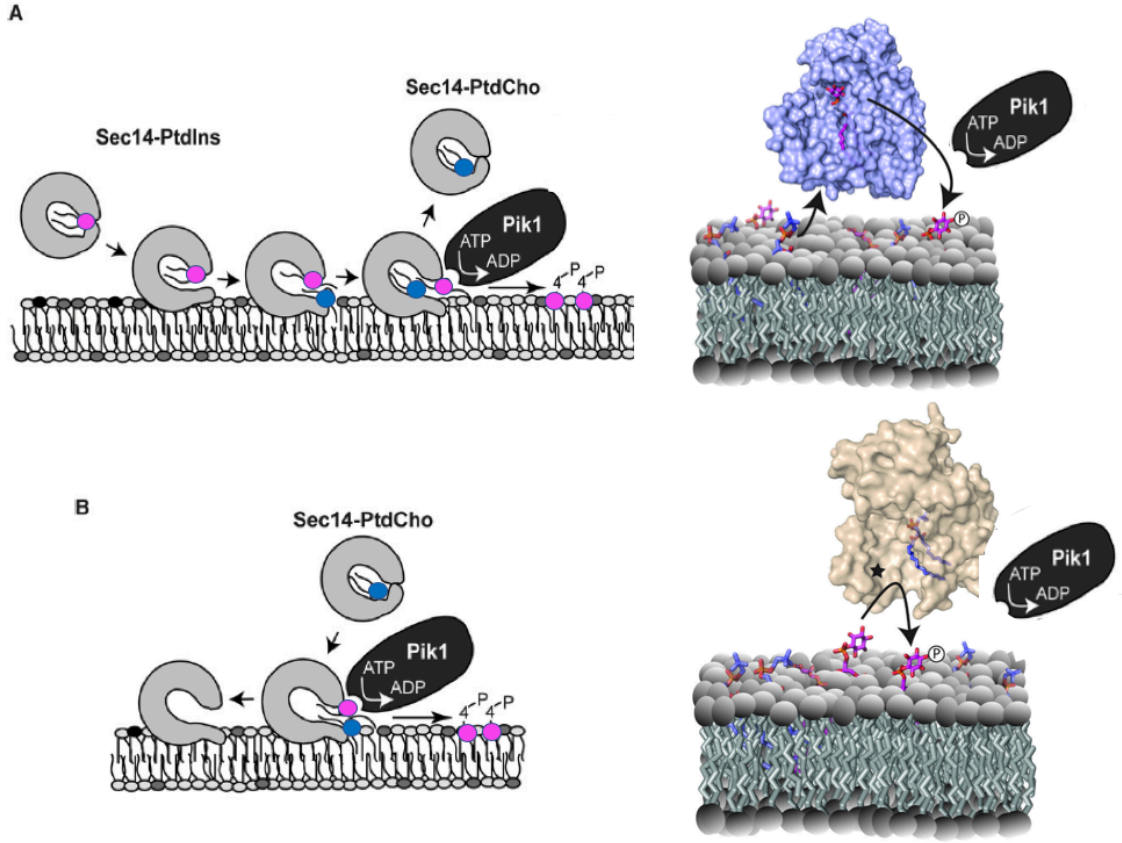

Figure 15: Proposed PI presentation model for the function of Sec14 in PIP homeostasis. A. Sec14 presentation of PI to Pik1 via heterotypic exchange of PI (pink) for PC (blue) through distinct entry and exit portals. **B.** Sec14 presentation of PI via heterotypic exchange through overlapping portals. Images modified with permission from (64, 65).

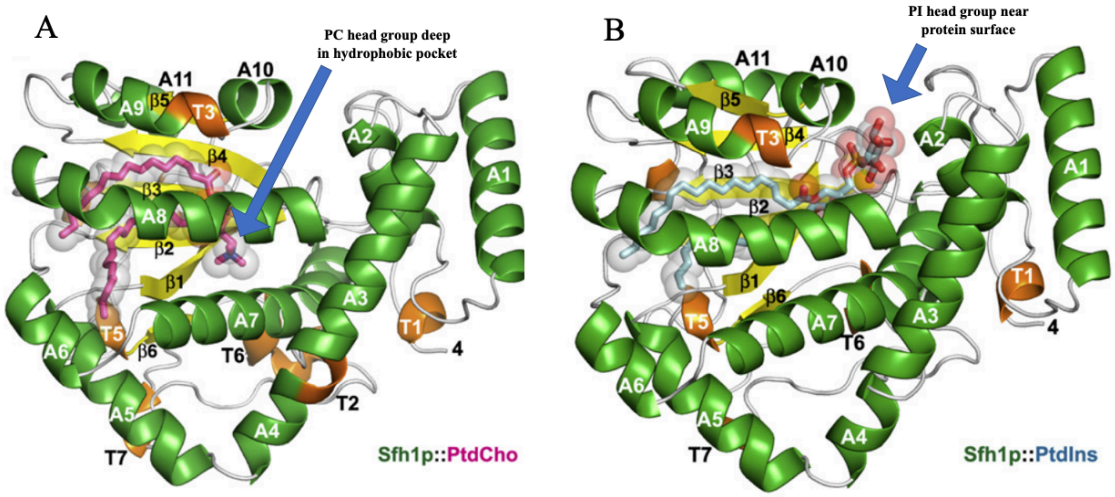

Figure 16: Ribbon diagram Sfh1 bound to PC (A) or PI (B). α-Helices shown in green, 3_{10} helices are shown in orange, and β strands are shown in yellow. Images modified with permission from (64).

1.3.3 Genetic and Structural Evidence of Mechanism

In 1989 the *SEC14* gene was observed to be essential for yeast vegetative growth and the *SEC14* gene product was identified as a cytosolic factor that was required for the transport of secretory proteins from the yeast Golgi complex (71). The *SEC14* gene was later determined to be identical to the independently characterized *PIT1* gene, which was known to encode a PI/PC transfer protein in yeast (72). This established an *in vivo* function (the stimulation of compartment-specific secretion) for a phospholipid transfer protein for the first time (72). To determine if the *in vivo* activity of Sec14 was represented by its *in vitro* PITP activity, rat PITP, which has very similar catalytic properties as Sec14 but no detectable primary sequence homology, was expressed in Sec14 mutants (73). Rat PITP mediated complementation of Sec14 defects but could not fully substitute for Sec14 function (73). There are two main possible explanations for this observation. First, the rat PITP and Sec14 act via different *in vivo* mechanisms, such that one may genuinely act as a PITP *in vivo* and the other's *in vitro* PITP activity reflects a different phospholipid binding activity *in vivo* (73). Second, the two proteins operate in a mechanistically similar way, but the rat PITP is missing an additional capability, such as the targeted binding of Golgi membranes, that is required for the *in vivo* activity of Sec14 (73). It was observed that Sec14 levels impact the apparent rate of PC biosynthesis via the CDP-choline pathway *in vivo* and this led to the hypothesis that

Sec14 senses the phospholipid composition of Golgi membranes and functions in the maintenance of proper composition of these membranes. This hypothesis also supposes that this is how Sec14 mediates secretion in yeast, because phospholipid composition is proposed as a critical determinant of Golgi secretory competence (73, 74).

The specific role that Sec14 has in secretion from the Golgi was investigated by generating suppressor mutations that are able to rescue temperature sensitive *sec14* mutants. *SAC1* encodes a phosphatase that hydrolyzes PI4P and some other PIPs. *sac1-22* is a full length but non-functional mutant of *SAC1* (75). *sac1-22* led to the accumulation of PI4P and was a suppressor mutation that rescued cells containing mutated non-functional *sec14* when inositol was provided in the media (75). This indicated that PI4P may be limited in cells having mutant *sec14* causing the observed secretory defects. This hypothesis was tested by measuring PI4P levels in the *sec14-3* mutant and by measuring the growth of mutant *sec14* cells carrying a plasmid for different PI kinases at normally non-permissive temperatures. This mutant is sometimes referred to as CTY1-1A and the genotype is *MATa ura3-52 Δhis3-200 lys2-801(*Am*) sec14-1(*Ts*)* (76). The *sec14-1*^{ts} mutation is a missense mutation that disrupts the T_5 helix (77). *sec14-3* mutants had decreased levels of PI4P and cells overexpressing *PIK1*, but not *STT4* (the other yeast PI4K gene) or *VPS34* (the yeast PI3K gene), could grow at an otherwise non-permissive temperature. Furthermore, two *pik1*^{ts} mutants both experienced an ~60% drop in PI4P level within 1h of growth at the restrictive temperature. A drop in the secretion of invertase was also observed; however, no change was seen in the maturation of the vacuolar enzyme carboxypeptidase Y. Overall, three conclusions were made from all these experiments. The first was that PI4P is limited in cells with mutant *sec14* and that this is a major factor in the secretory defect. The second was that *in vivo* function of Sec14 is coupled to the activity of Pik1. The final conclusion was that PI4P plays an important role in secretion between the Golgi and the plasma membrane (1).

PI(4)P and the other PIPs are involved in distinct outcomes in a cell, even sometimes when the PIP is produced by the same PI kinase (64). This suggests that additional layers of functional specification exist in PIP signaling (64). There is mounting evidence that PITPs are involved in PI kinase pathways and that they contribute

to the functional specification in PIP signaling (64). For example, both Sec14 and Sfh3 have been shown to influence the production of PI(4)P by Pik1. Sec14 regulates the activity of Pik1 in a pathway controlling the TGN and endosomal trafficking (1). Sfh3 stimulates PI(4)P production by Pik1 in modulation of the consumption of lipid droplets (78). Sfh2 and Sfh5 activate phospholipase D (PLD) by stimulating $PI(4,5)P_2$ synthesis in a way that is coupled to Stt4 (79). Sfh5 also works with Mss4 to facilitate Cdc42 activation and regulate both actin and protein trafficking (80). Overall, the genetic and biochemical data do not indicate that Sfh proteins stimulate PIP production directly, rather the evidence supports that they regulate the delivery of PI to the kinase (77) and that their involvement contributes to the signaling outcome of the PIP produced. PITPs are likely key players in PIP homeostasis.

The crystal structure of *Sacharomyces cerevisiae* Sec14 (1AUA) was published in 1998 (81). High resolution crystal structures of the yeast Sec14 homolog Sfh1 with phosphatidylethanolamine, phosphatidylcholine, or phosphatidylinositol were determined in 2008 (3B74, 3B7N, 3B7Q, 3B7Z) (64). From these structures, and from various genetic experiments, Bankaitis and colleagues made 5 conclusions (64). First, Sfh1/Sec14 bind PC and PI differently. Sfh1 binds PC or PI one phospholipid at a time in its hydrophobic cavity; however, the headgroup of PC is sequestered deep in the binding cavity, while the headgroup of PI is coordinated near but beneath the protein surface (Figure 16) (64). Second, the capacity of Sec14 to bind PC and PI is required for Sec14 to fulfill its essential *in vivo* roles. Three types of *sec14* mutants were made: pinch mutants (obstructed the acyl-chain space in the hydrophobic cavity), non-PI-binding mutants (exhibit steric or electrostatic incompatibility with PI phosphate binding), and non-PC-binding mutants (exhibited inability to coordinate PC headgroup). These mutants were studied using a variety of functional assays that investigated the complementation of $sec14\text{-}1^{ts}$ or employed plasmid shuffle assays. Pinch mutants were defective in all functional assays, non-PC-binding mutants were also defective, and the non-PI-binding mutants showed that PI binding is an essential event in Sec14 activity. Further experiments with mixed *in vivo* populations of non-PI-binding and non-PC-binding mutants provide evidence that the PI and PC binding activities must be in *cis* (on the same Sec14) (64). This led to the third conclusion, that Sec14 must have both PI and

PC binding activities on the same Sec14 molecule for biological activity (64). The fourth conclusion was that PI and PC binding are both required for Sec14-mediated regulation of PIP homeostasis. Non-PI-binding and non-PC-binding *sec14* mutants were expressed individually in a yeast strain that has only basal PIP levels; neither type of mutant was capable of restoring wild-type PIP profiles *in vivo* (64). The fifth conclusion was that the Kes1 oxysterol-binding protein (also known as Osh4) that antagonizes Pik1 kinase action is countered by Sec14-mediated regulation of PIP synthesis (64). Pik1 generates the PI4P in the Golgi that is required for efficient secretory trafficking from the Golgi to the plasma membrane, and Sec14 increases this kinase activity *in vivo*. Kes1 deficiencies create "bypass Sec14" and partial rescue of $pik1^{ts}$ alleles, providing evidence that Kes1 antagonizes the Sec14 pathway. Kes1 retrieves and removes PI(4)P as it delivers sterols to the Golgi, therefore Kes1 deficiencies would cause high PI(4)P levels in the Golgi therefore compensating for the *sec14* and *pik1* mutants and antagonizing the Sec14 pathway (82, 83).

1.4 Lipid Kinase Assays

A variety of methods have been developed to assay the activity of lipid kinases. These include radioactivity (84), bioluminescent (85–87), and electrochemical (88) based assays. Due to the sensitive and reliable nature of radioactive assays, they are commonly used to measure lipid kinase activity (2, 84, 89–92). However, the use of radioactive compounds is undesirable and labour intensive. In addition, these methods are not time resolved, and as a result kinetic data on kinase activity cannot easily be obtained. The standard approach of these existing assays is to measure the signal under standardized conditions at a single arbitrary time point. This is sufficient to measure the effect of inhibitors on the activity but does not reveal information on how the signal evolved to the point where it was measured. Therefore, a change in the conditions (a change in the phospholipid composition, the presence of an inhibitor, or the presence of a protein that may cooperate or impede kinase activity) may change the rate at which the kinase phosphorylates and therefore the rate at which the signal evolves, but this change could be invisible to the single time point assay methods (as seen in Figure 17). Therefore, a time resolved assay for the activity of a lipid kinase is more valuable for probing the activity and the mechanism of the kinase and its accessory and regulatory proteins.

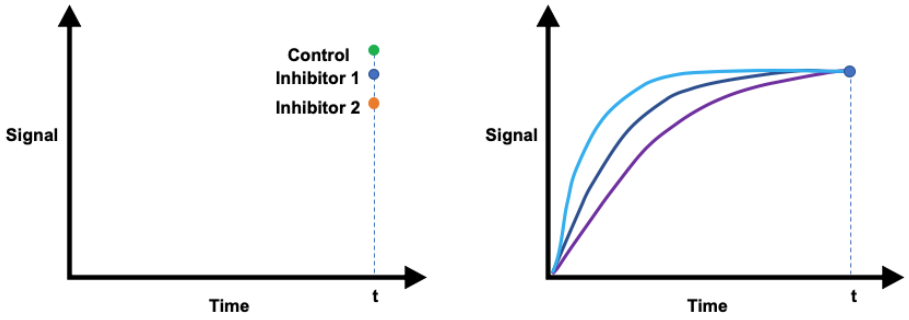

Figure 17: Arbitrary single time-point vs. time-resolved assays. Current available assays, including the Bellbrook Transcreener® ADP^2 FI Assay, are designed for end-point read-out, which is insufficient for measuring initial rates.

Many of the previously used lipid kinase assays use lipid substrates that are solubilized by detergents (2, 9, 50, 92). Therefore, the lipid substrates are soluble, likely in mixed micelles, and readily available to the kinase, but do not reside in a more appropriate model of biological membranes, such as vesicles. The goal of this project was to develop a lipid kinase assay to probe the presentation mechanism by which Sec14 is proposed to stimulate the activity of Pik1. If this presentation mechanism is correct

(*i.e.*, if Pik1 is not able to efficiently phosphorylate PI while PI is in the phospholipid bilayer, and therefore it needs Sec14 to present PI as a more suitable substrate) than using detergent micelles/detergent solubilized lipids as the substrate would abolish the need for Sec14 and it would be impossible to probe this mechanism. Therefore, it was imperative to design an assay that used phospholipid vesicles as the lipid substrates.

Sensitivity and ease of use are important factors in assay development. The assay that was developed in this project was a modification of Bellbrook Labs Transcreener® ADP² FI Assay. This kit can provide a high throughput screening assay platform with a simple fluorescence intensity (FI) readout. It is a simple, one-step homogenous detection assay that measures the production of ADP (Figure 18). The detection method employs an ADP² monoclonal antibody that is conjugated to an IRDye® QC-1 quencher and an ADP Alexa Fluor® 594 Tracer as the fluorophore. When the antibody-quencher conjugate is bound to the ADP Alexa Fluor® 594 Tracer the fluorescence is quenched. Then, as the enzyme produces ADP, the ADP displaces the ADP Alexa Fluor® 594 Tracer from the antibody-quencher conjugate. When the ADP Alexa Fluor® 594 Tracer is released, the fluorescence quenching is diminished and an increase in fluorescence intensity is measured. The increase in fluorescence is therefore proportional to the production of ADP. This commercial kit is designed for end-point reading and it was used to develop a time-resolved assay (93).

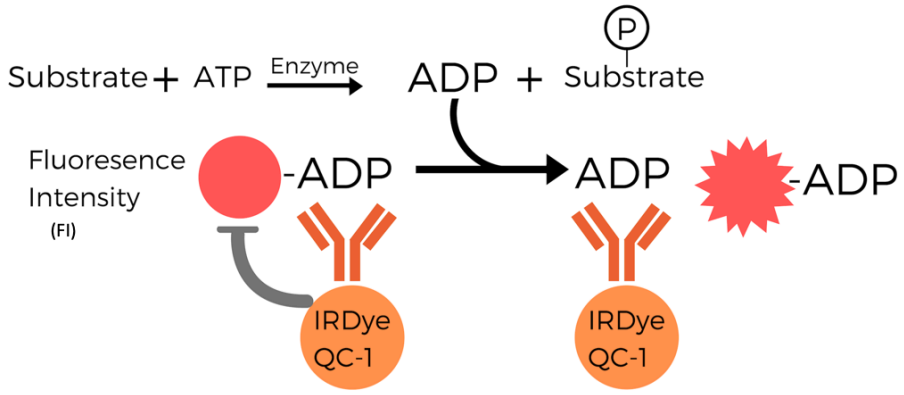

Figure 18: Schematic of the Transcreener® ADP² FI Assay. A commercial one-step homogenous detection assay designed to measure the production of ADP by any ADP-producing enzyme. FI: fluorescence intensity. Quenched ADP Alexa Fluor® 594 Tracer (red circle). IRDye QC-1: quencher (orange circle). ADP² Antibody-IRDye®QC-1: ADP antibody conjugated to quencher (orange antibody-dye conjugate). Free ADP Alexa Fluor® 594 Tracer (red star).

1.5 Purpose of the Project

There is genetic evidence and structural evidence for the presentation model that was outlined in Section 1.3.2, but there is no direct kinetic evidence. In this presentation model, Sec14 is proposed to mediate heterotypic exchange, binding both PI and PC, and during this exchange PI is presented to Pik1 making it a better substrate for phosphorylation. This thesis initiates work to test this proposed action of Sec14 on stimulating the production of PI(4)P by Pik1. This will require the lipid kinase activity of Pik1 to be measured in the presence and absence of Sec14, and with different substrates and conditions, *etc*. to probe this mechanism. The purpose of this project was to adapt the Bellbrook Labs Transcreener® ADP^2 FI Assay into a time-resolved and vesicle-based assay to measure the lipid kinase activity of Pik1.

2 Materials

2.1 Chemicals and Stock Solutions

2.2 DNA and Vectors

The cDNA for *CDC37* (YDR168W), *FRQ1* (YDR373W), and *PIK1* (YNL267W) were purchased in BG1805 from GE Dharmacon (94); BG1805 was developed by Eric Phizicky (University of Rochester) and Mike Snyder (Yale University).
CDC37 and *FRQ1* were cloned into the high copy number plasmid pESC-Trp (Agilent #217453 (95)) by Candace Panagabko (Brock University). pESC-Trp was received as a gift curtesy of Vince Qu (Brock University).
The low copy number plasmids pINIT_cat (Addgene plasmid #46858) and pYEXC3H (Addgene plasmid #49026) were purchased from Addgene, courtesy of Eric Geertsma (Goethe University) and Raimund Dutzler (University of Zurich), for the cloning and expression of *PIK1*. The cloning was done by Candace Panagabko.

2.3 Yeast and Bacterial Strains

Yeast: BJ2168 *Saccharomyces cerevisiae* was cultured for protein expression

MATa, ura3-52, trp1-289, leu2-3, 112, prb1-1122, prc1-407, pep4-3

B8NA: transformed BJ2168 with clone 8 (pYEXC3H+*PIK1*) and clone N (pESC-Trp+*FRQ1*+*CDC37*) at the same time, colony A

B8ND: transformed BJ2168 with clone 8 (pYEXC3H+*PIK1*) and clone N (pESC-Trp+*FRQ1*+*CDC37*) at the same time, colony D

10NE: transformed BJ2168 with clone 10 (pYEXC3H+*PIK1*) and clone N (pESC-Trp+*FRQ1*+*CDC37*) sequentially, colony E

B10NC: transformed BJ2168 with clone 10 (pYEXC3H+*PIK1*) and clone N (pESC-Trp+*FRQ1*+*CDC37*) at the same time, colony C

pVEX: BJ2168 transformed with empty pYEXC3H and pESC-Trp vectors

Naming Explanation:

B: transformed BJ2168 with both vectors (pYEXC3H+*PIK1* and pESC-Trp+*FRQ1*+*CDC37*) at the same time, no B means sequentially transformed

8 and 10: aka SC8 and SC10, SC= sub cloning and 8 and 10 refer to successful clone of

PIK1

*SC8 and SC10 were the bacterial colonies from which the DNA was sent for sequencing for carrying pYEXC3H with *PIK1*

N: successful clone of pESC-Trp with *FRQ1* and *CDC37*

A or C: colony "#"

NEB stable cells were the bacteria that were used for cloning and propagation. The propagation was done by plate. It was noted that the Pik1 expression plasmid was toxic to the bacteria.

2.4 Buffers, Solutions, and Media

2.4.1 Yeast Media

All yeast media was made with reverse osmosis (RO) H_2O and autoclaved (Panasonic MLS-3751L) using the liquid sterilization program (1-1: 121°C, 30min)

YPAD Plates (Yeast extract, Peptone, Adenine, Dextrose): 2.5g yeast extract, 5g peptone, 10mg adenine sulfate, 5g dextrose, 5g agar, 1 pellet NaOH (~50mg), dissolved in 250mL RO H_2O, autoclaved, poured plates

YPAD (Yeast extract, Peptone, Adenine, Dextrose): 2.5g yeast extract, 5g peptone, 10mg adenine sulfate, 5g dextrose, dissolved in 250mL RO H_2O, autoclaved

SCAT (Selective Complete, Adenine, Tryptophan): 1.74g/L yeast nitrogen base, 20g/L dextrose, 0.080g/L adenine sulfate, 0.040g/L tryptophan, 5g/L ammonium sulfate, 2g/L tryptophan dropout powder

SCUTA (Selective Complete, Ura^-Trp^- dropout, Adenine): 1.74g/L yeast nitrogen base, 5g/L ammonium sulfate, *sugar, 0.72g/L Trp^- Ura^- dropout powder, 0.08g/L adenine sulfate

*sugar:

SCUTA: no sugar

SCUTAD: 2% Dextrose – autoclaved as SCUTAD, or the components to make 100mL of SCUTA were weighed, dissolved in 95mL RO H_2O, and autoclaved, then 5mL of 20x dextrose stock was added to the 95mL of SCUTA to dilute to 100mL before use

SCUTAR: 2% Raffinose – autoclaved as SCUTA that was not completely diluted, then the appropriate volume of sterile raffinose stock was added after it

was autoclaved to produce the full volume and correct concentration of all components. The solution was autoclaved as SCUTA that was diluted to 95mL instead of all the way to 100mL and 6.9mL of 29% raffinose stock was added to 95mL of not fully diluted SCUTA before used (~100mL SCUTAR flasks). The solution was autoclaved as 93mL/100mL SCUTA and 7mL of 29% Raffinose was added before used (100mL SCUTAR flasks). The solution was autoclaved as 460mL SCUTA and 40mL of 25% Raffinose was added before used (500mL SCUTAR flasks).

SCUTAD Plates (Selective Complete, Ura^-Trp^- dropout, Adenine, Dextrose): 1.74g/L yeast nitrogen base, 5g/L ammonium sulfate, 20g/L dextrose (2%), 0.72g/L $Trp^- Ura^-$ dropout powder, 0.08g/L adenine sulfate, 20g/L agar (2%), pinch NaOH

SCUTAGE Plates (Selective Complete, $Ura^- Trp^-$ dropout, Adenine, Glycerol, Ethanol): 1.74g/L yeast nitrogen base, 5g/L ammonium sulfate, 0.720g/L $Ura^- Trp^-$ dropout powder, 0.08g/L adenine sulfate, 26g/L glycerol (~20.8mL), 22g/L agar, 27.5mL 95% ethanol

All ingredients except 95% ethanol were dissolved in RO H_2O, and the pH was adjusted to 5.5. The solution was diluted to 970mL and autoclaved, then 27.5mL 95% ethanol was added, the solution was mixed, and immediately poured into plates.

3xYEPG (Yeast Extract, Peptone, Galactose): 6% peptone, 3% yeast extract, 6% galactose. For 200mL 3x YEPG: 12g peptone, 6g yeast extract, 12g galactose dissolved in 200mL of RO H_2O.

2.4.2 Yeast Protein Extraction for SDS-PAGE

Lysis Buffer: 0.1M NaOH, 0.05M ethylenediaminetetraacetic acid (EDTA), 2% SDS, 2% β-mercaptoethanol (200mg NaOH, 730.6mg EDTA, 1000mg SDS, 895µL β-mercaptoethanol in 50mL RO H_2O)

Loading Buffer: 0.25M Tris-HCl pH 6.8, 50% Glycerol, 0.05% Bromophenol blue

Resolving Gel (10%): 3.8mL RO H_2O, 2mL 1.5M Tris-HCl pH 8.8, 2mL Acrylamide/ Bis-Acrylamide (37.5:1) 40% solution, 80µL 10% SDS, were all mixed then 80µL of

10% ammonium persulfate (APS) and 8μL of TEMED were added immediately before casting. This recipe makes two gels.

Stacking Gel (6%): 2.9mL RO H_2O, 1.25mL 0.5M Tris-HCl pH 6.8, 0.75mL Acrylamide/Bis-Acrylamide (37.5:1) 40% solution, 50μL 10% SDS, were all mixed then 50μL of 10% APS and 5μL of TEMED were added immediately before casting. This recipe makes two gels.

10x SDS-PAGE Running Buffer: 250mM Tris-HCl (pH 8.3), 1.92M Glycine, 1% SDS. 1L of 10x SDS-PAGE running buffer was made and stored at room temperature. The 10x solution was diluted to 1x (100mL 10x solution diluted to 1000mL) before it was used. The 1x SDS-PAGE running buffer was also stored at room temperature.

2.4.3 Glass Bead Lysis

Extraction Buffer (pH 8): 25mM Tris-HCl, 10mM $MgCl_2$, 10% glycerol, 150mM NaCl, 2mM β-mercaptoethanol, 0.5% Triton X-100.

One protease inhibitor tablet (cOmplete ULTRA Tablets, Mini, EDTA-free, EASYpack)/20mL of extraction buffer was added immediately before it was used in the extraction protocol. After the cells were resuspended in extraction buffer, 3μL of DNase (1000 units) and 50μL of 10mg/mL RNase were added to the extraction mixture.

2.4.4 IMAC Co^{2+} Affinity Chromatography

IMAC Resin Wash Solution: 50mM sodium acetate, 0.3M NaCl, pH 4.0

Co^{2+} IMAC Charging Solution: 0.2M $CoCl_2$

Buffer A (no imidazole): 25mM Tris-HCl, 300mM NaCl, pH 8

Buffer B (max imidazole): 25mM Tris-HCl, 300mM NaCl, 300mM or 500mM imidazole, pH 8

Co^{2+} Stripping Buffer: 1.5g sodium phosphate dibasic, 3.5g NaCl, 30g EDTA, pH 7.5, diluted to 200mL (All components did not dissolve until the solution was pH > 7)

2.5 Bellbrook Labs Transcreener® ADP² FI Assay

2.5.1 Materials Provided

ADP² Antibody-IRDye® QC-1: 1.4mg/mL solution in 100mM KH_2PO_4 (pH 8.5)

ADP Alexa Fluor® 594 Tracer: 800nM solution in 2mM HEPES (pH 7.5) containing 0.01% Brij-35

Stop and Detect Buffer B, 10x: 200mM HEPES (pH 7.5), 400mM EDTA, and 0.2% Brij-35

ATP: 5mM ATP, **ADP**: 5mM ADP

2.5.2 Assay Buffers and Solutions

Note: all solutions for the assay should be made with autoclaved mQH_2O

PKA Reconstitution Solution: 6mg/mL dithiothreitol (DTT), 10mM $MgCl_2 \bullet 6H_2O$

PKA Assay and Detect Buffer, 10x: 1000mM HEPES (pH 7.5), 0.2% Brij-35

Lipid Dilution Buffer, 2.5x: 62.5mM HEPES (pH 7.5), 1.25mM ethylene glycol-bis(β-aminoethyl ether)-N,N,N′,N′-tetraacetic acid (EGTA), sterile filtered then stored at -20°C

PIK3C3 Assay Buffer, 10x: 250mM HEPES (pH 7.5), 500mM NaCl, 30mM $MgCl_2$, 0.25mg/mL BSA, 50mM $MnCl_2$*

> * $MnCl_2$ was eventually omitted because it was causing precipitation problems with the KH_2PO_4 buffer which the antibody is dissolved in the Bellbrook kit

2.5.3 Enzymes and Substrates

Protein Kinase A catalytic subunit from bovine heart: purchased from Sigma-Aldrich (catalog number: P2645)

Casein from bovine milk: purchased from Sigma-Aldrich (catalog number C5890)

PIK3C3 (Vps34): purchased from Sigma-Aldrich as the active, GST, human PRECISIO® Kinase, recombinant (product number: SRP5306, lot number: Y1019-2). It was supplied in 50mM Tris-HCl (pH 7.5), 150mM NaCl, 10mM glutathione, 0.1mM EDTA, 0.25mM DTT, 0.1mM PMSF, and 25% glycerol.

L-*α*-Phosphatidylinositol (PI): Liver PI purchased from Avanti Polar Lipids

L-*α*-Phosphatidylserine (PS): Brain PS purchased from Avanti Polar Lipids

1,2-dioleoyl-*sn*-glycero-3-phosphocholine (DOPC): DOPC purchased from Avanti Polar Lipids

3 Methods

3.1 Creation of Pik1 Expression System

This procedure was written and performed by Candace Panagabko (Brock University). Unless otherwise stated, all materials were from New England Biolabs. This Pik1 expression system comprises 3 proteins: Pik1, Cdc37, and Frq1. Cdc37 is a molecular chaperone that assists in the correct folding of Pik1 (personal communication from Jeremy Thorner - University of California Berkeley) and Frq1 is the adaptor protein for Pik1 (3).

Yeast *FRQ1* and yeast *CDC37* genes were amplified from the cDNA clones from GE Dharmacon for insertion into the bidirectional yeast *E. coli* shuttle vector pESC-Trp vector. In *E. coli*, the vector confers ampicillin resistance whereas the vector enables growth of yeast in tryptophan deficient media. *FRQ1* was inserted under the control of the GAL10 promoter using EcoRI and NotI restriction sites to create a C-terminal FLAG-tag. *CDC37* was placed under the direction of the GAL1 promoter using BamHI and SalI creating a C-terminal c-myc fusion.

The yeast *PIK1* was cloned via the FX cloning system. Similar to the Gateway System (Invitrogen), the gene was cloned into an initial vector pINITIAL (pINIT) which can be a transition point for different expression hosts. The pINITIAL vector carried the chloramphenicol acetyltransferase (CAT) gene for selection on chloramphenicol media in *E. coli*. Primers for amplification were selected by the FX cloning website (http://www.fxcloning.org/) which appends SapI restriction sites to the gene without its start or stop codons. The pINIT-CAT vector also contains the ccdB gene that encodes transcriptional repressor of the ccdAB operon. Expression of the gene promotes cell survival of plasmid containing cells. The ccdB gene binds to DNA gyrase resulting in destruction of plasmid DNA. Thus, the pINIT-CAT vector was supplied in a DNA gyrase mutant *E. coli* strain DB3.1. Cloning of a gene into the pINIT-CAT vector disrupts the ccdB gene. Therefore, only cells containing recombinant plasmids should survive when the ligation mix is transformed into a ccdB susceptible *E. coli* strain.

For yeast expression, *PIK1* was subcloned from the pINIT-CAT–*PIK1* clone into pYEXC3H for creation of a C-terminal 10xHis-tag cleavable by PreScission protease (Human Rhinovirus 3C protease). The pYEXC3H vector carried both the CAT gene and the β-lactamase gene for ampicillin and chloramphenicol resistance in addition to the *B. subtilis* sacB gene. The sacB gene metabolizes sucrose to levan, leading to accumulation of levan within the periplasmic space and death of the cell. Sub-cloning of *PIK1* interrupted the sacB gene allowing selection of transformants by plating on ampicillin and 7% sucrose containing media. The pYEXC3H vector also carries the *URA3* gene for selection in uracil deficient media.

All genes for cloning were amplified by Pfu or Q5 polymerases. Plasmids were transformed into NEB Stable chemically competent cells following the manufacturer's instructions. Colony PCR using One Taq DNA polymerase enabled transformant selection for all three genes. DNA from successful transformants was recovered easily for pINIT-CAT-*PIK1* and pESC-Trp-*FRQ1-CDC37*. Despite pYEXC3H being a yeast expression vector, the *PIK1*-pYEXC3H clones appeared toxic to *E. coli* suggesting recognition by the bacterial transcriptional machinery. As such, upon identification of the clones, the cells were propagated solely on solid media (plates) at room temperature as transfer to liquid media or higher temperature led to loss of the *PIK1* gene. Clones from pESC-Trp-*FRQ1-CDC37* (clone N), pINIT-CAT-*PIK1* (clone 8) and pYEXC3H-*PIK1* (clones 8 and 10) were verified by sequencing.

Yeast cells (BJ2168) were transformed with the clones (*FRQ1-CDC37* (clone N) and *PIK1* clones (8 and 10)) either successively (N-series - *e.g.,* 10NE) or concurrently (B-N series - *e.g.,* B8NA) using lithium acetate for plating on selective complete media lacking both uracil and tryptophan. The presence of both plasmids in the yeast colonies was verified by colony PCR.

3.2 Growth Curves

3.2.1 Inoculation and Protein Expression

B8NA (transformed BJ2168 with clone 8 (pYEXC3H+PIK1) and clone N (pESC-Trp+FRQ1+CDC37) at the same time, colony A), and/or 10NE (transformed BJ2168 with clone 10 (pYEXC3H+PIK1) and clone N (pESC-Trp+FRQ1+CDC37) sequentially, colony E) were re-plated onto a fresh SCUTAD plate then placed in a static incubator (Thermo Electron Corporation REVCO or VWR Gravity Convection General Incubator) at 26°C for approximately 3 days. The cells did not grow as quickly from older plates; therefore, it was decided to always inoculate liquid cultures from plates that were less than 1 week old. SCUTAD pre-culture tubes (5 or 10mL) were inoculated from the plate with an inoculation loop in the presence of a flame. The pre-culture tubes were grown for at least 24h in a shaking incubator (New Brunswick Scientific I 26 Incubator Shaker Series or New Brunswick Scientific Series 25 Incubator Shaker) at 26°C and 300 RPM (Note: 30°C, and 220 RPM, 250 RPM, 260 RPM, and 310 RPM were also tried). The pre-culture tubes were poured into SCUTAR culture flasks (one 5mL pre-culture tube/100mL culture or two 10mL pre-culture tubes/500mL culture), which were subsequently placed in a shaking incubator for at least 24h at 26°C and 300 RPM. Optical density (OD) measurements were recorded at various time points to monitor cell growth. Galactose (2g of galactose/500mL culture) was used to induce expression and it was added at an OD between 1 and 3. Galactose was measured onto a piece of autoclaved tin foil using an autoclaved scoopula (however, sterile technique could not be used because of the balance). The solid galactose was added to the culture flask and was dissolved by swirling. A second induction method was also tested: 50mL of 3x YEPG were added to 100mL of culture at an OD of ~2. YEPG is a non-selective media that contains yeast extract, peptone, and galactose. The culture flasks were grown at 26°C and 300 RPM for at least 24h following the addition of galactose as a solid or in YEPG. OD measurements were taken at various time points to monitor growth. One of the times that this inoculation method was tested, a sample was taken approximately 24h post-induction and was used to inoculate a plate of SCUTAD, a selective medium. The plate was grown at 26°C for approximately 32h. This procedure was performed to check for plasmid loss or retention. Visually there appeared to be the same amount of growth, (*i.e.,*

the plasmid appeared stable). This small test was carried out by Candace Panagabko (Brock University).

3.2.2 Sample Harvesting

Optical density measurements, and in certain cases cell counts, were measured at different time points before and after induction to monitor the growth of the yeast. The time that the sample was taken from the flask was recorded along with each cell count and/or OD. The OD measurements and the cell counts could not be performed using sterile conditions; however, the sample was removed from the culture tube or flask in the presence of a flame, thus preventing contamination of the culture tube or flask. After the measurement was taken, the contents of the cuvette were transferred to an Eppendorf tube, placed in a microcentrifuge (ThermoIEC Micromax), and centrifuged at 14,000 RPM for 7 min. The media was decanted with a pipette into a waste beaker to be bleached and the Eppendorf tube with the cell pellet was stored at -20°C.

3.2.3 Optical Density Measurements

Optical density (OD) measurements were taken to monitor growth. All of the OD measurements were measured at 600nm and the instrument (Thermo Scientific GENESYS 10S UV-Vis) was blanked using uninoculated media that matched the media of the sample being measured. The culture tube or flask was mixed to agitate any settled cells before the sample volume was taken. A 1mL sample was taken to measure the OD, unless the OD was (or was suspected to be) 1 or greater; in this case, a smaller sample was taken and diluted with media to 1mL. A 1:5 dilution was the most common, in which 200µL of culture was taken and diluted with 800µL of the appropriate media. The cuvettes were covered with parafilm, inverted multiple times, and the sides wiped with a Kimwipe prior to insertion into the instrument. The OD was measured and multiplied by the appropriate factor (5 for a 1:5 dilution) to obtain the OD of the culture tube or flask.

3.2.4 Correlating OD to an Approximate Cell Count

To correlate OD to an approximate cell count, both measurements were made at each time point during the first 7h of the first growth curve that was completed. Untransformed BJ2168 was grown in YPAD at 26°C and 260RPM. A 1mL sample of

culture was taken every 1-2 h for approximately 11 h on the first day and samples and OD measurements were carried out at various time points during the subsequent 3 days. During the first 7 h of the first day, both OD measurements and cell counts were carried out. After the OD was measured, 10μL of the sample was taken from the cuvette, pipetted onto a hemocytometer, and a cover slip was added. The cells were counted using a microscope (Zeiss ID 03) under 10x magnification. The number of cells/mL was determined by taking the average of the cell count total from each set of 16 corner squares (one set of 16 corner squares is boxed in blue in Figure 19) and multiplying it by 10^4. This growth curve was conducted before it was known that the sample should be diluted if the OD was greater than 1, therefore no dilutions were made except the last two measurements. The approximate number of cells was determined using the OD prior to centrifugation and the average number of cells per mL per OD unit was determined to be 9.02×10^7 cells/mL/OD unit.

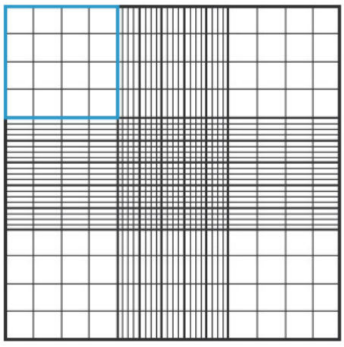

Figure 19: Hemocytometer gridlines. The blue box designates one of four sets of 16 corner squares that were used for counting. Figure reproduced from (96).

3.2.5 Specific Conditions of the Growth Curve Experiments

The specific conditions for each of the growth curve experiments can be seen in Table 3. The experiments are organized based on purpose and conditions. The purpose of the first set was to establish baseline/normal growth in rich and selective media. The purpose of the second set of experiments was to establish how temperature and agitation influence growth. The purpose of the third set was to investigate the effect on growth upon inducing with solid galactose at different ODs. The fourth, fifth, and sixth sets include experiments that used SCUTAD* (0.2% dextrose) instead of SCUTAD (2% dextrose) as the pre-culture medium. The fourth set studied the impact of the carbon

source on growth and compared growth in dextrose *verses* raffinose containing media. The fifth and sixth sets investigated growth related to induction by solid galactose and YEPG respectively.

Table 3: The details for the growth experiments with different transformants, media, carbon sources, and induction methods. BJ2168: untransformed yeast strain, pVEX: BJ2168 transformed with both empty vectors, B8NA: a transformant of BJ2168 in which the cells were transformed with both vectors at the same time (transformed BJ2168 with clone 8 (pYEXC3H+PIK1) and clone N (pESC-Trp+FRQ1+CDC37) at the same time, colony A). 10NE: a transformant of BJ2168 in which the cells were sequentially transformed with each vector (transformed BJ2168 with clone 10 (pYEXC3H+PIK1) and clone N (pESC-Trp+FRQ1+CDC37) sequentially, colony E).

Growth Curve	Cell	Media, Temperature, RPM, Culture Volume		
		Plate	Pre-Culture	Culture Tube or Flask
BJ2168 in SCAT	BJ2168	YPAD 26°C	SCAT 26°C 310 RPM 5mL	SCAT 26°C 310 RPM 5mL pre-culture into 50mL in 250mL flask
pVEX in SCUTAD	pVEX	SCUTAD 26°C	SCUTAD 26°C 310 RPM 5mL	SCUTAD 26°C 310 RPM 5mL pre-culture into 50mL in 250mL flask
Growth Condition Test: 26°C, 250 RPM	BJ2168	YPAD 26°C	SCAT 26°C 250 RPM Overnight 5mL	SCAT 26°C 250 RPM 24 hours 500µL used to inoculate culture tube (5mL)
Growth Condition Test: 30°C, 250 RPM	BJ2168	YPAD 26°C	Used pre-culture from above	SCAT 30°C 250 RPM 24 hours 500µL used to inoculate culture tube (5mL)
Growth Condition Test: 26°C, 220 RPM	BJ2168	YPAD 26°C	Used pre-culture from above	SCAT 26°C 220 RPM 500µL used to inoculate culture tube (5mL)

Table 3: continued

Growth Curve	Cell	Media, Temperature, RPM, Culture Volume		
		Plate	Pre-Culture	Culture Tube or Flask
B8NA Non-Induced	B8NA	SCUTAD 26°C	SCUTAD 26°C 300 RPM Overnight (~24h) 5mL	SCUTAR 26°C 300 RPM Whole 5mL pre-culture used to inoculate 100mL culture in 500mL flask
B8NA Induced OD ~2 with solid Gal	B8NA	SCUTAD 26°C	SCUTAD 26°C 300 RPM Overnight (~24h) 5mL	SCUTAR 26°C 300 RPM Whole 5mL pre-culture used to inoculate 100mL culture in 500mL flask
B8NA Induced OD ~3 with solid Gal	B8NA	SCUTAD 26°C	SCUTAD 26°C 300 RPM Overnight (~24h) 5mL	SCUTAR 26°C 300 RPM Whole 5mL pre-culture used to inoculate 100mL culture in 500mL flask
B8NA Induced OD~2 with solid Gal	B8NA	SCUTAD 26°C	SCUTAD 26°C 300 RPM Overnight (~24h) 5mL	SCUTAR 26°C 300 RPM Whole 5mL pre-culture used to inoculate 100mL culture in 500mL flask
pVEX in SCUTAR (SCUTAD* pre-culture)	pVEX	SCUTAD 26°C	SCUTAD* 26°C 300 RPM Overnight 5mL	SCUTAR 26°C 300 RPM Whole 5mL pre-culture used to inoculate ~100mL culture in 500mL flask
B8NA in SCUTAD (SCUTAD* pre-culture)	B8NA	SCUTAD 26°C	SCUTAD* 26°C 300 RPM Overnight 5mL	SCUTAD 26°C 300 RPM Whole 5mL pre-culture used to inoculate ~100mL culture in 500mL flask
B8NA in SCUTAR (SCUTAD* pre-culture)	B8NA	SCUTAD 26°C	SCUTAD* 26°C 300 RPM Overnight 5mL	SCUTAR 26°C 300 RPM Whole 5mL pre-culture used to inoculate ~100mL culture in 500mL flask

Table 3: continued

Growth Curve	Cell	Media, Temperature, RPM, Culture Volume		
		Plate	Pre-Culture	Culture Tube or Flask
10NE in SCUTAD	10NE	SCUTAD 26°C	SCUTAD 26°C 300 RPM Overnight 5mL	SCUTAD 26°C 300 RPM 1mL of pre-culture used to inoculate ~100mL culture in 500mL flask
10NE in SCUTAR	10NE	SCUTAD 26°C	SCUTAD 26°C 300 RPM Overnight 5mL	SCUTAR 26°C 300 RPM 1mL of pre-culture used to inoculate ~100mL culture in 500mL flask
B8NA Induced OD ~1.5 with solid Gal	B8NA	SCUTAD 26°C	SCUTAD* 26°C 300 RPM Overnight 5mL	SCUTAR 26°C 300 RPM Whole 5mL pre-culture used to inoculate 100mL culture in 500mL flask
B8NA Induced OD ~2 with solid Gal	B8NA	Same plate as above	SCUTAD* 26°C 300 RPM Overnight 5mL	SCUTAR 26°C 300 RPM Whole 5mL pre-culture used to inoculate 100mL culture in 500mL flask
B8NA Induced OD ~2 with YEPG	B8NA	Same plate at 6a	SCUTAD* 26°C 300 RPM Overnight 5mL	SCUTAR 26°C 300 RPM Whole 5mL pre-culture used to inoculate 100mL culture in 500mL flask
10NE Induced OD ~2 with YEPG	10NE	SCUTAD 26°C	SCUTAD* 26°C 300 RPM Overnight 5mL	SCUTAR 26°C 300 RPM Whole 5mL pre-culture used to inoculate 100mL culture in 500mL flask

3.3 Yeast Protein Extraction for SDS-PAGE

3.3.1 SDS-PAGE Sample Preparation

This method was based on the one outlined by von der Haar (97). A pellet of ~10^8 yeast cells was resuspended in 200µL of lysis buffer and the mixture was vortexed then placed in a 90°C water bath for 10min. Acetic acid (5µL, 4M) was added, the mixture was vortexed for ~30s, and then placed in a 90°C water bath for an additional 10min. In an attempt to increase the extraction of high molecular weight proteins, the two 10min incubations were lengthened to two 18min incubations for some samples. Loading buffer (50µL) was added, and the mixture was vortexed. The volumes of each step were scaled up accordingly for pellets with a greater number of cells. The approximate number of cells was determined using the OD prior to centrifugation and average number of cells per mL per OD unit determined to be 9.02 x 10^7 cells/mL/OD unit. The prepared samples were stored at -20°C. After thawing, the samples were centrifuged at 5000rpm for 5min to clear the lysate prior to loading into the gel. (Note: This method of cell lysis was insufficient to extract proteins with molecular weights higher than approximately 95kDa, even when boiled for 18min. Some samples were also taken at various points in the process of the glass bead lysis protocol; this method was more effective at extracting protein especially proteins of higher molecular weights.)

Sample calculation for scale up:
Sample: B8NA OD1 Uninduced
Lysis Buffer:

$$OD = 1.495$$

$$1.495 \cdot \frac{9.0223 \cdot \frac{10^7 cells}{mL}}{OD\ unit} \cdot 1mL \cdot \frac{200\mu L}{1 \cdot 10^8 cells} = 269.8\mu L \approx 270\mu L$$

Therefore, the pellet was resuspended in 270µL of lysis buffer.

Acetic Acid:

$$270\mu L \cdot \frac{5\mu L}{200\mu L} = 6.75\mu L$$

Therefore, 6.75µL of 4M acetic acid was used.

Loading Dye:

$$270\mu L \cdot \frac{50\mu L}{200\mu L} = 67.5\mu L$$

Therefore, 67.5µL of loading dye was used.

3.3.2 Casting SDS-PAGE Gels (6% Stacking, 10% Resolving)

The resolving and the stacking buffers were prepared, and the pH was adjusted in 50mL Falcon® tubes. Two sets of plates were cleaned, wrapped in Parafilm®, assembled into the casting stand, and RO H_2O was added to check for leaks; the RO H_2O was then poured out, and the plates were patted dry with a Kimwipe®. The 10% resolving gel was prepared, the 10% APS and the TEMED were added right before casting, and two sets of plates were filled ¾ of the height of the plate with resolving gel. Isopropanol (200µL) was pipetted on top of the resolving gel to eliminate air bubbles, then the gel was left to polymerize on the counter for 30-40min. The isopropanol was poured out and the plates were patted dry with a Kimwipe®, then residual isopropanol was rinsed out with 3 rinses of RO H_2O, and the plates were patted dry with a Kimwipe®. The 6% stacking gel was prepared, the 10% APS and the TEMED were added right before casting, and the top portion of both sets of plates were filled with stacking gel. A comb was inserted such that there were no bubbles below the teeth and the gel was left to polymerize on the counter for 30-40min. The gels were wrapped in a damp paper towel, placed in a sealed plastic bag, and stored at 4°C until they were used.

3.3.3 SDS-PAGE

The SDS-PAGE gel was run at 120V for approximately 1h using a Bio-Rad Mini-PROTEAN® Tetra System. The gel was stained overnight with a mixture of 45mL of Protoblue Safe Colloidal stain and 10mL of absolute ethanol. The gel was de-stained with RO H_2O and imaged with a Bio-Rad Gel Doc® EZ Imager (white tray).

3.4 Glass Bead Lysis

3.4.1 Pellet Formation

Centrifuge bottles (250mL) were labelled, filled with cell culture, weighed, and balanced, and then centrifuged (Beckman Coulter Allegra X-30R Centrifuge) for 20min at 4700 RPM and 4°C using a SX 4400 rotor. Most of the media was removed and pooled in a beaker for bleaching; a small amount of media was left in the tubes to resuspend and combine the pellets. The combined pellet(s) were centrifuged (Beckman Coulter Allegra X-30R Centrifuge or Thermo Scientific Sorvall RC6+ Centrifuge) again for 20min at 4700 RPM and 4°C using the SX 4400 rotor or the F12-6x500 LEX rotor, depending on the sample size and the centrifuge used. The media supernatant was carefully poured off and the pellet was stored at -80°C.

3.4.2 Glass Bead Acid Wash

The glass beads were washed by soaking them for 1h in concentrated nitric acid. The beads were then rinsed thoroughly with water, autoclaved, and then dried in an oven at 100°C. The beads were cooled to room temperature, then stored at 4°C.

3.4.3 Yeast Cell Lysis

The yeast cell lysis was completed while the IMAC (Immobilized Metal Affinity Chromatography) resin was equilibrating with 0.2M $CoCl_2$ (see Preparation of the IMAC Resin). The TissueLyser (Qiagen TissueLyser II) Eppendorf tube holders were placed in the -80°C freezer to pre-cool. The protease inhibitor tablet was added to the extraction buffer (1 tablet/20mL of extraction buffer). The cell pellet was resuspended in just enough extraction buffer to get the consistency of an iced cappuccino (~1-2mL for a 15g pellet). DNase (3µL, 1000 units) and 50µL of 10mg/mL RNase were added to the suspension, which was then mixed, and aliquoted into Eppendorf tubes (1mL into each 2mL tube). Approximately 1mL of glass beads was added to each tube and the tubes were placed in the pre-cooled TissueLyser holders. The tubes were agitated for 6min at a frequency of 30.0 oscillations/s, then the holders containing the tubes were placed in the -80°C freezer to cool for 6min. The cycle of agitation and cooling was repeated 5 additional times. To ensure adequate lysis, two tubes were centrifuged at 13 800 RPM

for 3min at 4°C; additional rounds of beating and cooling would be needed if the supernatant was clear. The preparation of the IMAC resin was completed during the TissueLyser and the extraction buffer washing wait times.

The Eppendorf tubes were placed on ice, and the supernatants from each tube were decanted and pooled into a 50mL centrifuge tube. Extraction buffer (500µL) was added to each Eppendorf tube, the tube was vortexed, then the extraction buffer was decanted into the same thin centrifuge tube after the beads settled. The pooled lysate was centrifuged (Thermo Scientific Sorvall RC6+ Centrifuge) for 25min, at 17,500 RPM and 4°C, using rotor 521-8x-50y. The supernatant was carefully poured onto the prepared IMAC resin, and the Falcon® tube was placed on a rocker in the 4°C fridge overnight.

3.5 IMAC Co^{2+} Affinity Chromatography

3.5.1 Preparation of IMAC Resin

The resin was disrupted to form a slurry with the 20% EtOH that it was stored in and a graduated cylinder was used to measure 4mL of settled resin (settled volume of resin = column volume). The 20% EtOH was decanted, one column volume of IMAC Resin Wash Solution was added and used to make a slurry; the slurry was transferred to a 50mL Falcon® tube. This step was repeated until 5 column volumes had been used and all of the resin had been transferred to the 50mL Falcon® tube. The Falcon® tube was inverted ~10 times, then the IMAC Resin Wash Solution was decanted off. Four column volumes of 0.2M $CoCl_2$ was added to the Falcon tube and the tube was placed on a rocker in a 4°C fridge to equilibrate for at least 2 h. During this equilibration the yeast cells were lysed.

The Falcon® tube containing IMAC resin was retrieved from the 4°C fridge and was placed upright on the counter to allow the resin to settle. The 0.2M $CoCl_2$ solution was decanted off and was stored in a glass bottle at room temperature for reuse. The resin was washed twice each with 2.5 column volumes (5 column volumes total) of IMAC Resin Wash Solution (washed = added solution, inverted multiple times, settled, decanted). The resin was then washed twice each with 5 column volumes (10 column volumes total) with RO H_2O. The resin was then washed with at least 5 column volumes of extraction buffer or buffer A. After buffer A was decanted the resin was ready for the supernatant of the glass bead lysate.

3.5.2 Setting Up the FPLC Column

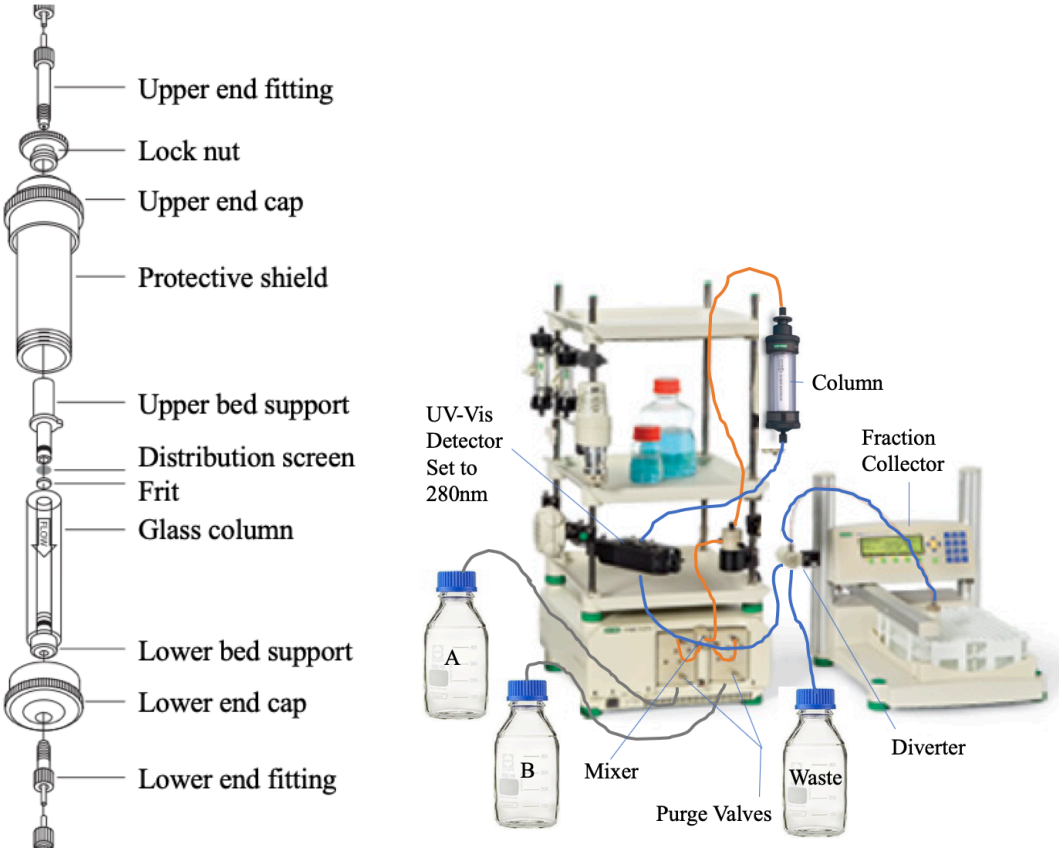

Figure 20: Diagram of the FPLC (Fast Protein Liquid Chromatography) set up. **A.** Column assembly. **B.** Column attachment. Images adapted from Bio-Rad user manuals.

The distribution screen, the frit, and the lower bed support were placed in the bottom of the glass column and the glass column was clamped to a retort stand with a beaker under it. The Co^{2+} loaded resin incubated with cell lysate from the previous day was poured into the glass column. Some lysate was allowed to flow through and drip into the beaker, but the level of liquid was kept above the resin. The flow through collected by the beaker was used to rinse all of the resin out of the Falcon® tube into the glass column. A pipette bulb was used to apply pressure to encourage the lysate to drip out until there was approximately 0.5cm of lysate left above the resin; this was to ensure the resin did not dry since the lysate continues to drip as the column was being assembled. The upper bed support was placed in the top of the glass column. Next the plastic protective shield was screwed into the lower end cap. Then the lock nut was

screwed into the upper end cap and this was placed on the top of the glass column such that the notch of the upper bed support matched the groove on the upper end cap. The glass column and the upper end cap were then assembled and screwed together with the protective shield and lower end cap until tight. If the lysate did not drip out of the bottom of the apparatus, this was an indication of an internal leak, and the apparatus was adjusted and tightened until the lysate properly dripped out of the bottom. The upper end fitting and the lower end fitting were screwed into the upper and lower end caps respectively. The lysate was allowed to drip out of the lower end fitting until the lysate level was only a few millimeters above the resin. The whole apparatus was then attached to the FPLC as seen in Figure 20.

3.5.3 Using the FPLC

The FPLC and the fraction collector were turned on, then the Bio-Logic Duo Flow program was opened on the computer. The system was washed with 70% EtOH, mQH_2O, and buffer A (no imidazole): Flow rate = 5mL/min, Inlet A= 50%, Inlet B=50%, Time = 3min, Pressure: high limit = 130psi, low limit = 1psi. Both lines A and B were in the same jar for all 3 washes and the lines were purged of air bubbles when switching between the jars of wash solutions. Lines A and B were set up and purged with buffer A (no imidazole) and buffer B (max imidazole) respectively. The column was attached to the system as seen in Figure 20. The desired FPLC protocol was run. The column was removed from the system and the 70% EtOH and mQH_2O wash steps were repeated. The program was closed then the FPLC and the fraction collector were turned off.

3.5.4 The FPLC Protocol

The first FPLC protocol that was attempted for the purification of the Pik1-Frq1 complex was a protocol that is standard in the Atkinson lab group for isolating a His-tagged version of the wtOSBP (wild type Oxysterol-binding protein 1) protein designed and standardized by Parthajit Mukherjee (Brock University). Solution A was the running buffer (25mM Tris-HCl, 300mM NaCl, pH = 8) and Solution B was the elution buffer (25mM Tris-HCl, 300mM NaCl, 300mM imidazole, pH = 8). This protocol can be seen in Table 4. However, no sample was detected by the UV-Vis detector that was monitoring the eluate during the elution step. Therefore, the column was subjected to a

second elution protocol that consisted of an elution gradient that went up to 100% of a 500mM imidazole Solution B (Table 5), however, no peaks were observed. Another attempt at expression and purification was carried out, and another gradient elution was attempted with a 500mM imidazole Solution B (Table 6).

Table 4: The FPLC protocol for the first attempt to purify the Pik1-Frq1 complex from Co^{2+}-loaded IMAC resin. Solution B contained 300mM imidazole. The concentration of imidazole for the wash step was 24mM and elution was attempted at 240mM imidazole. Protocol designed and standardized by Parthajit Mukherjee.

	Volume (mL)	Description	Parameters
1	0	Collection fractions within 1 time window(s) ending at 120.0mL	
2	0.00	Lamp (UV detector)	ON
3	0.00	Isocratic flow	A: 100% B: 0% V= 40.00mL Flow = 3.0mL/min
4	40.00	Isocratic flow	A: 92% B: 8% V = 40.00mL Flow = 3.0mL
5	80.00	Isocratic flow	A: 20% B: 80% V = 40.00mL Flow = 3.0mL/min
	120.00	End of Protocol	

Table 5: The second FPLC elution protocol for the first attempt to purify the Pik1-Frq1 complex from Co^{2+}-loaded IMAC resin. Solution B contained 500mM imidazole. A gradient elution from 300mM imidazole to 500mM imidazole was used.

	Volume (mL)	Description	Parameters
1	0.00	Collection fractions within 1 time window(s) ending at 240.00mL	
2	0.00	Lamp (UV detector)	Turn ON
3	0.00	Isocratic flow	A: 100% B: 0% V = 40.00mL Flow = 3mL/min
4	40.00	Linear Gradient	A: 40% → 0% B: 60% → 100% V = 200mL Flow = 3mL/min
	240.00mL	End of Protocol	

Table 6: The FPLC protocol for the second attempt to purify the Pik1-Frq1 complex from Co^{2+}-loaded IMAC resin. Solution B contained 500mM imidazole. The wash step contained 40mM imidazole and it was followed by a gradient elution from 100mM to 500mM imidazole.

	Volume (mL)	Description	Parameters
1	0.00	Collection fractions within 1 time window(s) ending at 240.00mL	
2	0.00	Lamp (UV detector)	Turn ON
3	0.00	Isocratic flow	A: 100% B: 0% V = 40.00mL Flow = 3mL/min
4	40.00	Isocratic flow	A: 92% B: 8% V = 40.00mL Flow = 3mL/min
5	80.00	Linear Gradient	A: 80% → 0% B: 20% → 100% V = 200mL Flow = 3mL/min
	280.00mL	End of Protocol	

3.5.5 Stripping Co^{2+} From the IMAC Resin

The FPLC was used to strip the Co^{2+} from the IMAC resin (Table 7). The IMAC resin was washed with Strip Co^{2+} buffer, 70% EtOH, then Buffer A for 20min each at 2mL/min. Then the column was washed with water at 2mL/min for 10min. To do this, the Strip IMAC resin FPLC protocol was set up with Strip Co^{2+} buffer and 70% EtOH as A and B respectively and the protocol was run. During the pause, A and B was switched to Buffer A and water respectively, then the protocol was resumed. After the Co^{2+} was stripped, the resin can be stored in 20% EtOH for future use.

Table 7: The FPLC protocol for stripping the IMAC resin of the Co^{2+} ions

	Volume (mL)	Description	Parameters
1	0.00	Collection fractions within 1 time window(s) ending at 20.0 min.	
2	0.00	Lamp (UV detector)	Turn ON
3	0.00	Isocratic flow	A: 100% B: 0% Time: 20.00min Flow = 2mL/min
4	20.00	Isocratic flow	A: 0% B: 100% Time: 20.00min Flow = 2mL/min
5	40.00	Pause	No timeout
6	40.0	Isocratic flow	A: 100% B: 0% Time: 20.00min Flow = 2mL/min
7	60.0	Isocratic flow	A: 0% B: 100% Time: 10.00min Flow = 2mL/min
	280.00mL	End of Protocol	

3.6 The Assays

3.6.1 Defining the FI Assay Window

The Bellbrook Labs Transcreener® ADP^2 FI Assay kit requires that minimum and maximum fluorescence values be assessed so that the breath of the detection window is known. The Fluorescence Intensity (FI) Assay Window was determined by measuring the lowest and highest possible signals at the conditions and concentrations used for the assay (low = tracer with antibody + quencher, high = tracer but no antibody + quencher). The compositions of the low and high RFU mixtures are found in Table 8 and 9 for the PKA assay and Table 10 and 11 for the PIK3C3 assay respectively. The components of each were measured into 1.5mL Eppendorf tubes that were labelled either High or Low. The tubes were then rotated at room temperature for at least 15min, then the mixtures were aliquoted into the assay microplate with 50µL/well. The fluorescence was measured with either the Endpoint FI Assay Window protocol, the PKA Kinetic Assay protocol, or the PIK3C3 Kinetic Assay protocol.

Table 8: Low Relative Fluorescence Units (RFUs) Mixture PKA Assay Conditions (to make 200µL)

Component	[Stock]	[Final]	Volume
ADP^2 Antibody-IRDye® QC-1	1.4mg/mL	5µg/mL	0.71µL
10x PKA Assay and Detect Buffer	10x	0.5x	10µL
ADP Alexa Fluor® 594 Tracer	800nM	4nM	1µL
mQH_2O *			188.29µL
		Total	200µL

*mQH_2O was used but autoclaved mQH_2O should have been used

Table 9: High RFU Mixture PKA Assay Conditions (to make 200µL)

Component	[Stock]	[Final]	Volume
10x PKA Assay and Detect Buffer	10x	0.5x	10µL
ADP Alexa Fluor® 594 Tracer	800nM	4nM	1µL
mQH_2O *			189µL
		Total	200µL

*mQH_2O was used but autoclaved mQH_2O should have been used

Table 10: Low Relative Fluorescence Units (RFUs) Mixture PIK3C3 Assay Conditions (to make 200µL)

Component	[Stock]	[Final]	Volume
ADP[2] Antibody-IRDye® QC-1	1.4mg/mL	28.25µg/mL	4.04µL
10x PIK3C3 Assay Buffer	10x	1x	20µL
ADP Alexa Fluor® 594 Tracer	800nM	4nM	1µL
mQH_2O *			174.96µL
		Total	200µL

*mQH_2O was used but autoclaved mQH_2O should have been used

Table 11: High RFU Mixture PIK3C3 Assay Conditions (to make 200µL)

Component	[Stock]	[Final]	Volume
10x PIK3C3 Assay Buffer	10x	1x	20µL
ADP Alexa Fluor® 594 Tracer	800nM	4nM	1µL
mQH_2O *			179µL
		Total	200µL

*mQH_2O was used but autoclaved mQH_2O should have been used

3.6.2 Preparation of the Kinase Substrates

3.6.2.1 Dephosphorylation of Casein

Casein was dephosphorylated based on the method used by Mayer *et al.* (98). Casein (5.02g) was measured, poured into a 250mL graduated cylinder and 40mL of RO H_2O were added. The pH was adjusted to 9.5 very slowly. Water was heated in a 1L beaker using a hot plate; the top of the beaker was covered in aluminum foil. When the temperature of the water was approximately 95°C the graduated cylinder was placed in the water and the graduated cylinder and the top of the beaker were wrapped in aluminum foil to assist the hot plate in maintaining a temperature around 95°C. The pH of the casein solution was monitored with a pH meter and 1M NaOH was added as needed to maintain the pH of the solution at 9.5, while the solution was in the water bath for 10min. The aluminum foil was removed, and the graduated cylinder was taken out of the water bath and was placed on a stir plate. The casein solution in the graduated cylinder was stirred until it reached room temperature (~1h), then it was diluted to 60mL with RO H_2O. During cooling the pH rose to 10.74. Next the pH of the solution was adjusted

very slowly while stirring vigorously to 5.75 with 1N HCl. The solution was poured in centrifuge tubes, which were then balanced and placed at -20°C overnight.

The centrifuge tubes were placed on the counter to thaw, then were centrifuged (Thermo Scientific Sorvall RC6+ Centrifuge) using rotor 521-8x-50y for 20min at 20 000 RPM. The infranatant was carefully removed using a pipette while avoiding floating particulates and pooled into a 250mL flask. The pH was adjusted to 5.9 and the centrifugation step was repeated. A Bradford Assay was conducted to determine the concentration of casein in each tube (121.92mg/mL in tube 1). A working stock of 60 mg/mL of dephosphorylated casein was made from the solution in tube 1.

3.6.2.2 Preparation of 50nm PI:3PS Vesicles

To prepare 1.5mL of PI:3PS, 18.75µL of 10mg/mL liver PI and 56.25µL of 10mg/mL brain PS were measured into a glass vial. The chloroform was evaporated using a stream of nitrogen, then the vial was placed under high vacuum for at least 1h. The lipid mixture was resuspended in 1.5mL of 2.5x Lipid Dilution Buffer and was stored at 4°C. The same protocol was followed for the PC:3PS control, except 7.5µL of 25mg/mL DOPC and 56.25µL of 10mg/mL brain PS was used.

The sonicator (Qsonica sonicators, Model CL-334) was set to a 35% duty cycle (amp), 5 min, pulse 1s on 1s off, and enter was pressed to set (on these settings the sample is subjected to sonication for 5 min over 10min, 1s on 1s off). The sonication probe was carefully set up with the vial to ensure that the tip of the probe was in the lipid solution but did not touch the bottom of the glass vial. The vial of lipids was sonicated on ice with the above parameters; following the 10min, the ice was replaced, and the sonication was repeated (total of 20min). The content of the vial was transferred to an Eppendorf® tube and centrifuged (ThermoIEC Micromax) at 15000 RPM for 5min to remove particulates from the tip of the sonicator probe. The lipid mixture was then immediately transferred to a large glass vial to minimize contact with plastic and to allow the syringes to fit through the mouth of the vial. The large glass vial was placed in a water bath at ~40°C for ~10min, during this time the Mini-Extruder apparatus (Avanti Polar Lipids) was set up. A small amount of 2.5x Lipid Dilution Buffer was passed

through the Mini-Extruder apparatus to wet the apparatus with the buffer to be used and to check for leaks. The lipid mixture was passed through the apparatus at least 5 times, then deposited into a new and labelled large glass vial. The cap of the glass vial was wrapped in parafilm and the vial was stored at 4°C, and the lipids were used within 1 week.

3.6.3 Preparation of the Enzyme Mix

3.6.3.1 Preparation of PKA and of the PKA Enzyme Mix

PKA (400units) was purchased as a dried solid (9-11units/1μg PKA). The PKA was reconstituted to 550units/mL (50μg/mL) by adding 272μL of PKA Reconstitution Solution to the commercial vial of dried PKA and the solution was mixed with a pipette. The PKA Reconstitution Solution was composed of 6mg/mL DTT and 10mM Mg^{2+} and the freshly reconstituted PKA was left on the benchtop at room temperature for 10min, as per the instructions on the PKA product information sheet. The reconstituted PKA solution acted as the 550units/mL PKA stock, and a second 11units/mL PKA stock was made by diluting 2μL of 550units/mL PKA stock with 98μL of PKA Reconstitution Solution.

The Enzyme Mix was composed of PKA stock and PKA Reconstitution Solution. The PKA Reconstitution Solution was used to dilute the PKA stock so that the concentration of DTT and Mg^{2+} was consistent between the assays independent of the enzyme concentration. An enzyme titration was carried out in which different Enzyme Mixes were made with different concentrations of PKA. Since the optimal concentration of PKA for this assay was unknown, the concentrations of PKA chosen for the titration were chosen to cover a wide range and based on ease of pipetting/calculating. Enzyme concentration titrations were carried out using the values listed in Table 12 and the columns labelled Vol PKA Stock/Assay and Vol PKA Reconstitution Solution/Assay were multiplied by (the number of assays to be completed with that enzyme concentration +0.5 or 1). The +0.5 or +1 is to make a little bit of extra to account for small volumes that stick to the sides of the Eppendorf® tubes or small variations in pipette calibrations that cause problems with repeated pipetting (*e.g.,* if a pipette actually pipettes 20.5μL when it is set to 20μL, repeated pipetting from the same stock will cause a person to run out if

only the exact theoretical amount was made). Those respective volumes were then added to Eppendorf tubes such that there was one tube per concentration of PKA in the titration. The assays were carried out on PKA within two days after it was reconstituted.

Table 12: PKA Enzyme Concentration Titration. The concentrations of PKA tested in the time-resolved version of the Bellbrook assay to determine the optimal concentration of PKA for these conditions.

[PKA] Stock		Vol PKA Stock/ Assay	Vol PKA Reconstitution Solution /Assay	[PKA] in 20µL Enzyme Mix		[PKA] in 50µL Assay	
µg/mL	Units/ mL			µg/mL	Units/ mL	µg/mL	Units/ mL
50	550	20µL	0µL	50	550	20	220
50	550	18.2µL	1.8µL	45.5	500	18.2	200
50	550	13.6µL	6.4µL	34	375	13.6	150
50	550	9.1µL	10.9µL	22.75	250	9.1	100
50	550	4.5µL	15.5µL	11.25	125	4.5	50
50	550	2µL	18µL	5	55	2	22
1	11	10µL	10µL	0.5	5.5	0.2	2.2
1	11	1µL	19µL	0.05	0.55	0.02	0.22
-	-	-	20µL	0	0	0	0

3.6.3.2 Preparation of PIK3C3 and of the PIK3C3 Enzyme Mix

The PIK3C3 was purchased as a 100µg/mL solution of PIK3C3 in 50mM Tris-HCl (pH 7.5), 150mM NaCl, 10mM glutathione, 0.1mM EDTA, 0.25mM DTT, 0.1mM PMSF, and 25% glycerol. To make the working stock for the assay, 25µL of this solution was diluted with 475µL of mQH_2O, then ~100µL was aliquoted into 4 Eppendorf® tubes, and the tubes were stored at -80°C. The smaller aliquots in separate tubes were used to prevent freeze-thaw cycles. The PIK3C3 titration was carried out as seen in Table 13.

Table 13: The PIK3C3 Enzyme Concentration Titration. The concentrations of PIK3C3 tested in the time-resolved version of the Bellbrook assay to determine the optimal concentration of PIK3C3 for these conditions.

[PIK3C3] in Assay	[PIK3C3] in Stock	Vol of PIK3C3 Stock/Assay	Vol mQH_2O* / Assay	Vol PIK3C3 Stock/4 Assays	Vol mQH_2O* / 4 Assays
10µg/mL	100µg/mL	5µL	15µL	17.5µL**	52.5µL **
5µg/mL	100µg/mL	2.5µL	17.5µL	8.75µL **	61.25µL **
2µg/mL	5µg/mL	20µL	0µL	80µL	0µL
0.5µg/mL	5µg/mL	5µL	15µL	20µL	60µL
0.2µg/mL	5µg/mL	2µL	18µL	8µL	72µL
0.05µg/mL	5µg/mL	0.5µL	19.5µL	2µL	78µL
0µg/mL		0µL	20µL	0µL	80µL

*used autoclaved mQH_2O
**volumes were for 3.5 assays instead of 4 assays, this was because measuring for 4 assays was wasteful

3.6.4 Preparation of the Bellbrook Labs Transcreener® ADP^2 FI Assay Mix

The appropriate volume of autoclaved mQH_2O, ADP Alexa Fluor® 594 Tracer, and ADP^2 Antibody-IRDye® QC-1 were added into a 1.5mL Eppendorf tube according to Table 14 or Table 15. In the case of the PKA assay, the dephosphorylated casein was also added at this time. The tube was vortexed and rotated at room temperature for at least 15min. The ATP, and the lipid substrate for PIK3C3 Assay Mix, were only added after everything was ready (See section 3.6.5 Running the Assay for more details) and immediately before the mixture was aliquoted into the assay wells. This was to prevent contact between lipid substrate and the plastic tube. Following the addition of ATP and lipid substrate, the mixture was vortexed, and if necessary, it was pulsed quickly in a microcentrifuge to collect the mixture from the walls of the Eppendorf® tube.

Table 14: PKA Assay Mix

Component	[Stock]	Vol of Stock/ Assay	Concentration in 30µL Assay Mix	Concentration in 50µL Assay
ATP	500µM	1µL	16.67µM	10µM
Dephosphorylated Casein	60mg/mL	4µL	8mg/mL	4.8mg/mL
ADP[2] Antibody-IRDye® QC-1	1400µg/mL	0.345µL	16.1µg/mL	9.66µg/mL
ADP Alexa Fluor® 594 Tracer	800nM	0.25µL	6.67nM	4nM
10x PKA Assay and Detect Buffer	10x: 1000mM HEPES 0.2% Brij-35	2.5µL	0.83x: 83.33mM HEPES 0.017% Brij-35	0.5x: 50mM HEPES 0.01% Brij-35
mQH_2O *		21.905µL		

*mQH_2O was used but autoclaved mQH_2O should have been used

Table 15: PIK3C3 Assay Mix

Component	[Stock]	V of Stock/ Assay	Concentration in 30µL Assay Mix	Concentration in 50µL Assay
ATP	500µM	3µL	50µM	30µM
Lipid Substrate	0.5mg/mL lipid in 62.5mM HEPES 1.25mM EGTA	20µL	0.33mg/mL lipid in 41.7mM HEPES 0.83mM EGTA	0.2mg/mL lipid in 25mM HEPES 0.5mM EGTA
ADP[2] Antibody-IRDye® QC-1	1400µg/mL	1µL	46.67µg/mL	28.25µg/mL
ADP Alexa Fluor® 594 Tracer	800nM	0.25µL	6.67nM	4nM
10x PIK3C3 Assay Buffer	10x: 250mM HEPES 500mM NaCl 30mM $MgCl_2$ 0.25mg/mL BSA 50mM $MnCl_2$**	5µL	1.67x: 41.67mM HEPES 83.33mM NaCl 5mM $MgCl_2$ 0.042mg/mL BSA 8.33mM $MnCl_2$**	1x: 25mM HEPES 50mM NaCl 3mM $MgCl_2$ 0.025mg/mL BSA 5mM $MnCl_2$**
mQH_2O *		0.75µL		

*Used autoclaved mQH_2O

**$MnCl_2$ was used in the initial stages of assay development, but was not present in the final working assay conditions

Assay substrates were either ATP and dephosphorylated casein, or ATP and 50nm vesicles made from PI:3PS. A PKA assay concentration of 10μM ATP was chosen, as this was supposedly within the range of the kit (0.1μM ATP - 1000μM ATP) and seemed like a reasonable but not wasteful amount. The ATP concentration (30μM) was chosen for the PIK3C3 assay because this was the concentration found in literature (99) and this is at or below the reported K_m and ADP-Glo technical manual reports the apparent K_m to be 40μM. Casein (4.8mg/mL) was used as the substrate concentration because 4μL of the 60mg/mL dephosphorylated casein stock was a convenient volume, and calculations were done to ensure that there was excess casein, assuming the maximum specific activity of PKA (based on the product data sheet) and assuming only one phosphorylation site per casein subunit (even though there are multiple sites, because the number of sites available to be phosphorylated was unknown, and the goal was to make sure that casein was not limiting). A concentration of 4.8mg/mL dephosphorylated casein is approximately 8×greater than the amount of casein that would be phosphorylated in 2h assuming maximum specific activity and if casein was only phosphorylated once. The vesicle size, lipid composition and ratio, and the lipid dilution buffer for the lipid substrate for the PIK3C3 assay were taken from the description of the lipid substrates in the Promega ADP-Glo Lipid Kinase Systems technical manual (100).

The concentration of ADP^2 Antibody-IR Dye® QC-1 that was used for each assay was calculated using a slight modification of the equation in the technical manual.

Equation from the technical manual: $y = 0.93x + 0.7$

$y =$ [ADP^2 Antibody-IR Dye® QC-1 (μg/mL)] in the 25μL Detection mixture for the end-point format

$x =$ [ATP (μM)] in the 25μL Enzyme Reaction for the end-point format

The equation was designed to be used with the 25μL Enzyme Reaction + 25μL Detection Mixture end-point format. To adjust to the 50μL assay volume (20μL Enzyme Mix + 30μL Assay Mix) for the time-resolved assay format, the [ATP] for the assay was multiplied by two, substituted into the equation as x, solved for y, and y was divided by 2 to get the antibody concentration in the 50μL assay.

[ATP] for time-resolved 50μL PKA assay = 10μM

$10\mu M * 2 = 20\mu M$

$y = 0.93(20\mu M) + 0.7$

$y = 19.3\mu g/mL$ antibody

$\frac{y}{2} = 9.65\mu g/mL$ antibody in time-resolved 50µL PKA assay

The assay concentration of the ADP Alexa Fluor® 594 Tracer is always 4nM, independent of the other assay conditions as inferred from the technical manual (93).

The PKA assay buffer recipe was based on information included in the Bellbrook Labs Transcreener® ADP^2 FI Assay kit technical manual (93). The PIK3C3 assay buffer was taken from the Promega ADP-Glo technical manual (100), then was adjusted based on the challenges that were faced in the development of the assay. This process is outlined in the Results and Discussion Section 5.5.1 10x PIK3C3 Assay Buffer: Precipitation Problems.

The length of the assay was determined in proportion to the [ATP], the [enzyme], and the specific activity reported on the material data sheets. The equilibration time of the displacement of the ADP Alexa Fluor® 594 Tracer by the non-fluorescent ADP produced by the enzyme is greater than 15min (93). Therefore, the kit cannot confidently be used with short-term enzyme reactions. Thus, the length of time, the [ATP], and the [enzyme] were chosen to ensure that the enzyme was working slowly enough that ADP was being produced at a slower rate than the displacement. This was to ensure that the rate measured by the assay was the rate of ADP production and not the rate of displacement.
It was also important to ensure initial rate conditions as there would be less than 10% ATP conversion during the length of the assay.

3.6.5 Running the Assay

Prior to beginning the assay everything was prepared and set up – the enzyme solution, the assay mix, the pipettes, the autoclaved pipette tips, the plate reader, the plate, and the map of which samples go where in the assay plate was already planned out. Then the last components of assay mix were added (lipid substrate and ATP), the Eppendorf® tube was vortexed, and the contents of the tube were spun down in a

microcentrifuge if necessary. The Assay Mix (30µL) was aliquoted into each well, then 20µL of the Enzyme Mix was added into each well to start the reaction. The plate was placed into plate reader, and the Read button was clicked immediately. The "set first point to zero" box was unchecked to ensure that the raw data was displayed instead of data that was arbitrarily normalized.

3.6.6 ATP/ADP Standard Curves

Twelve autoclaved 1.5mL Eppendorf® tubes were labeled 0%-100% according to the first column of Table 16. Autoclaved mQH_2O was pipetted into each tube according to column 7 in Table 16, followed by the proper volume of the ATP and ADP stock solutions (columns 5 and 6, Table 16). Next, the Assay Mix was made (Table 17). The volumes of each component necessary for 52 microtiter wells were measured into a 2mL Eppendorf® tube, the tube was mixed and rotated at room temperature for at least 15 min. Then 108.38uL of Assay Mix was added to each % ATP conversion Eppendorf® tube, the tubes were vortexed and were rotated at room temperature for at least 15min. 50µL of each %ATP conversion was pipetted into 3 wells and the FI was measured using the Endpoint FI Assay Window protocol/settings. The same procedure was followed for the PIK3C3 ATP/ADP standard curve with a few exceptions. The volumes used are found in Tables 18 and 19. When the Assay Mix was made the lipid substrate was not added until right before the Assay Mix was aliquoted into the % ATP conversion tubes, this was to reduce the contact of the lipid substrate with plastic. The Assay Mix (105µL) was added to each % ATP conversion Eppendorf® tube.

Table 16: The volumes required to make the ATP/ADP solutions to make 200µL total of each % ATP conversion for the PKA ATP/ADP standard curve (91.62µL ATP/ADP solution + 108.38µL of Assay Mix = 200µL of the % ATP Conversion).

% ATP Conversion	[ATP] (µM)	[ADP] (µM)	Vol of 100µM ATP Stock (µL)	Vol of 10µM ADP stock (µL)	Vol of 100µM ADP stock (µL)	Vol of autoclaved mQH_2O (µL)	Total Volume (µL)
0	10	0	20	0		71.62	91.62
2	9.8	0.2	19.6	4.0		68.02	91.62
4	9.6	0.4	19.2	8.0		64.42	91.62
6	9.4	0.6	18.8	12.0		60.82	91.62
8	9.2	0.8	18.4		1.6	71.62	91.62
10	9.0	1.0	18.0		2.0	71.62	91.62
15	8.5	1.5	17.0		3.0	71.62	91.62
20	8.0	2.0	16.0		4.0	71.62	91.62
30	7.0	3.0	14.0		6.0	71.62	91.62
40	6.0	4.0	12.0		8.0	71.62	91.62
60	4.0	6.0	8.0		12.0	71.62	91.62
100	0	10	0		20.0	71.62	91.62

Table 17: Assay Mix for the PKA ATP/ADP Standard Curve (Volumes to make 200µL of each % Conversion, 108.38µL of Assay Mix per % Conversion)

Component	[Stock]	Vol per well (µL)	Vol for 52 wells (µL)
PKA Buffer	6mg/mL DTT 10mM $MgCl_2$	20µL	1040µL
Casein	60mg/mL	4µL	208µL
ADP[2] Antibody-IR Dye® QC-1	1400ug/mL	0.345µL	17.94µL
ADP Alexa Fluor® 594 Tracer	800nM	0.25µL	13µL
10x PKA Assay + Detect Buffer	10x 1000mM HEPES 0.2% Brij	2.5µL	130µL
Total			1408.94µL

Table 18: The volumes required to make the ATP/ADP solutions to make 175µL total of each % ATP conversion for the PIK3C3 ATP/ADP standard curve (70µL ATP/ADP solution + 105µL of Assay Mix = 175µL of the % ATP Conversion).

% ATP Conversion	[ATP] (µM)	[ADP] (µM)	Vol of 100µM ATP Stock (µL)	Vol of 100µM ADP stock (µL)	Vol of autoclaved mQH_2O (µL)	Total Volume (µL)
0	30.0	0.0	52.5	0	17.5	70
2	29.4	0.6	51.45	1.05	17.5	70
4	28.8	1.2	50.4	2.1	17.5	70
6	28.2	1.8	49.35	3.15	17.5	70
8	27.6	2.4	48.3	4.2	17.5	70
10	27.0	3.0	47.25	5.25	17.5	70
15	25.5	4.5	44.62	7.88	17.5	70
20	24.0	6.0	42.0	10.5	17.5	70
30	21.0	9.0	36.75	15.75	17.5	70
40	18.0	12.0	31.5	21.0	17.5	70
60	12.0	18.0	21.0	31.5	17.5	70
100	0.0	30.0	0	52.5	17.5	70

Table 19: Assay Mix for the PIK3C3 ATP/ADP Standard Curve (Volumes to make 175µL of each % Conversion, 105µL of Assay Mix per % Conversion)

Component	[Stock]	Vol per well (µL)	Vol for 45.5 wells (µL)
PI:3PS Lipid Substrate	0.5mg/mL	20µL	910µL
ADP^2 Antibody-IR Dye® QC-1	1400ug/mL	1µL	45.5µL
ADP Alexa Fluor® 594 Tracer	800nM	0.25µL	11.38µL
10x PIK3C3 Assay Buffer	10x	5µL	227.5µL
Autoclaved mQH_2O		3.75µL	170.62µL
Total		30µL	1365µL

3.6.7 Assay Controls

Control assays in which the enzyme, a substrate, or both were omitted, were conducted for the same time and with the same conditions as the respective assay, having all of the components. The volume of the missing component was compensated for with autoclaved mQH_2O for the Background (no antibody and no tracer), No Antibody, No Tracer, No ATP, No Casein, No PIK3C3, No Lipid, and the No Lipid and No PIK3C3

controls. In the case of the PKA controls without PKA, the respective volume of PKA reconstitution solution was added. In the case of the PC:3PS control, the volume and concentration of lipid substrate was the same as the assay conditions, the vesicles were just composed of PC:3PS instead of PI:3PS. The PI:3PS + mQH_2O control contained 0.2mg/mL PI:3PS and autoclaved mQH_2O. The PI:3PS + Buffer control contained 0.2mg/mL PI:3PS, 1x PIK3C3 Assay Buffer, and autoclaved mQH_2O. 0% ATP conversion and 100% ATP conversion controls were completed as the first and last points of the ATP/ADP standard curves.

3.6.8 Sneaking Mn^{2+} into the Assay

The "sneak" Mn^{2+} assay was conducted in the same way as the PIK3C3 assay with two key changes. The first change was that the 10x PIK3C3 assay buffer was made without $MgCl_2$ and without $MnCl_2$. The second change was that $MnCl_2$ was added to the enzyme mix such that the final assay concentration of Mn^{2+} was either 3mM or 3μM.

3.6.9 Fluorescence Plate Reader

Molecular Devices SpectraMax M2

Software: SoftMax pro 7.03

Assay Plates: Corning, Assay Plate, 96 Well Half Area, No Lid, Flat Bottom, Non-Binding Surface, Black Polystyrene (REF 3686)

Settings for Endpoint FI Assay Window:

Endpoint

Fluorescence

Excitation Wavelength: 575nm, Emission Wavelength: 620nm

Auto-cutoff: 610nm

PMT and Optics: Auto, 6 flashes/read

More Settings: shake once before 1st read, calibrate on, carriage speed normal, column priority

Temperature: room temperature (~22°C)

Settings for PKA Kinetic Assay:

Kinetic, Time: 1h, Interval: 2min, Reads: 31

Fluorescence

Excitation Wavelength: 575nm, Emission Wavelength: 620nm

Auto-cutoff: 610nm

PMT and Optics: Medium, 6 flashes/read

More Settings: shake on, calibrate on, carriage speed normal, column priority

Temperature: room temperature (~22°C)

Settings for PIK3C3 Kinetic Assay:

Kinetic, Time: 3h, Interval: 2min, Reads: 91

Fluorescence

Excitation Wavelength: 575nm, Emission Wavelength: 620nm

Auto-cutoff: 610nm

PMT and Optics: Medium, 6 flashes/read

More Settings: shake on, calibrate on, carriage speed normal, column priority

Temperature: room temperature (~22-24°C)

4 Results and Discussion: Protein Expression and Purification

Notes for whole Results and Discussion section: the colour code
BJ2168 = pink, pVEX = green, B8NA = blue, 10NE = purple
● Not Induced ▲ Induced with solid Galactose ■ Induced with YEPG
Black fit line: 2% Dextrose SCUTAD pre-culture
Coloured fit line + black outline around symbols: 0.2% Dextrose SCUTAD* pre-culture

4.1 Growth Curve Experiments: pVEX in SCUTAD and BJ2168 in SCAT and YPAD

BJ2168 was grown in SCAT (Figure 21). The time to reach mid-log phase was approximately 700min. The maximum OD (600nm) predicted by the fit was 5.353 and the data began to plateau around 1000min. pVEX (BJ2168 transformed with empty pYEXC3H and pESC-Trp vectors) was grown in SCUTAD (Figure 21). The time to reach the mid-log phase was approximately 1000min and a maximum OD around 3.6 was reached by 1900min. The maximum OD predicted by the fit was 3.722.

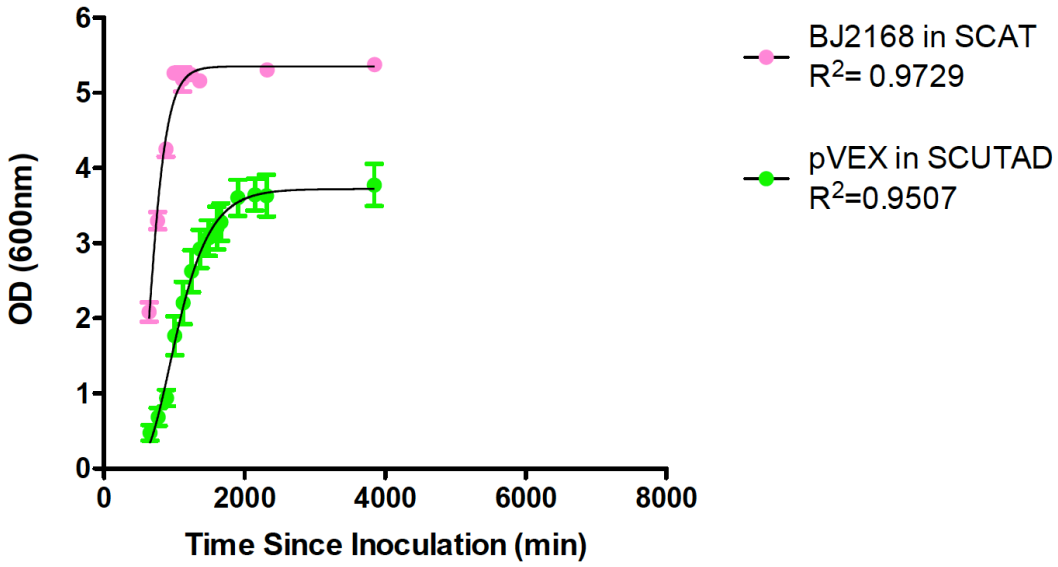

Figure 21: BJ2168 and pVEX were grown in either SCUTAD or SCAT. pVEX: BJ2168 transformed with empty vectors pYEXC3H and pESC-Trp. Growth was measured by following the optical density (OD) measured at 600nm. The growth curves were fit using a Gompertz growth model.

It took longer for pVEX in SCUTAD to reach its mid-log and its maximum OD than for BJ2168 in SCAT. This makes sense because SCAT is not a selective medium,

while SCUTAD is a selective medium that works based on the principle that BJ2168 is a tryptophan (Trp) and uracil (Ura) auxotroph, meaning that BJ2168 is not capable of making either on its own. SCAT has both of these nutrients while SCUTAD does not. The two vectors that pVEX is transformed with confer the ability to make Trp and Ura respectively, therefore, when pVEX is grown on media that does not contain Trp and Ura, only cells that contain both vectors can make these amino acids and survive. Therefore, pVEX in SCUTAD are not expected to grow as efficiently as BJ2168 in SCAT because they have the additional work of producing Trp and Ura (resources have to go into that instead of into growth and division) and any cells that have lost a plasmid die, therefore also slowing the overall population growth. pVEX in SCUTAD also have the additional work of replicating the plasmids. BJ2168 (which does not contain the plasmids) in SCAT was expected to have the fastest growth as it is a non-selective medium.

The first time that BJ2168 was grown in YPAD both OD and cell count measurements were made at each time point; this was to correlate OD with approximate cell counts. This data can be seen in Figure 22. The same samples were plotted two different ways, one with the OD measurements and one with the cell counts. OD vs Time (min) and #cells/mL vs. Time (min) are both approximately linear and follow the same trend. It was calculated that there were approximately 9.02 x 10^7 cells/mL per OD unit.

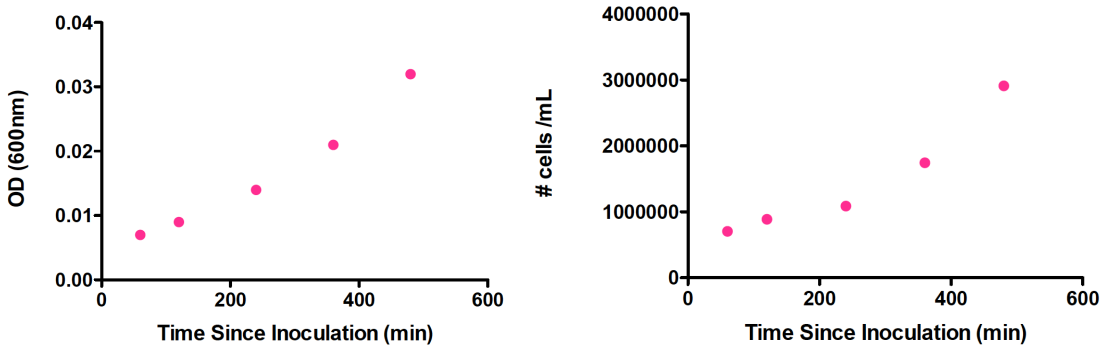

Figure 22: Correlation of optical density at 600nm and cell counts from BJ2168 grown in YPAD. The same samples were plotted two different ways, one with the OD measurements and one with the cell counts.

4.2 Growth Curve Experiments: Pre-Culture Tube Growth Condition Tests

BJ2168 was grown in 5mL of SCAT in culture tubes for 24h at different conditions (Figure 23). There was a slight decrease in growth at 220 RPM compared to 250 RPM, which is likely due to a decrease in aeration. Given that the maximum ODs did not change substantially with temperature or shaking speed, 26°C and 300 RPM were the conditions that were chosen based on practicality; 26°C was chosen over 30°C because 26°C is the recommended growth temperature for this strain (101).

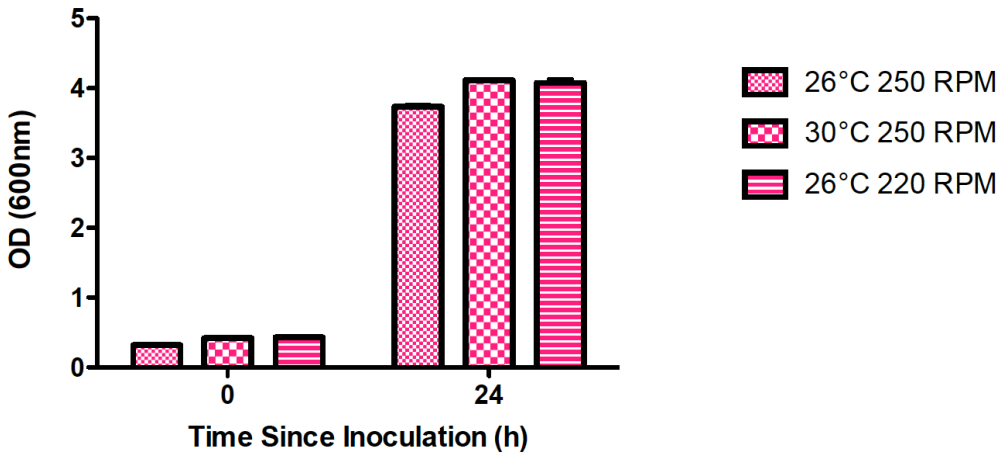

Figure 23: Pre-culture tube growth condition tests. Growth as determined by OD (600nm) measurements for BJ2168 grown in 5mL of SCAT medium in culture tubes for 24h at different conditions of temperature and agitation.

4.3 Growth Curve Experiments: B8NA in SCUTAR – Non-induced and Induced with Solid Galactose

B8NA (transformed BJ2168 with clone 8 (pYEXC3H+PIK1) and clone N (pESC-Trp+FRQ1+CDC37) at the same time, colony A) was grown in SCUTAR (Figure 24). The time to reach the mid-log phase was approximately 940min. The maximum OD (600nm) predicted by the fit was 3.585 and it began to plateau around 2300min.

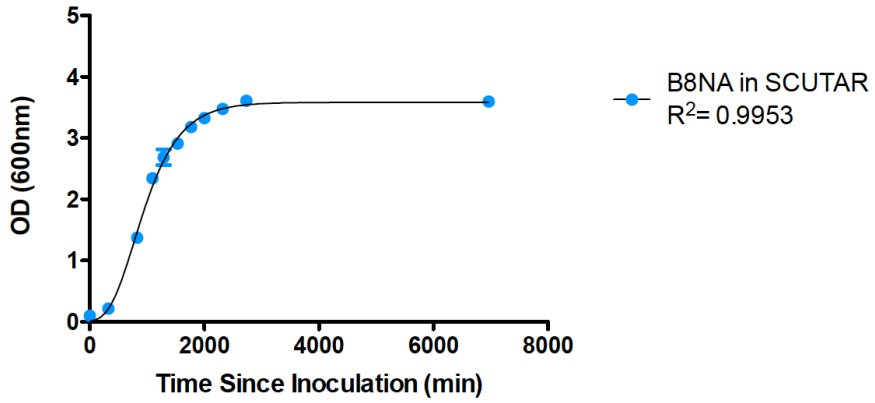

Figure 24: B8NA grown in SCUTAR. B8NA: transformed BJ2168 with clone 8 (pYEXC3H+PIK1) and clone N (pESC-Trp+FRQ1+CDC37) at the same time, colony A. No induction. Grown at 26°C and 300 RPM. The growth curves were fit using a Gompertz growth model.

B8NA was grown in SCUTAR and protein expression was induced by the addition of solid galactose at different ODs. The time to reach mid-log phase was approximately 1050min for the majority of the curves (Figure 25). The growth plateaued between about OD 3.8-4 by 3000min. The maximum values predicted by the Gompertz growth model fits are 4.207 (baby blue), 4.005 (navy blue), and 3.857 (teal). Non-induced B8NA grown in SCUTAR (blue) is also shown in Figure 25 for comparison. There was not a drastic difference in growth if B8NA was not induced or if it was induced with solid galactose, and there was not a drastic difference between the growth of B8NA when it was induced with solid galactose at different ODs. This indicated either that adding the sugar galactose (the inducer) added an additional carbon source that assisted the cells to grow despite the extra burden of protein expression or that following induction with solid galactose, B8NA was not producing a substantial amount of protein, so the energy drain on the growth and division was not large. These experiments

monitored cell growth via measuring the OD at 600nm; therefore, the level of protein expression based on these different conditions is not known, and it will be the work of a future student to optimize protein expression.

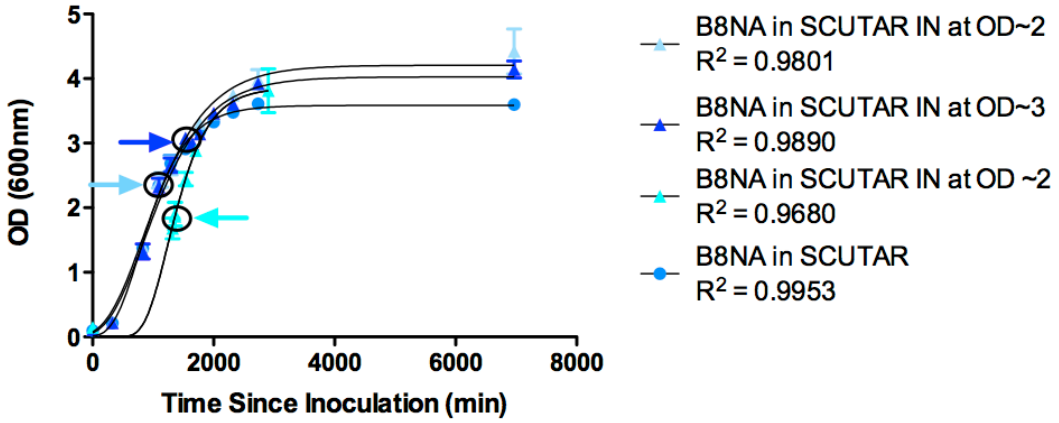

Figure 25: B8NA grown in SCUTAR, induced with solid galactose at different optical densities. B8NA: transformed BJ2168 with clone 8 (pYEXC3H+PIK1) and clone N (pESC-Trp+FRQ1+CDC37) at the same time, colony A. Grown at 26°C and 300 RPM. All plateau OD ~3-4. The growth curves were fit using a Gompertz growth model.

4.4 Growth Curves: SCUTAD vs SCUTAD*

Other growth curve experiments were completed prior to the ones shown in Sections 4.1-4.3. However, after their completion it was realized that the SCUTAD pre-culture tubes used for these experiments contained 10-fold less dextrose than they were supposed to (0.2% dextrose instead of 2%). This error is denoted by SCUTAD* in this document when this 0.2% dextrose media was used. The cells in the SCUTAD* pre-cultures grew less in 24h than those in SCUTAD, therefore the inoculum used to inoculate the SCUTAR flasks for these growth curve experiments was smaller than that of the SCUTAD pre-cultures used in the growth curve experiments discussed in the previous sections. As a result, the growth curves took a longer time to evolve, as seen in Figure 26. The difference in the time to reach mid-log phase for B8NA (transformed BJ2168 with clone 8 (pYEXC3H+PIK1) and clone N (pESC-Trp+FRQ1+CDC37) at the same time, colony A) in SCUTAR for SCUTAD* vs SCUTAD pre-cultures was 1050min (~17h). However, given the time, the cultures grown from SCUTAD* pre-cultures still reached a plateau in OD between 3 and 4. Overall these experiments are still meaningful, but the timing of the growth cannot be compared with the experiments that used SCUTAD pre-cultures. The data presented in Section 4.4 (4.4.1 - 4.4.3) was gathered from cultures that were grown in SCUTAD* pre-cultures except where otherwise stated. The 10NE (transformed BJ2168 with clone 10 (pYEXC3H+PIK1) and clone N (pESC-Trp+FRQ1+CDC37) sequentially, colony E) experiments were not grown in the SCUTAD* pre-cultures, the pre-culture used as the inoculum for this experiment was grown in SCUTAD. However, only 1mL of pre-culture was used instead of 5mL to inoculate 100mL of SCUTAR for the growth curve. This is why these cultures follow the same delayed growth as the ones grown in SCUTAD* pre-cultures as both of them began with fewer cells as the inoculum.

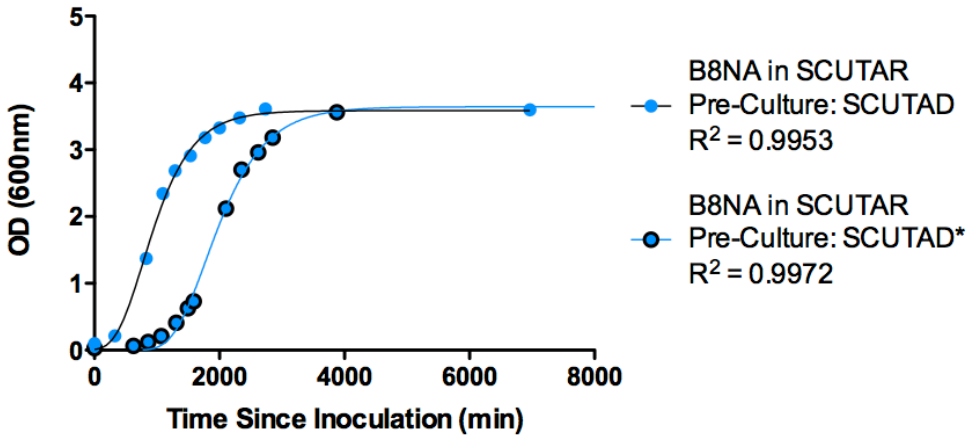

Figure 26: B8NA grown in SCUTAR from either SCUTAD (2% dextrose, black trendline) or SCUTAD* (0.2% dextrose, coloured trendline) pre-cultures. B8NA: transformed BJ2168 with clone 8 (pYEXC3H+PIK1) and clone N (pESC-Trp+FRQ1+ CDC37) at the same time, colony A. No induction. Grown at 26°C and 300 RPM. The growth curves were fit using a Gompertz growth model. An additional data point around 10000min exists for the SCUTAD* pre-culture data set; it was used to generate the fit, but it was truncated for consistency and clarity in the visual representation.

4.4.1 Maximum Plateau

It is easily observed from Figures 24-28 that all the growth curves of B8NA (transformed BJ2168 with clone 8 (pYEXC3H+PIK1) and clone N (pESC-Trp+FRQ1+CDC37) at the same time, colony A) in SCUTAR or SCUTAD have a maximum OD value very close to or between 3 and 4. This is observed independent of the various growth conditions- if the cultures were induced with solid galactose or not, if they were grown in dextrose or raffinose, or if pre-culture dextrose concentration was 0.2% or 2%. The two growth curves of 10NE (transformed BJ2168 with clone 10 (pYEXC3H+PIK1) and clone N (pESC-Trp+FRQ1+CDC37) sequentially, colony E) also seem to follow this trend (Figure 27).

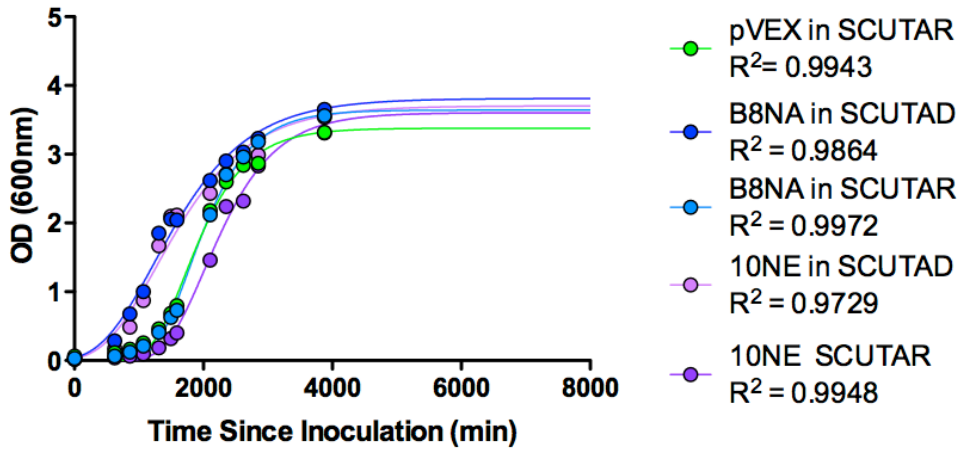

Figure 27: A comparison of growth in dextrose vs raffinose, pVEX, B8NA, and 10NE grown in SCUTAD and SCUTAR. pVEX: BJ2168 transformed with empty vectors pYEXC3H and pESC-Trp. B8NA: transformed BJ2168 with clone 8 (pYEXC3H+PIK1) and clone N (pESC-Trp+FRQ1+CDC37) at the same time, colony A. 10NE: transformed BJ2168 with clone 10 (pYEXC3H+PIK1) and clone N (pESC-Trp+FRQ1+CDC37) sequentially, colony E). SCUTAD* pre-cultures. No induction. Grown at 26°C and 300 RPM. All plateau OD ~3-4. The growth curves were fit using a Gompertz growth model. Additional data points around 10000min exist; they were used to generate the fits but were truncated for consistency and clarity in the visual representation.

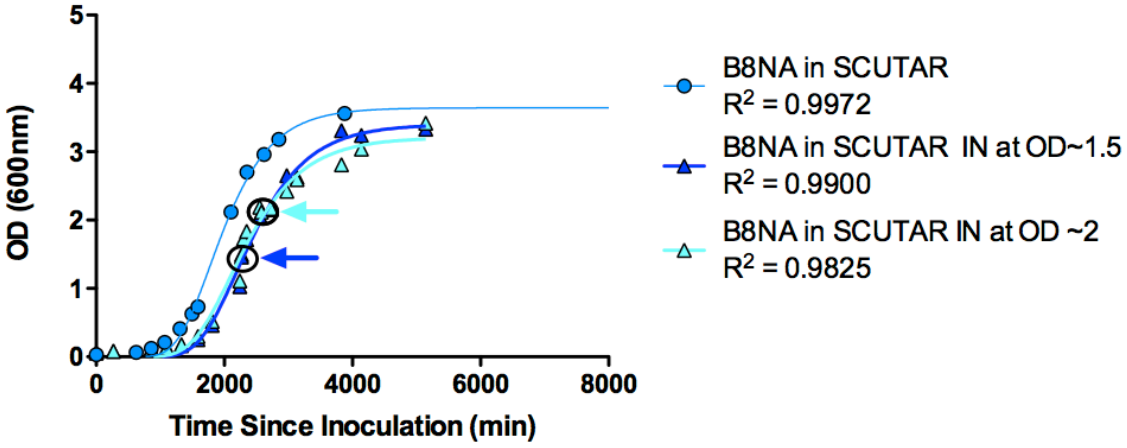

Figure 28: B8NA grown in SCUTAR, induced with solid galactose at different optical densities. B8NA: transformed BJ2168 with clone 8 (pYEXC3H+PIK1) and clone N (pESC-Trp+FRQ1+CDC37) at the same time, colony A. SCUTAD* pre-cultures. Grown at 26°C and 300 RPM. All plateau OD ~3-4. The growth curves were fit using a Gompertz growth model. An additional data point around 10000min exists for the B8NA in SCUTAR data set; it was used to generate the fit, but it was truncated for consistency and clarity in the visual representation.

4.4.2 B8NA in Dextrose vs Raffinose

A comparison between growth in dextrose vs raffinose containing media was carried out with pVEX (BJ2168 transformed with empty vectors pYEXC3H and pESC-Trp), B8NA (transformed BJ2168 with clone 8 (pYEXC3H+PIK1) and clone N (pESC-Trp+FRQ1+CDC37) at the same time, colony A), and 10NE (transformed BJ2168 with clone 10 (pYEXC3H+PIK1) and clone N (pESC-Trp+FRQ1+CDC37) sequentially, colony E) (Figure 27). These experiments were not done in replicates; however, a trend can be seen between the cultures grown in SCUTAD vs the cultures grown in SCUTAR. B8NA and 10NE grown in SCUTAD reached the mid-log phase at least 9h faster than pVEX, B8NA, and 10NE grown in SCUTAR. This trend indicated that growth was more efficient when the culture was grown in dextrose vs raffinose containing media. This makes sense as glucose is the favoured carbon and energy source in yeast (102). However, raffinose did not negatively impact overall growth, as the growth curves in SCUTAR still plateaued between an OD of 3 and 4, and they reached their maximum OD around a similar time as the SCUTAD cultures. This is advantageous for this expression system because it means that growth is not sacrificed when raffinose is used. Raffinose is advantageous because it is a non-glucose and non-inducing sugar. Glucose is the favoured carbon source in yeast and it suppresses the expression of galactose metabolism genes, along with other sugar metabolism genes (102, 103). Galactose induction occurs when the concentration of glucose is low enough and the concentration of galactose is high enough to create the appropriate glucose:galactose ratio (103). Growing the cells in a non-inducing, non-glucose sugar containing medium prior to induction with galactose eliminates the repression of galactose metabolizing genes, allowing them to be quickly activated upon the addition of galactose (102, 103).

4.4.3 B8NA and 10NE Induced with YEPG

B8NA (transformed BJ2168 with clone 8 (pYEXC3H+PIK1) and clone N (pESC-Trp+FRQ1+CDC37) at the same time, colony A) and 10NE (transformed BJ2168 with clone 10 (pYEXC3H+PIK1) and clone N (pESC-Trp+FRQ1+CDC37) sequentially, colony E) were grown in SCUTAR and induced at an OD of ~2 with YEPG (rich media containing galactose) (Figure 29). There was a dip in OD between the time points taken

immediately before and after the addition of YEPG (between 2500min-2800min in Figure 29). YEPG (50mL, 3x) was added to 100mL of growing culture, this diluted the culture, thus causing the dip in the observed OD. YEPG is a rich media that lifts the selection, therefore these cells received fresh nutrients, and they no longer had to make their own Ura and Trp to survive. This relieved the cells of this work and allowed them to channel more energy and resources into growing and dividing. This was probably why the OD of the final measurement was so high (OD = ~9). The lack of selection may have also led to loss of the vectors, and this also may have caused the large amount of growth. Measurements were ceased due to time constraints and due to suspicions that the cells were losing the plasmids as a result of the lack of selection. As a result, the plateau (max OD) for YEPG induced B8NA or 10NE is unknown. A test of plasmid stability was subsequently conducted and 24h after induction with YEPG a sample was taken and plated on SCUTAD and SCUTA and grown for 32h. Visually there appeared to be the same amount of growth regardless of selective or non-selective media, which indicated that the plasmids were stable. Therefore, the growth was likely due to the fresh nutrients and the relief of the auxotrophic selection.

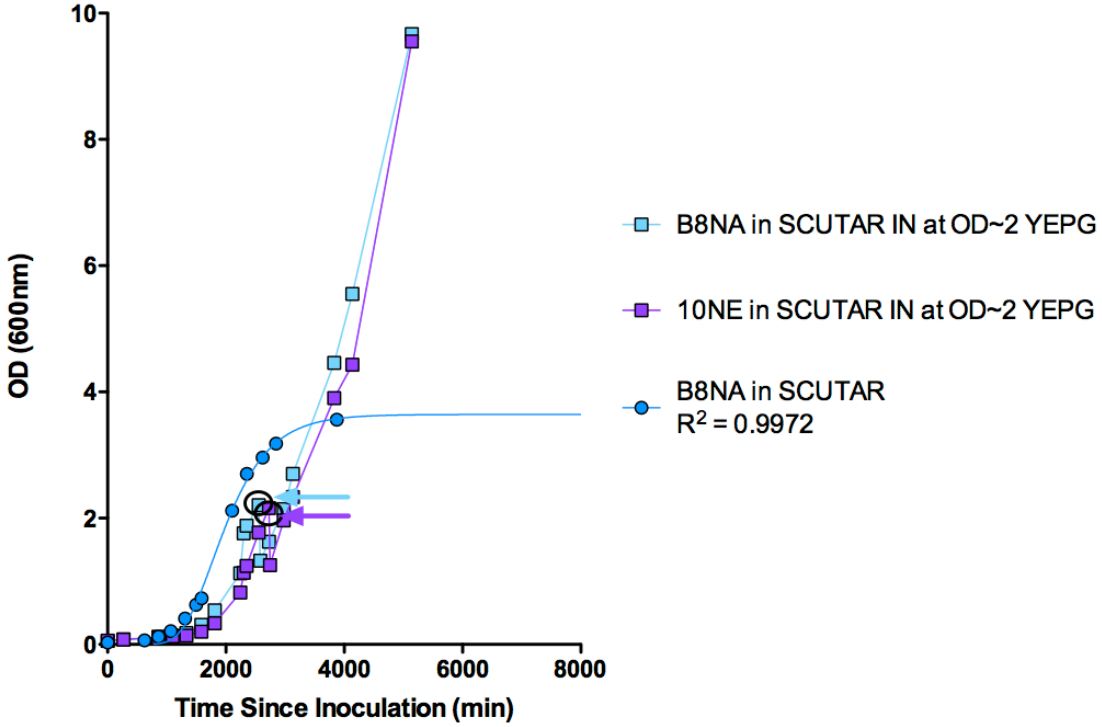

Figure 29: B8NA and 10NE grown in SCUTAR, induced with YEPG at different OD ~2. B8NA: transformed BJ2168 with clone 8 (pYEXC3H+PIK1) and clone N (pESC-Trp+FRQ1+CDC37) at the same time, colony A. 10NE: transformed BJ2168 with clone 10 (pYEXC3H+PIK1) and clone N (pESC-Trp+FRQ1+CDC37) sequentially, colony E. SCUTAD* pre-cultures. Grown at 26°C and 300 RPM. Huge amounts of subsequent growth were observed after addition of rich YEPG media and as a result the plateau/maximum OD was not reached. An additional data point around 10000min exists for the B8NA in SCUTAR data set; it was used to generate the fit, but it was truncated for consistency and clarity in the visual representation.

4.5 Analyzing Growth Curve Experiments Using SDS-PAGE

4.5.1 Method of Yeast Cell Lysis Matters

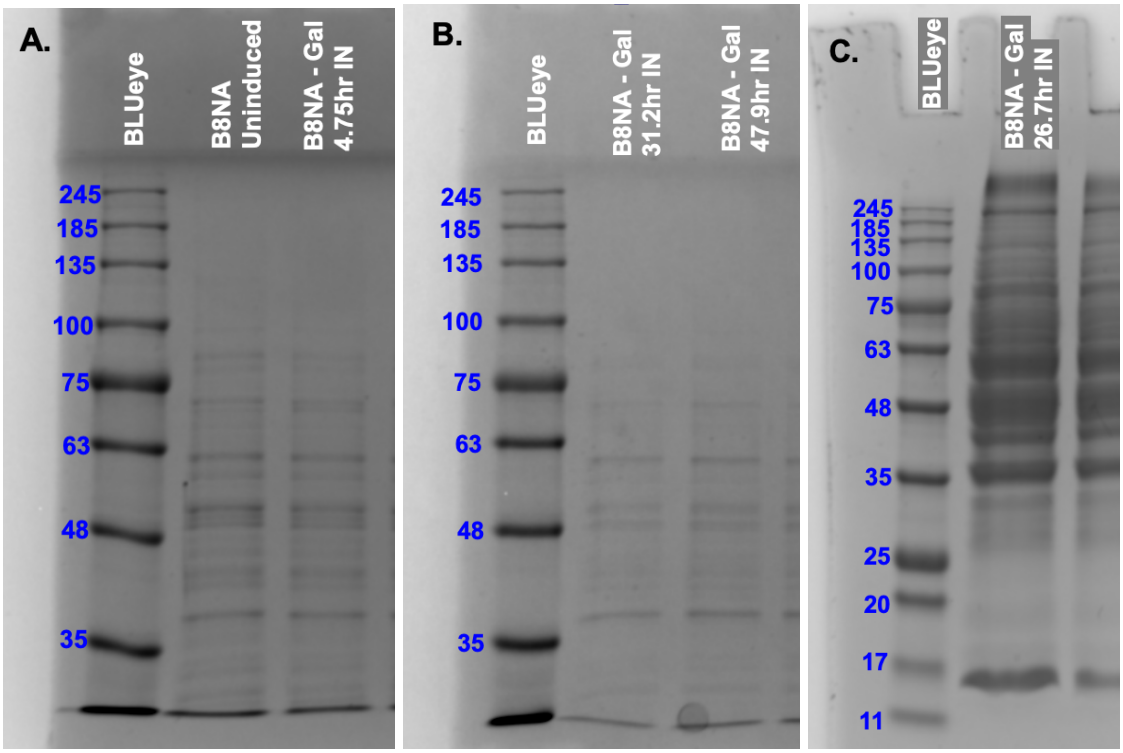

Figure 30: A comparison of the methods of yeast cell lysis. **A.** The samples were prepared by boiling for 10min at 90°C with lysis buffer (0.1M NaOH, 0.05M EDTA, 2% SDS, and 2% β-mercaptoethanol) and acetic acid. The gel was a 6% stacking, 10% resolving SDS-PAGE gel and it was run at 120V for ~1.75h. **B.** The samples were prepared the same as A. except they were boiled for 18min instead of 10min. The gel was a 6% stacking, 10% resolving SDS-PAGE gel and it was run at 120V for ~2h. **C.** The cells were lysed by vortexing (VWR Analog Vortex Mixer) five times with glass beads, at maximum speed (10) for 30s, with 1.5min in between to cool on ice. The gel was a precast commercial 12% SDS-PAGE gel.

Three methods of yeast cell lysis were tried; the first two involved boiling the cells at 90°C with lysis buffer (0.1M NaOH, 0.05M EDTA, 2% SDS, and 2% β-mercaptoethanol) and acetic acid for different amounts of time, while the third method involved the use of glass beads. The first method of yeast cell lysis (boiling for 10min 90°C with lysis buffer and acetic acid) did not effectively extract proteins that were larger than approximately 100kDa. This is seen in the sample lanes shown in Figure 30A and it was also observed with all of the samples that were prepared using this method. The second method was the same as the first except the cells were boiled for 18min. Extending the boiling time from 10min to 18min did not improve the protein extraction

problem with respect to the extraction of high MW proteins; no proteins larger than 100kDa were observed in any of the lanes with any of the samples that were prepared in this manner. The samples in Figure 30B are examples of this. However, proteins larger than 100kDa could be seen on the SDS-PAGE gels when glass beads were used for the cell lysis. This can be seen in Figure 30C.

The difference in the size of extracted proteins was caused by a difference in the degree to which the cell membrane and cell wall were disrupted by the lysis technique. Boiling the cells in lysis buffer (0.1M NaOH, 0.05M EDTA, 2% SDS, and 2% β-mercaptoethanol) disrupted the cell membrane and the cell wall, making them more permeable, without completely breaking the cells open (97). This explains the size cut-off that was observed; the cells became permeable enough to let out proteins of smaller molecular weight, but proteins with molecular weights greater than ~100kDa were too big to be released. However, glass beads collide with the cells and mechanically break the membranes by shear force (104). Cell membranes can be completely disintegrated using glass beads, therefore this method is a very efficient method for lysing cells and the entire contents of the cell is released independent of molecular weight (104).

4.5.2 Western Blot

A western blot was performed on galactose-induced transformants (B8NA: transformed BJ2168 with clone 8 (pYEXC3H+PIK1) and clone N (pESC-Trp+FRQ1+CDC37) at the same time, colony A, and 10NE: transformed BJ2168 with clone 10 (pYEXC3H+PIK1) and clone N (pESC-Trp+FRQ1+CDC37) sequentially, colony E) by Candace Panagabko (Brock University) (Figure 31). Frq1 was tagged with FLAG and an anti-FLAG (Sigma) antibody was used for the western blot. There was some cross reactivity, but the largest and darkest bands between 20-25kDa correspond to Frq1, a 22kDa protein. Bands corresponding to the Pik1-Frq1 complex can be seen at ~100kDa. The non-induced pVEX and B8ND controls, and the induced pVEX control, did not have any bands (lanes 1-3 in Figure 31). No distinct bands were observed in lanes 5 and 6. The induced B8NA sample in lane 5 was an old sample that was lysed using the boiling protocol. It is very likely that the sample was not completely

neutralized leading to the degradation of the protein in the sample. This smearing was observed as the samples that were lysed with this method aged. The induced B8NA sample in lane 6 was lysed with a different method and it is likely that this method was ineffective. The western blot confirmed that the transformants were expressing Pik1 and Frq1 and that the two form a complex that is stable during lysis.

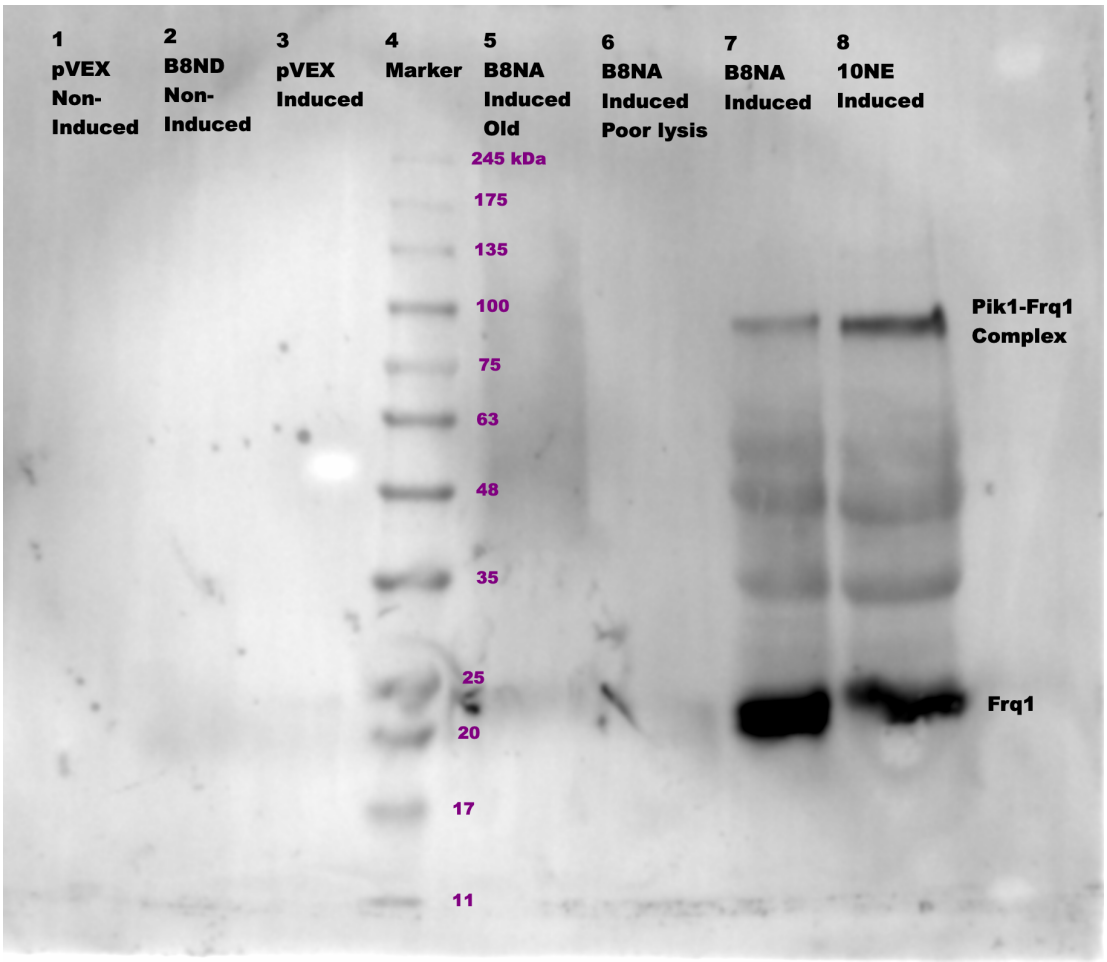

Figure 31: A Western blot showing the expression of Frq1 and the Pik1-Frq1 complex in B8NA and 10NE induced with galactose. B8NA: transformed BJ2168 with clone 8 (pYEXC3H+PIK1) and clone N (pESC-Trp+FRQ1+CDC37) at the same time, colony A. 10NE: transformed BJ2168 with clone 10 (pYEXC3H+PIK1) and clone N (pESC-Trp+FRQ1+CDC37) sequentially, colony E. The Western blot was performed by Candace Panagabko (Brock University). The samples of yeast cells were lysed using the boiling protocol or glass beads prior to subjection to SDS-PAGE. The proteins where blotted onto a PVDF membrane and an anti-FLAG primary antibody was used for detection.

4.6 Purification

The complete expression and purification of the Pik1-Frq1 complex was attempted twice; however, both attempts were unsuccessful at yielding the complex. The FPLC was set up with a UV-Vis detector to monitor the eluate from the IMAC column at 280nm to detect protein. No protein peak was detected during the imidazole elution steps for either attempt. This is possibly due to low expression levels; however, protein expression was not measured in these experiments. The expression of the Pik1-Frq1 complex was confirmed by the Western blot, and therefore the expression and purification of the complex just needed to be fine-tuned and optimized. It was deemed more critical to move on to the development of a time-resolved assay and therefore this work was set aside for future students to continue and focus was placed on assay development.

5 Results and Discussion: Development of the Assay

Assay development requires answers to questions regarding buffer components and their concentrations, the concentrations of assay components, signal intensity, and the reliability and sensitivity of the instrument. The following sections describe efforts to elucidate this information.

5.1 Assay Plates and Instrument Settings and Sensitivity

The first questions that were addressed were regarding the plate reader. Which plate reader should be used? Is the plate reader sensitive enough to distinguish between the high and low FI signals? If so, what settings are required so that the plate reader can do that? Which excitation, emission, and cutoff wavelengths should be used? Which microplates should be used for the assay?

These questions were answered over the course of 3 months as 4 different plate readers were attempted in succession: Cary Eclipse (Agilent Technologies), POLARstar Optima (BMG LABTECH), SpectraMax i3 (Molecular Devices), and SpectraMax M2 (Molecular Devices). The FI assay window experiment was used to determine the sensitivity of the instrument and the settings required to achieve a FI window in which the high signals are at least 5 times greater than the low signals. The narrow difference between the optimal excitation and emission wavelengths of the ADP Alexa Fluor® 594 Tracer posed an issue (especially for the older machines, thus making the use of the newer machines essential). It was determined that 575nm, 620nm, and 610nm should be used for the excitation, emission, and cutoff wavelengths respectively. The use of ½ area plates instead of full area plates was also deemed essential. The Cary Eclipse and POLARstar Optima were not sensitive enough to distinguish the difference between the high and low FI samples. Both SpectraMax i3 and SpectraMax M2 were adequate for this assay but SpectraMax M2 was used because it was more readily available for use. A default setting of the software of SpectraMax M2 when performing kinetic measurements is to "Set first data point to zero". When this data reduction setting was on, it normalized all the data to 0, making the high and low FI measurements the same, resulting in illogical and meaningless data. This setting must therefore be turned off. One benefit is that this setting effects the processing and presentation of the data, but not the acquisition of the data. Therefore, file(s) that were recorded with this setting on were opened, this box unchecked, and the file saved with the raw/unnormalized data.

5.2 How the Commercial Bellbrook Transcreener ADP FI Assay Is Designed to Work and How the Protocol Was Modified to Make the Assay Time-Resolved

The assay kit was designed as an endpoint assay in which the enzyme reaction occurs in 25µL for a particular amount of time, then the enzyme activity is stopped by adding 25µL of the 1x Detection Mixture which contains EDTA. EDTA strips the metal cation from the active site of the enzyme effectively stopping the reaction from continuing. During the 1-hour incubation period, the ADP that was produced during the enzyme reaction displaces the ADP Alexa Fluor® 594 Tracer from the ADP^2 Antibody-IR Dye® QC-1. After the 1-hour incubation, the fluorescence intensity is measured once.

The key changes that needed to be made and/or accounted for to make this a time-resolved assay, were a change in the enzyme reaction volume from 25µL to 50µL, the removal of EDTA, and an increase in the number of FI measurements. The enzyme reaction and the detection components need to be added together and at the beginning of the assay, thus increasing the enzyme reaction volume to 50µL instead of 25µL. The amounts of the assay components need to be increased to account for this increase in volume so that the concentrations were sufficient. The buffer does not contain EDTA so that the enzyme remains functional throughout the duration of the measurements. The last key change is a change in the data acquisition, such that the FI is measured at regular time intervals for the duration of the assay.

The two solutions defined in the endpoint protocol are the Enzyme Reaction Mix and the 1x ADP Detection Mixture. How these two solutions are defined, what is in each of them and how they are used, were not conducive to a time-resolved assay (one for enzyme reaction, one to stop the reaction and detect the signal). Therefore, two different solutions were defined: the Enzyme Mix and the Assay Mix (to be mixed with each other at the beginning to start the reaction) (Table 20). The ATP and acceptor substrate were included in the Assay Mix instead of with the enzyme, and the concentrations in the Enzyme Mix and Assay Mix were such that when 20µL of Enzyme Mix was added to 30µL of Assay Mix, each component had the desired concentration in the 50µL assay. It

was decided to change the recipe from 25µL + 25µL = 50µL to 20µL + 30µL = 50µL because the solutions were getting mixed at the beginning of the reaction anyway, so the volume proportions did not matter with respect to the enzyme reaction volume. It made it easier to pipette all the components into the assay mix and keep the volume below 30µL/assay, and 20µL of "space" for the enzyme titration was helpful to get a wide range of enzyme concentrations. For example, if the volume split was 40/10 instead, then the highest concentration of enzyme available would be 10µL/50µL of the reconstituted/commercial (highest concentration) enzyme stock, instead of 20µL of this stock, which would give a lower maximum enzyme concentration and a smaller enzyme concentration window to work in for the titration.

Table 20: The components of the two solutions for the Endpoint and Time-Resolved assay formats.

Endpoint	Time-Resolved
Complete Enzyme Reaction Mix: Enzyme Autoclaved mQH_2O ATP Acceptor Substrate	Enzyme Mix: Enzyme Autoclaved mQH_2O
1x ADP Detection Mixture: ADP^2 Antibody-IRDye® QC-1 ADP Alexa Fluor® 594 Tracer Stop and Detect Buffer B Autoclaved mQH_2O	Complete Assay Mix: ADP^2 Antibody-IRDye® QC-1 ADP Alexa Fluor® 594 Tracer Assay Buffer Autoclaved mQH_2O ATP Acceptor Substrate

Figure 32 and 33 outline the procedures for the endpoint and time-resolved assays. The colour coding in Table 20 matches the colour coding in Figures 32 and 33.

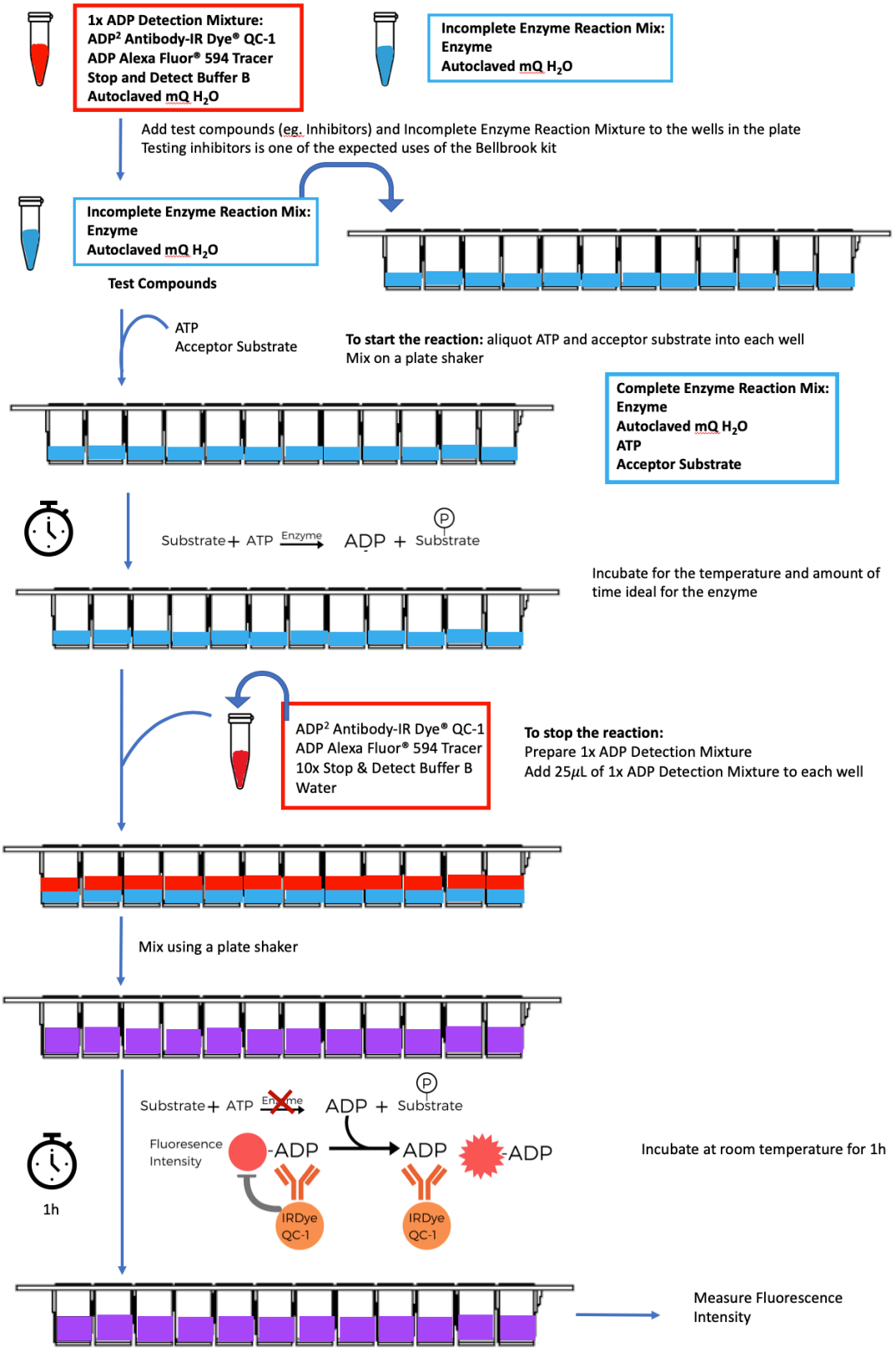

Figure 32: Endpoint Format. The commercial design for the Bellbrook Transcreener® ADP² FI Assay.

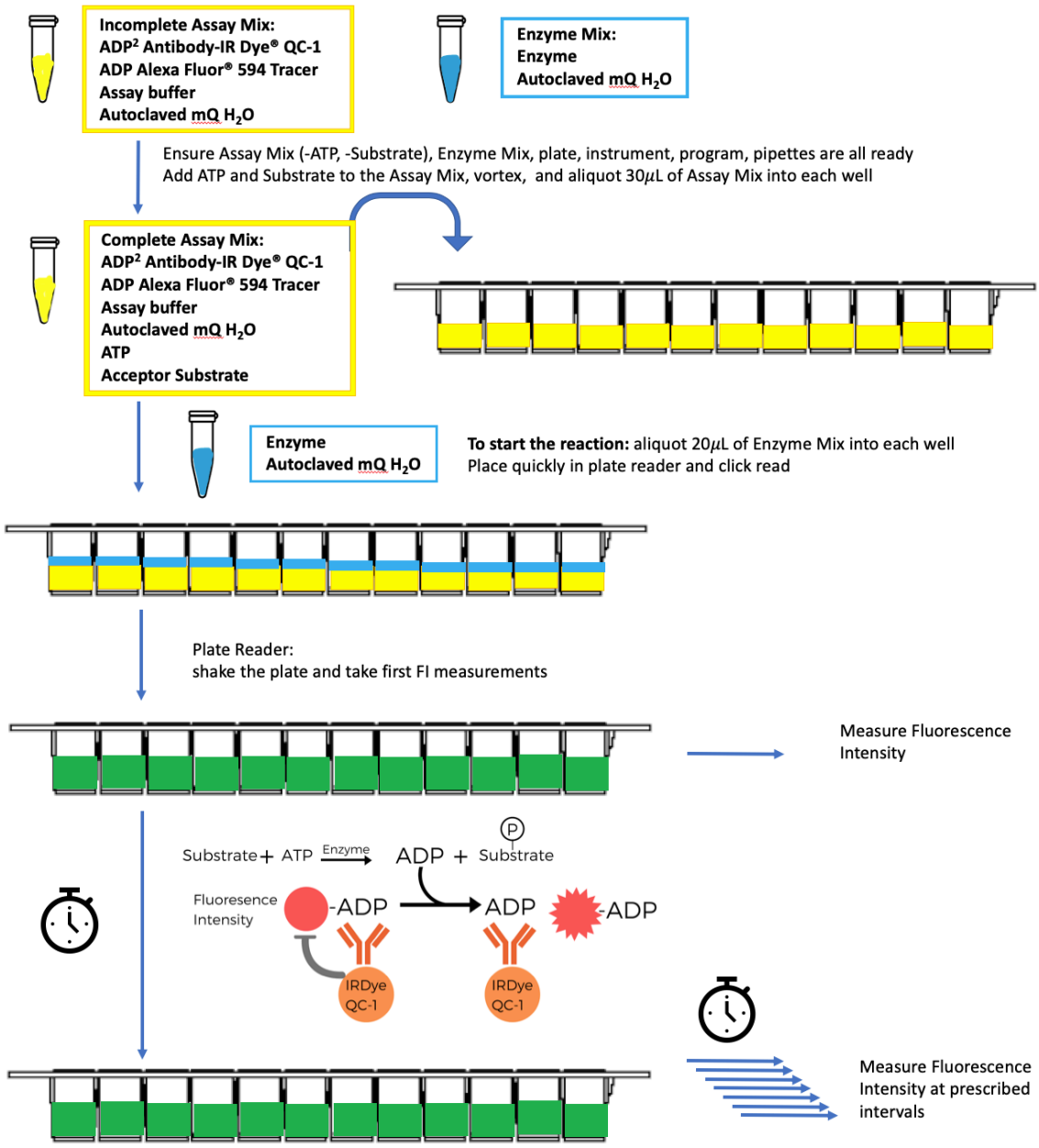

Figure 33: Time-resolved Format. The application of the Bellbrook Transcreener® ADP² FI Assay that was developed and described in this thesis.

The end-point assay format measures the FI at a single arbitrary time-point. The time-resolved assay format measures the FI at many time points throughout the progression of the reaction. As a result, kinetic data on kinase activity can easily be obtained. A diagram of the type of data generated by each format can be seen in Figure 34.

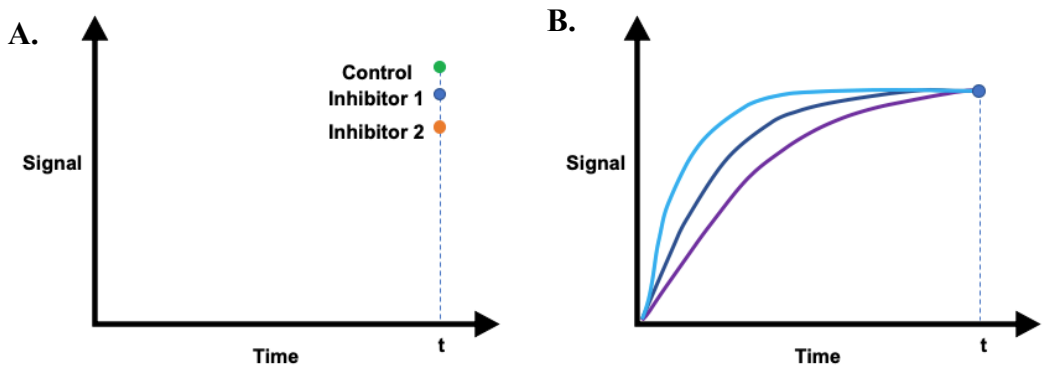

Figure 34: A comparison between the data gathered from the end-point vs time-resolved formats. **A.** A representation of typical data gathered from the end-point format. A FI signal is measured at a single arbitrary time point, which is insufficient for measuring initial rates. This format is typically used to measure the effect of inhibitors on kinase activity. **B.** A representation of typical data gathered from the time-resolved format. The FI is measured at regular intervals during the course of the assay, and thus gives sufficient information for measuring initial rates.

5.3 The PKA Assay

The purpose of the PKA assay was to learn how to use the plate reader, how to use the Bellbrook Transcreener® ADP^2 FI Assay kit, and to figure out how to adapt this commercial kinase kit into a time-resolved assay. This process was detailed above. The following section presents the data that shows the successful development of a time-resolved assay.

5.3.1 The Maximum FI Window for the PKA Assay Conditions

Before the assay could be carried out, it was essential to determine the FI window for the PKA assay conditions (Figure 35). The mean FI for the minimum FI sample (Min FI) was 0.65 RFUs and that of the maximum FI sample (Max FI) was 8.29 RFUs. Max FI was over 12-fold greater than Min FI, which was excellent because the ratio of Max FI:Min FI must be greater than 5 for the window to be wide enough for the assay. The maximum FI window for the PKA assay conditions was 7.65 RFUs.

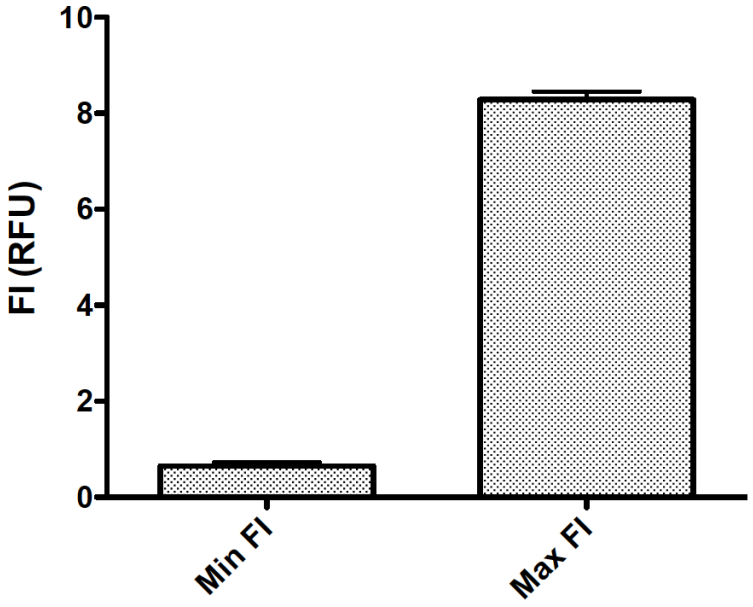

Figure 35: The FI window for the PKA assay conditions. Min FI: 9.66µg/mL ADP^2 Antibody-IRDye® QC-1, 0.5x 10x PKA Assay and Detect Buffer, 4nM ADP Alexa Fluor® 594 Tracer. Max FI: 0.5x 10x PKA Assay and Detect Buffer, 4nM ADP Alexa Fluor® 594 Tracer.

5.3.2 The ATP/ADP Standard Curve for the PKA Assay Conditions

An ATP/ADP standard curve was obtained for the PKA assay conditions (Figure 36). This standard curve mimicked an enzyme reaction over 12 points in which ATP was decreasing and ADP was increasing proportionally. The FI was plotted against the log[ADP] and a linear regression of the ATP/ADP standard curve was conducted to give the equation: $y = 1.361x + 4.424$. This curve correlates FI and the concentration of ADP produced; therefore, the equation could be used to calculate %ATP conversion based on FI and vice versa. The [ATP] used in this assay was 10µM, therefore 10% ATP conversion corresponds to 1µM ADP. Based on the equation, an FI equal to or lower than 4.42 RFUs corresponds with a % ATP conversion that is 10% or lower. It is important to have this estimate for the assays because the aim is to choose enzyme and substrate concentrations and run the assay for the time corresponding to less than 10% ATP conversion to ensure that the assumption of initial rates of conversion hold true, where the change in [ATP] is small enough to not significantly decrease the rate of the enzyme (99, 100).

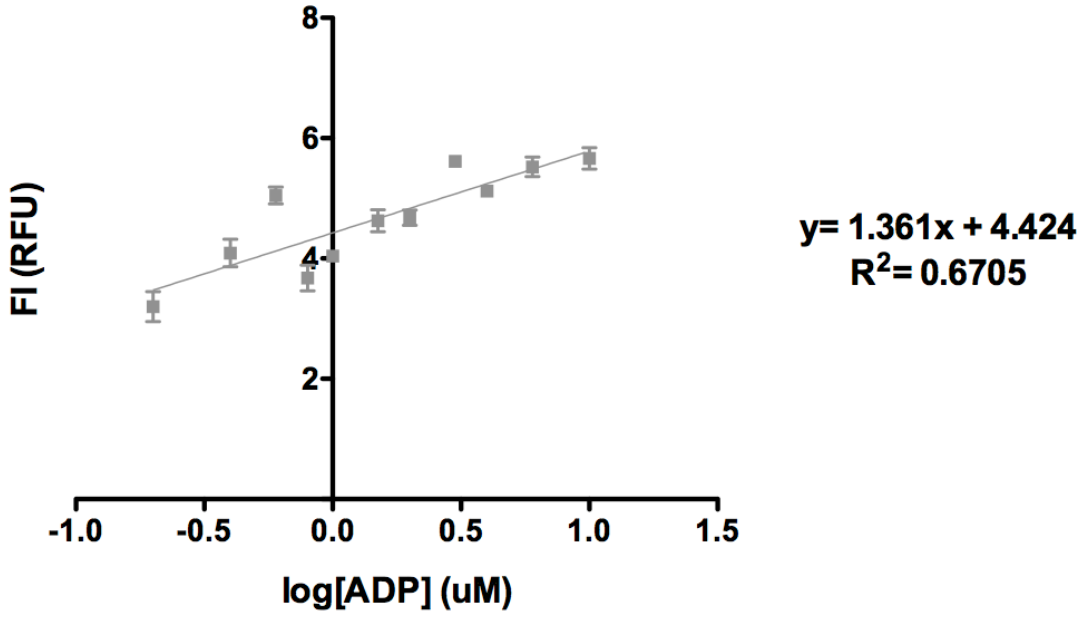

Figure 36: ATP/ADP standard curve for the PKA assay conditions. Varied [ATP] and [ADP], 2.4mg/mL DTT, 4mM Mg^{2+}, 4.8mg/mL casein, 9.66µg/mL ADP^2 Antibody-IRDye® QC-1, 4nM ADP Alexa Fluor® 594 Tracer, 50mM HEPES, 0.01% Brij

5.3.3 Assay Results

The time-resolved assay of PKA was conducted at 8 different concentrations of PKA ranging between 0.22 units/mL and 220 units/mL (Figures 37 and 38). An increase in signal over the time of the assay was observed for all concentrations of PKA except 0.22 units/mL and 2.2 units/mL. The evolution of a FI signal over time that was dependent on the kinase concentration and therefore dependent on the production ADP by a kinase was observed. Therefore, this data showed that the goal of adapting the Bellbrook Transcreener® ADP² FI Assay kit into a time-resolved assay was accomplished.

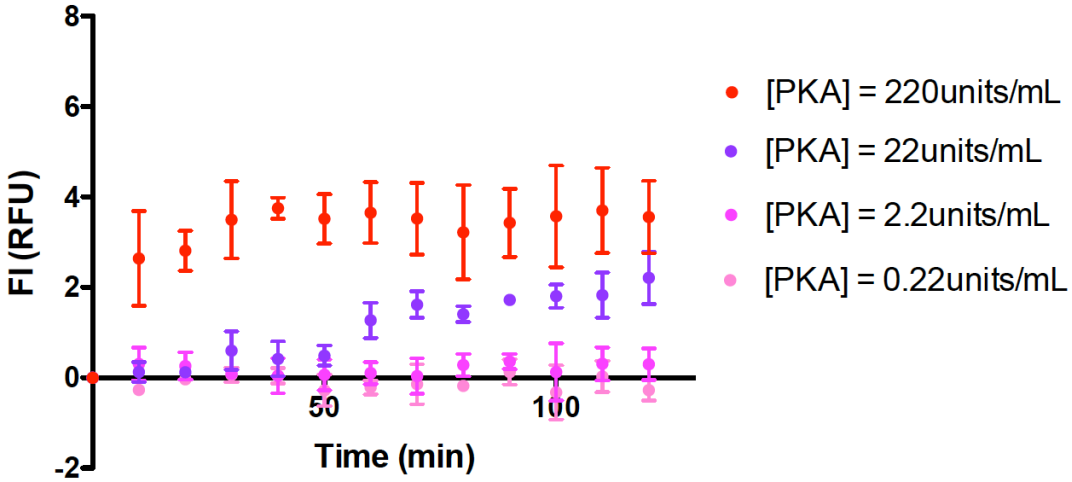

Figure 37: Time-Resolved assay of PKA using the Bellbrook Transcreener® ADP² FI Assay. The evolution of FI was measured over 120min for 4 different concentrations of PKA. 10µM ATP, 2.4mg/mL DTT, 4mM Mg^{2+}, 4.8mg/mL casein, 9.66µg/mL ADP² Antibody-IRDye® QC-1, 4nM ADP Alexa Fluor® 594 Tracer, 50mM HEPES, 0.01% Brij

The enzyme titration had two purposes, first to establish if the evolution of the signal was dependent the concentration of enzyme (as it would be expected to), and second to determine the optimal PKA concentration for these assay conditions (Figure 38). To ensure that kinase reactions are performed under initial rate conditions it is important to use a concentration of enzyme that results in less than 10% ATP conversion over the time of the assay. Based on the ATP/ADP standard curve for the PKA assay conditions, an FI equal to or lower than 4.42 corresponds with a % ATP conversion that is 10% or lower. It is also important that the enzyme concentration is chosen such that

the time of the assay is much longer than 20min. This is because the equilibration time for the ADP Alexa Fluor® 594 Tracer and the ADP^2 Antibody-IRDye® QC-1 is greater than ≥ 15min, making it difficult to quantify ADP production during short term enzyme reactions. Based on the enzyme titration shown in Figure 38, the enzyme concentrations between 100-220 units/mL (inclusive) are too high; they all reach a FI around or above 4 by 20min. Therefore, past 20min the enzyme reactions are no longer in initial rate conditions and before 20min the reaction time is too short to reliably quantify the rate of production of ADP because of the equilibration time of the ADP Alexa Fluor® 594 Tracer and the ADP^2 Antibody-IRDye® QC-1. These traces all also overlap during the first 20 min and there is no significant difference between them; thus, increasing the concentration of PKA past 100 units/mL does not result in a significant change in rate. This likely indicates that at or above ~100units/mL the speed of ADP production is quicker than the displacement of ADP Alexa Fluor® 594 Tracer from the ADP^2 Antibody-IRDye® QC-1. Therefore, the rate of signal production measured in these assays was actually likely the rate of displacement rather than the rate of phosphorylation by PKA. Based on Figures 37 and 38, 22units/mL is the most optimal assay concentration of PKA out of the ones that were tested. This is because the signal increased off the baseline and the % ATP conversion did not exceed 10%.

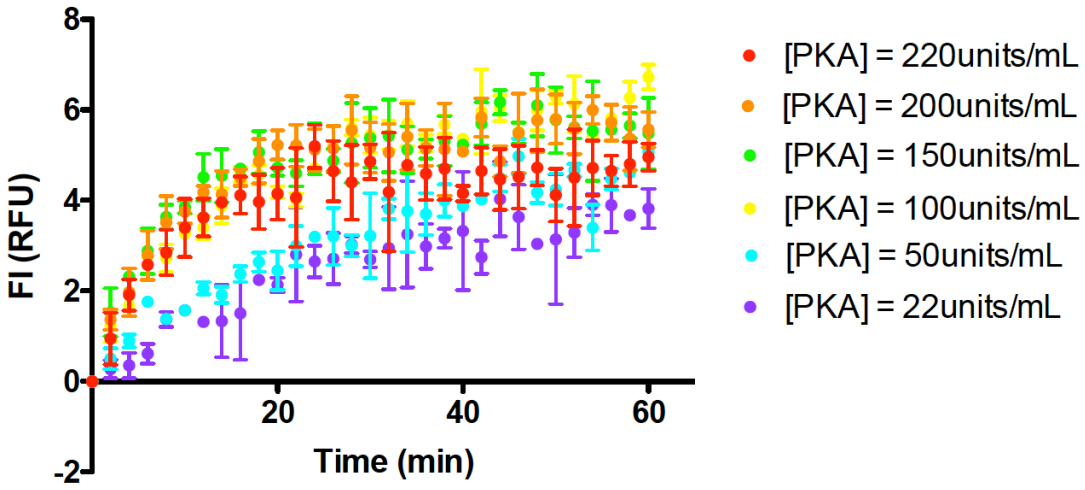

Figure 38: PKA titration for the time-Resolved assay of PKA using the Bellbrook Transcreener® ADP^2 FI Assay. The evolution of FI was measured over 60min for 6 different concentrations of PKA. 10µM ATP, 2.4mg/mL DTT, 4mM Mg^{2+}, 4.8mg/mL casein, 9.66µg/mL ADP^2 Antibody-IRDye® QC-1, 4nM ADP Alexa Fluor® 594 Tracer, 50mM HEPES, 0.01% Brij.

5.3.4 Controls

The Background, the No Antibody, and the No Tracer controls all gave the expected results (Figure 39). There was no ADP Alexa Fluor® 594 Tracer to give the FI signal in the Background and in the No-tracer controls, therefore the baseline FI measurements that were observed, was expected. In the No Antibody control there was no ADP^2 Antibody-IRDye® QC-1 to quench the fluorescence of the ADP Alexa Fluor® 594 Tracer, therefore a FI around the Max FI was expected and that was observed. There was no evolution of signal in the absence of ATP (No ATP control). This was the expected result and shows that the signal generated in the assays is from the hydrolysis of ATP to ADP. The enzyme titration in light of the No ATP control shows that the signal generated was from the hydrolysis of ATP to ADP by the enzyme as the signal evolution is dependent on the concentration of the PKA.

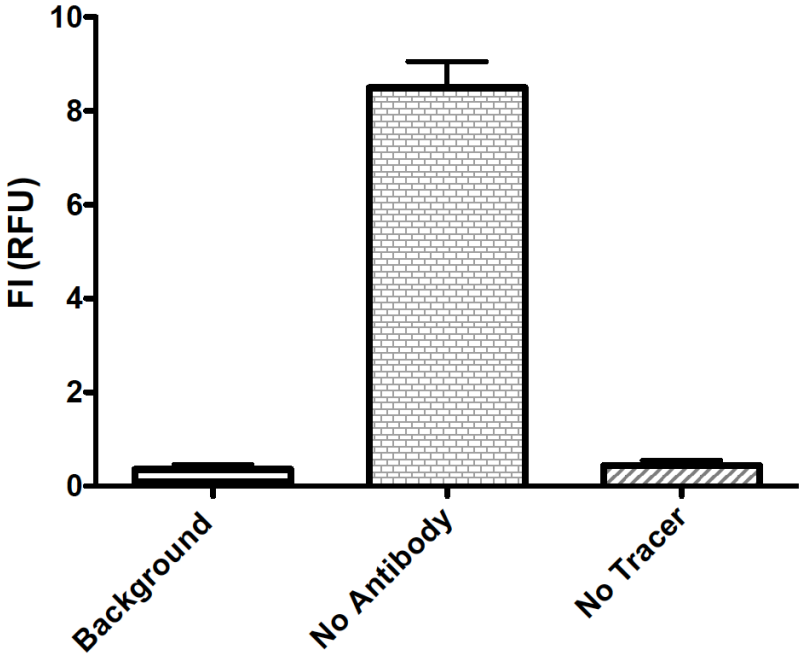

Figure 39: The Background, the No Antibody, and the No Tracer controls for the time-resolved PKA assay. None of these controls contained PKA. Background: Assay conditions but no antibody and no tracer. No Antibody: Assay conditions but no antibody. No Tracer: Assay conditions but no tracer. Assay conditions: 10µM ATP, 2.4mg/mL DTT, 4mM Mg^{2+}, 4.8mg/mL casein, 9.66µg/mL ADP^2 Antibody-IRDye® QC-1, 4nM ADP Alexa Fluor® 594 Tracer, 50mM HEPES, 0.01% Brij.

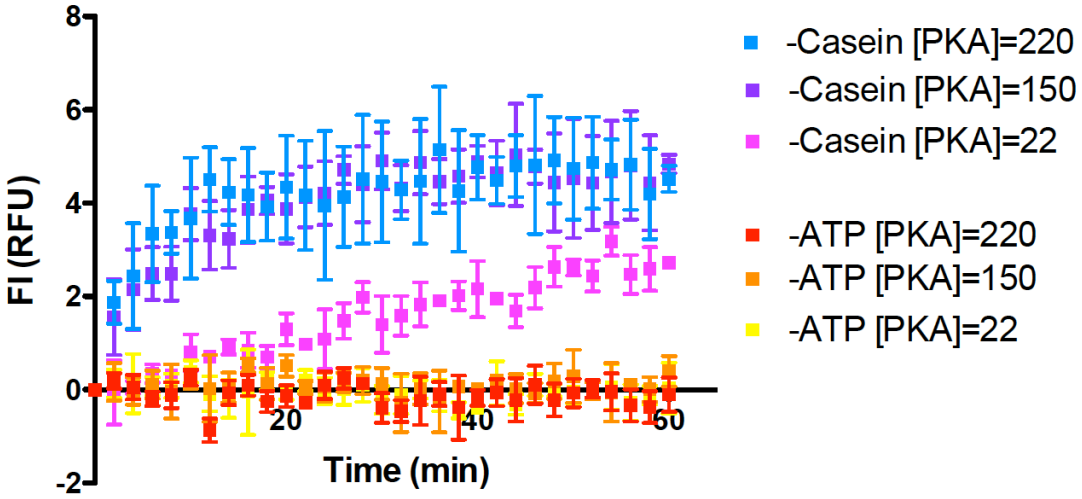

Figure 40: The No Casein (-Casein) and No ATP (-ATP) controls for the time-resolved PKA assay. [PKA] is found in the figure in units/mL. No Casein: Assay conditions but no casein. No ATP: Assay conditions but no ATP. Assay conditions: 10µM ATP, 2.4mg/mL DTT, 4mM Mg^{2+}, 4.8mg/mL casein, 9.66µg/mL ADP^2 Antibody-IRDye® QC-1, 4nM ADP Alexa Fluor® 594 Tracer, 50mM HEPES, 0.01% Brij.

This data also showed some inconsistencies and results that raise questions. The No Casein control was expected to result in no evolution of signal because one of the enzyme substrates was not included in the assay. However, signal did evolve, and the evolution was dependent on the concentration of the enzyme (Figure 40). This indicated PKA was either conducting non-productive ATP hydrolysis, auto-phosphorylation, or phosphorylation of other molecules of PKA. In addition, the data presented in Figure 37 and Figure 38 were collected on two consecutive days and the signal intensity and speed of evolution of the signal were very different for the same concentrations of PKA on the two consecutive days. These were inconsistencies that would have been important to address if PKA or another protein kinase was the protein of interest. However, the purpose of doing a PKA assay was to learn to how to use the plate reader, to learn how to use the Bellbrook Transcreener® ADP^2 FI Assay kit, and to adapt the kit into a time-resolved assay. These things were accomplished with the PKA assay. Additionally, the overall goal of the project was the develop a vesicle-based time-resolved assay for the lipid kinase Pik1. Therefore, these concerns were left unaddressed as it was deemed more advantageous for the project to progress to a PI kinase related to Pik1 to develop the time-resolved assay relevant for a vesicle-based for the activity assay of a lipid kinase.

5.4 The PIK3C3 Assay

5.4.1 10x PIK3C3 Assay Buffer: Precipitation Problems

Table 21: The recipe for the 10x PIK3C3 Assay Buffer

Original Plan	Final Recipe
250mM HEPES (pH 7.5) 500mM NaCl 30mM $MgCl_2$ 0.25mg/mL BSA 50mM $MnCl_2$ 20mM DTT Stored at -20°C	250mM HEPES (pH 7.5) 500mM NaCl 30mM $MgCl_2$ 0.25mg/mL BSA Made with autoclaved mQH_2O, filter sterilized, and stored at room temperature

The original composition of the assay buffer was derived from the ADP-Glo® Lipid Kinase Systems technical manual (100) with some influence from (99). 50mM HEPES (pH 7.5), 50mM NaCl, 3mM $MgCl_2$, 0.025mg/mL BSA, 5mM $MnCl_2$ is the PI3K reaction buffer described in the ADP-Glo® technical manual for PIK3C3. It was decided to use 250mM HEPES (pH 7.5) instead of 500mM HEPES for the 10x Assay buffer because 25mM HEPES (pH 7.5) is contributed to the assay by the lipid dilution buffer. DTT was included in the original plan because it was in the kinase reaction buffer in (99). Mn^{2+} is instructed to be added specifically for assaying PIK3C3 because the enzyme is more active with Mn^{2+} than in Mg^{2+} (38). The ADP-Glo technical manual said to use Mn^{2+} and Bellbrook Transcreener® ADP^2 FI Assay technical manual said to use either Mg^{2+} or Mn^{2+} and that either would be okay to use with the kit.

Many precipitation problems were encountered when making the 10x PIK3C3 Assay Buffer. The first time it was made, DTT was not used and something precipitated. The second attempt included DTT and something precipitated. DTT and Mn^{2+} are both redox sensitive, and since the presence or absence of DTT did not stop the precipitation, and the Promega ADP-Glo manual described an assay buffer for PIK3C3 that contained $MnCl_2$ but not DTT, it was decided to omit DTT until it was deemed necessary or beneficial to the assay. The precipitation occurred when $MnCl_2$ was added to the buffer; therefore, it was concluded that it was precipitating with another component of the assay

buffer. To figure out which two components were precipitating, a solution of ~250mM HEPES and ~50mM $MnCl_2$ (pH 7.5) was made and each buffer component was sequentially added and observed for precipitation. A white precipitate was observed upon the addition of 1mg/mL BSA. It was discovered that the BSA was in a solution of PBS and that $Mn_3(PO_4)_2$ is very insoluble and precipitates (pK_{sp} = 23.83 (105)) . A white precipitate was observed when PBS was added to another solution of ~250mM HEPES and ~50mM $MnCl_2$ (pH 7.5) but no precipitate was observed when a solution of BSA in RO H_2O was used to make 10x PIK3C3 Assay Buffer. This confirmed the precipitate was $Mn_3(PO_4)_2$ and it eliminated the first precipitation problem.

The second precipitation problem was encountered when the pH of the 10x PIK3C3 Assay Buffer was adjusted after all the components of the buffer were in solution. A white precipitate was observed when NaOH was added to adjust the pH to 7.5. From previous research about Mn^{2+} precipitation, it was known that $Mn(OH)_2$ precipitates ($K_{sp} = 4.6 \times 10^{-14}$ (106), pK_{sp} = 13.34) . The solution of $MnCl_2$ was added after the pH was adjusted to 7.5 and no precipitate was observed. This eliminated the second precipitation problem.

Once the 10x PIK3C3 Assay Buffer was successfully made without precipitation, it was filter sterilized and stored at -20°C overnight. This was how the PKA buffer was stored and there were no issues with storing the PKA buffer at this temperature. However, when the 10x PIK3C3 Assay Buffer was thawed the next day a cream-coloured solid had formed and collected at the bottom of the tube. The FI Window Experiment was done with this precipitated 10x PIK3C3 Assay Buffer and the 10x PKA Assay Buffer to compare them. In addition, 10x PIK3C3 Assay Buffer -$MnCl_2$ (no $MnCl_2$) and fresh, never frozen 10x PIK3C3 Assay Buffer were made. The FI Window Experiment was done with these buffers before and after they were stored overnight at either room temperature, 4°C, or -20°C. The buffers were judged by the size of the FI assay window and by the presence of precipitate based on crude visual observations.

The best results (determined by the widest FI window and no turbidity) were achieved using the 10x PIK3C3 Assay Buffer -$MnCl_2$ that was stored at room

temperature. The FI window for this buffer was 7.40 RFUs. The fresh 10x PIK3C3 Assay Buffer stored at room temperature resulted in an FI window of 4.04 RFUs, which is a narrower FI window than the one without $MnCl_2$. However, no turbidity was observed, and the Max FI:Min FI ratio was 8.5, which is sufficient for the assay. In addition, PIK3C3 is more active with Mn^{2+} than Mg^{2+}, therefore the 10x PIK3C3 Assay Buffer (containing Mn^{2+}) was chosen to proceed with in assays. Storing the 10x PIK3C3 Assay Buffer at room temperature eliminated the third precipitation problem. It was noticed that the FI assay window was not always consistent. In the future the FI window should be measured each time the assay is run, and the data normalized to be presented as a percentage of the maximum signal.

By eliminating the first 3 precipitation problems, the 10x PIK3C3 Assay Buffer could be prepared, adjusted to a pH of 7.5, filter sterilized, and stored without precipitation occurring. However, a fourth precipitation problem was observed when the ADP^2 Antibody-IRDye® QC-1 was added to the Assay Mix. The components of the Assay Mix were added in a different order each time and it was noticed that the solution became turbid when the ADP^2 Antibody-IRDye® QC-1 and the 10x PIK3C3 Assay Buffer were both present. However, the cause of the turbidity was still unclear. Therefore, each component of the assay and each step of assay component preparation was scrutinized to determine possible sources of problems. Two key things were identified, the first being the use of water with varying degrees of purity. Nucleases can degrade nucleotide substrates and products, therefore, using water that is contaminated with nucleases reduces assay performance. Just in case the water purity was compromising the assay performance, all of the stock solutions and buffers involved in the assay and in the preparation of assay components were re-made using autoclaved mQH_2O (*eg.,* 2.5x Lipid Dilution Buffer, the 1N HCl and 1N NaOH for adjusting the pH, 500µM ATP, 10x PIK3C3 Assay Buffer, 5µg/mL PIK3C3, the Enzyme Mix and the Assay Mix). The second key thing that was identified was the fact that the ADP^2 Antibody-IRDye® QC-1 comes in a 100mM KH_2PO_4 buffer. Mn^{2+} is known to precipitate with phosphate, therefore, this was suspected to be the source of the fourth precipitation problem. This was investigated by making 5 simplified buffers of the following compositions:

1. 250mM HEPES (pH 7.5)
2. 250mM HEPES (pH 7.5), 500mM NaCl
3. 250mM HEPES (pH 7.5), 30mM $MgCl_2$
4. 250mM HEPES (pH 7.5), 0.25mg/mL BSA
5. 250mM HEPES (pH 7.5), 50mM $MnCl_2$

ADP[2] Antibody-IRDye® QC-1 (2µL) was added to 10µL of each of the simplified buffers. All of the resulting solutions were clear and colourless except for #5, which contained $MnCl_2$, where a white precipitate formed. To investigate the hypothesis that the precipitation was caused by the KH_2PO_4 buffer and not the antibody itself, a solution of 100mM KH_2PO_4 (pH 8.5) was made and 2µL of this buffer was added to 10µL of each of the following solutions:

1. 250mM HEPES (pH 7.5)
2. 250mM HEPES (pH 7.5), 30mM $MgCl_2$
3. 250mM HEPES (pH 7.5), 50mM $MnCl_2$
4. 250mM HEPES (pH 7.5), 30mM $MgCl_2$, 50mM $MnCl_2$

No turbidity was observed with solutions 1 and 2, but a white precipitate was observed with solutions 3 and 4. This confirmed that Mn^{2+} was precipitating with the phosphate from the KH_2PO_4 buffer of the ADP[2] Antibody-IRDye® QC-1. This also confirmed that the other metal cation, Mg^{2+}, does not cause this effect. The removal of $MnCl_2$ from the 10x PIK3C3 Assay Buffer eliminated the fourth precipitation problem.

The effect of the precipitation on the assay signal is reported and discussed in the following section. The requirement that PIK3C3 has for Mn^{2+} and the necessity of Mn^{2+} to the assay is explored and discussed in Assay Results.

5.4.2 "False Signal" Troubleshoot: Precipitate or Lipids?

The assay was attempted for the first time before all of the precipitation problems had been solved. The data that was gathered was "meaningless" because all of the trials overlapped each other despite differences in the concentration of enzyme, and all are elevated off the baseline and do not change substantially overtime (Figure 41). Especially odd was that the no enzyme control in which no ADP was being produced overlapped with the other trials. It was suspected that the false signal was caused by light scattering from the precipitate. However, this was also the first time that lipid vesicles

were used as the substrate. Therefore, the lipids could not be ignored as a potential source of false signal and this was also investigated.

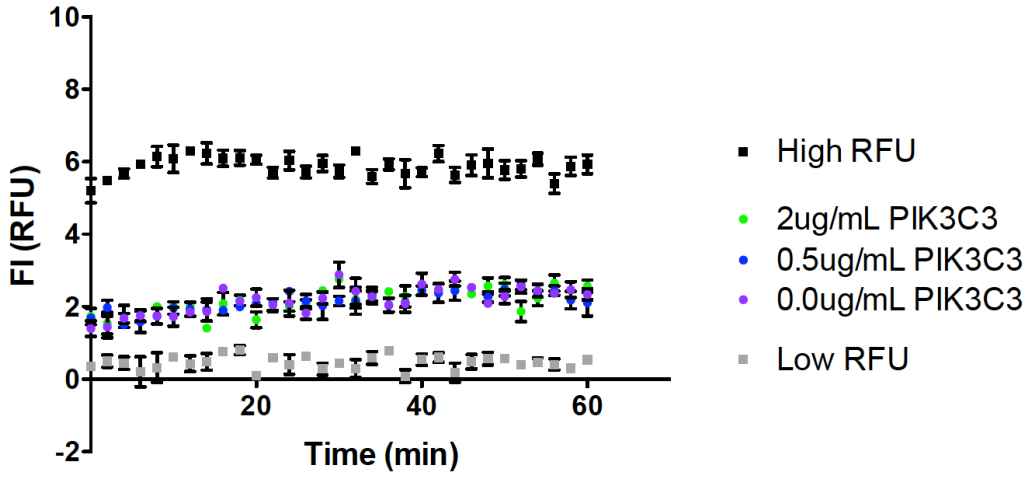

Figure 41: PIK3C3 time-resolved assay when precipitate was present. Variable [PIK3C3]. Assay conditions: 30µM ATP, 0.2mg/mL PI:3PS, 1x Lipid Dilution Buffer (25mM HEPES, 0.5mM EGTA), 28.25µg/mL ADP^2 Antibody-IRDye® QC-1, 4nM ADP Alexa Fluor® 594 Tracer, 1x PIK3C3 Assay Buffer (25mM HEPES, 50mM NaCl, 3mM $MgCl_2$, 0.025mg/mL BSA, 5mM $MnCl_2$).

There were two hypotheses regarding the lipids as a source of a false signal. The first was that the lipid vesicles were aggregating (caused by the negatively charged lipids and the positively charged metal cations in the buffer) and getting large enough to scatter the light. The second hypothesis was that the lipids provide a different environment for the fluorophore and change the fluorescence, leading to the false signal. A series of lipid controls were completed, and the results can be seen in Figure 42.

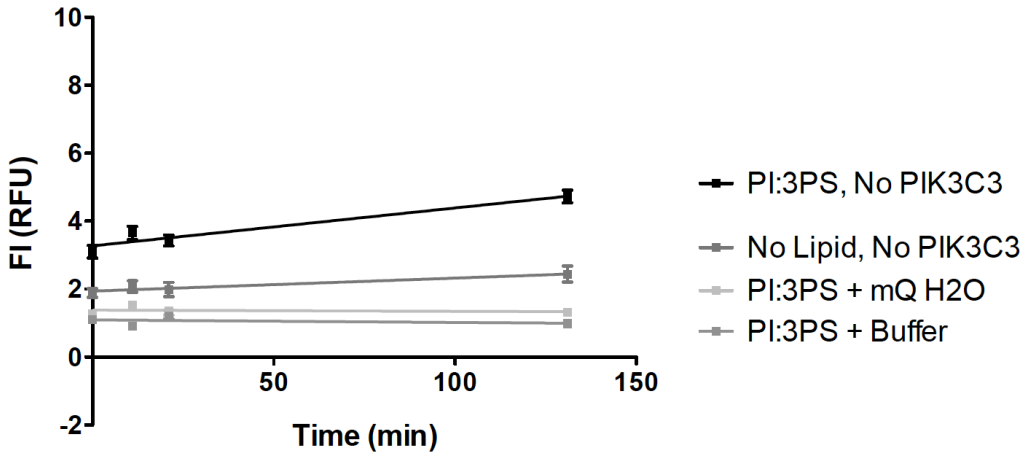

Figure 42: Lipid Controls in Mn^{2+} containing buffer. PI:3PS, No PIK3C3: Assay conditions with no PIK3C3. No Lipid, No PIK3C3: 30µM ATP, 28.25µg/mL ADP[2] Antibody-IRDye® QC-1, 4nM ADP Alexa Fluor® 594 Tracer, 1x PIK3C3 Assay Buffer (25mM HEPES, 50mM NaCl, 3mM $MgCl_2$, 0.025mg/mL BSA, 5mM $MnCl_2$). PI:3PS + mQH_2O: 0.2mg/mL PI:3PS, 1x Lipid Dilution Buffer (25mM HEPES, 0.5mM EGTA). PI:3PS + Buffer: 0.2mg/mL PI:3PS, 1x Lipid Dilution Buffer (25mM HEPES, 0.5mM EGTA), 1x PIK3C3 Assay Buffer (25mM HEPES, 50mM NaCl, 3mM $MgCl_2$, 0.025mg/mL BSA, 5mM $MnCl_2$).

The PI:3PS + mQH_2O and the PI:3PS + Buffer controls showed that the phospholipid vesicles on their own did not aggregate over time or even in the presence of the metal cations from the assay buffer. The FI is approximately "baseline" (*i.e.,* the Min FI), but there was no fluorophore or antibody in these controls, therefore, the vesicles may have contributed in a small way to the signal via light scattering. Precipitation was observed in two of the controls (PI:3PS, No PIK3C3 and No Lipid, No PIK3C3, Figure 42). These controls had elevated FI and seemed to increase slightly over time even though there was no enzyme. This may be because of increased precipitation as particles became larger over the time of the assay. The only difference between the PI:3PS, No PIK3C3 control (everything but enzyme) and the No Lipid, No PIK3C3 control was the presence of lipid, but the PI:3PS, No PIK3C3 control was much higher in signal. This could mean that the lipid was making the precipitation problem worse by co-precipitating, by scattering some light without aggregating or precipitating, or the lipid environment may be influencing the fluorophore. However, it was not very likely that the ADP Alexa Fluor® 594 Tracer was entering into the lipid environment of the vesicles because the headgroups of the phospholipids (PS) are negatively charged and the ADP Alexa Fluor® 594 Tracer is also negatively charged. It was, therefore, concluded that the

inorganic precipitate was likely the problem instead of the lipid. The solution was to remove $MnCl_2$ from the 10x PIK3C3 Assay Buffer. The assay was attempted with this new buffer recipe and the results of the PIK3C3 assays are reported in the following Section.

5.4.3 The Maximum FI Window for the PIK3C3 Assay Conditions

Before the assay could be carried out, it was essential to determine the FI window for the PIK3C3 assay conditions (Figure 43). The mean FI for the minimum FI sample (Min FI) was 0.73 RFUs and that of the maximum FI sample (Max FI) was 7.56 RFUs. Max FI was over 10-fold greater than Min FI, which was excellent because the ratio of Max FI:Min FI must be greater than 5 for the window to be wide enough for the assay. The FI window for the PIK3C3 assay conditions was 6.83 RFUs. This FI window is 1.41 RFUs greater than that measured with Mn^{2+} containing buffer (Figure 41). The FI of the mean of the Max FI sample increases from 5.88 RFUs when Mn^{2+} is present to 7.56 RFUs when Mn^{2+} is not present. An absorption spectrum of 5mM $MnCl_2$ was measured (GENESYS 10S UV-Vis) from 190nm-800nm. A peak with an absorbance of 2.5 was observed at 200nm, but no absorbance was observed between 250-800nm. Therefore Mn^{2+} was not decreasing the fluorescence by absorbing some of the excitation or emission light. It is possible that Mn^{2+} was quenching some of the fluorescence; Mn^{2+} is known to quench the fluorescence of a different fluorophore called Fura-2 (107, 108).

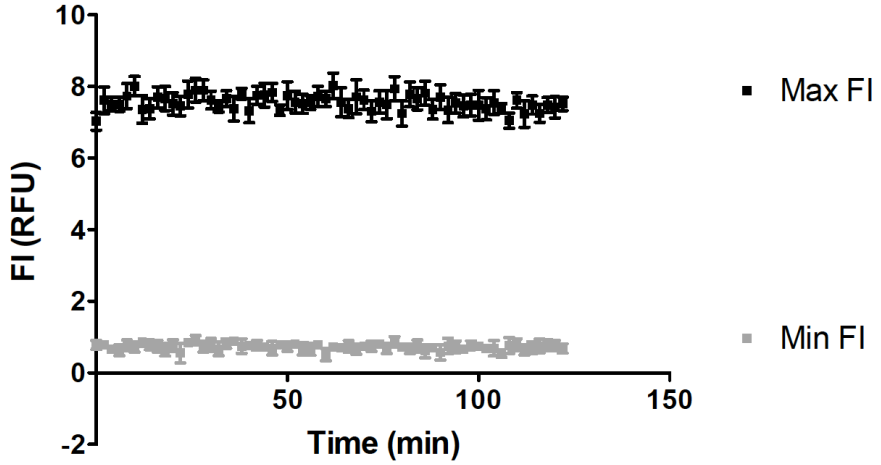

Figure 43: The FI window for the PIK3C3 assay conditions. Min FI: 28.25µg/mL ADP[2] Antibody-IRDye® QC-1, 1x PIK3C3 Assay Buffer (25mM HEPES, 50mM NaCl, 3mM $MgCl_2$, 0.025mg/mL BSA), 4nM ADP Alexa Fluor® 594 Tracer. Max FI: 1x PIK3C3 Assay Buffer (25mM HEPES, 50mM NaCl, 3mM $MgCl_2$, 0.025mg/mL BSA), 4nM ADP Alexa Fluor® 594 Tracer.

5.4.4 The ATP/ADP Standard Curve for the PIK3C3 Assay Conditions

An ATP/ADP standard curve was conducted for the PIK3C3 assay conditions (Figure 44). This standard curve mimicked an enzyme reaction over 12 points in which ATP was decreasing and ADP was increasing proportionally. The FI was plotted against the log[ADP] and a linear regression of the ATP/ADP standard curve was conducted to give the equation: $y = 2.499x + 5.360$. This curve correlates FI and the concentration of ADP produced, therefore, the equation could be used to calculate %ATP conversion based on FI and vice versa. The [ATP] used in this assay was 30μM, therefore 10% ATP conversion corresponds to 3μM ADP. Based on the equation, a FI equal to or lower than 6.55 RFUs corresponds with a % ATP conversion that is 10% or lower. It is important to have this estimate for the assays because the aim is typically to choose enzyme and substrate concentrations and run the assay for the time corresponding to less than 10% ATP conversion to ensure initial rates of conversion (99, 100).

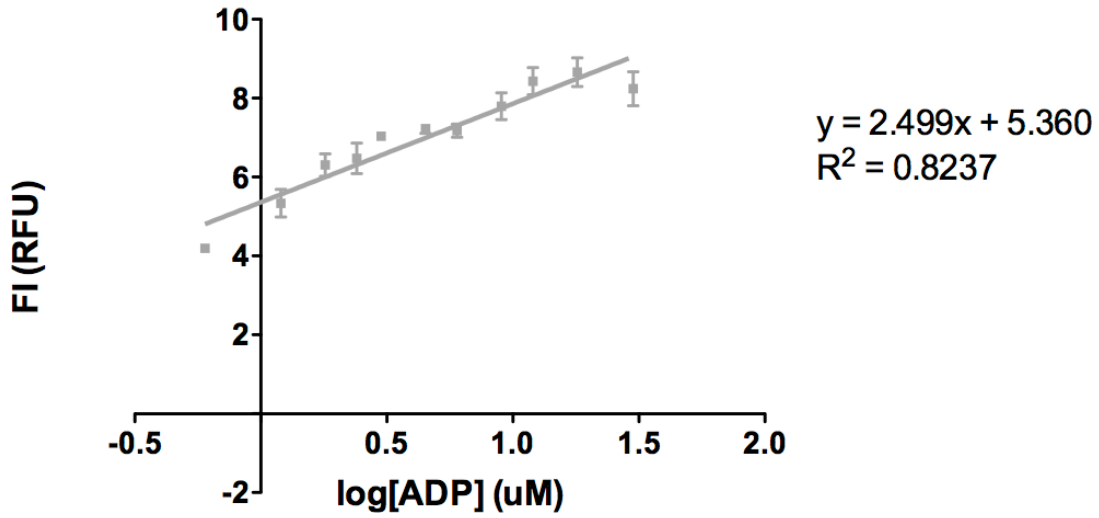

Figure 44: ATP/ADP standard curve for the PIK3C3 assay conditions. Variable [ATP] and [ADP], 0.2mg/mL PI:3PS substrate, 1x Lipid Dilution Buffer (25mM HEPES, 0.5mM EGTA), 28.25μg/mL ADP^2 Antibody-IRDye® QC-1, 4nM ADP Alexa Fluor® 594 Tracer, 1x PIK3C3 Assay Buffer (25mM HEPES, 50mM NaCl, 3mM $MgCl_2$, 0.025mg/mL BSA).

5.4.5 Assay Results

The time-resolved assay of PIK3C3 was conducted at 4 different concentrations of PIK3C3 between 0.5µg/mL and 10µg/mL (Figure 45). The evolution of the signal was dependent on the concentration of enzyme. An increase in signal past the baseline was observed for 10µg/mL and 5µg/mL PIK3C3 over the 120min that the assay was conducted. The baseline was judged by the no enzyme control (purple trace in Figure 45, black trace in Figure 46). PIK3C3 at concentrations of 0.5µg/mL and 2µg/mL did not result in a signal that increased significantly from the baseline (Figure 45). Based on the ATP/ADP standard curve in Figure 44, the a FI equal to or lower than 6.55 RFUs corresponds with a % ATP conversion that is 10% or lower. Over the 120min of the assay, none of the traces exceeded a FI of 6 RFUs, therefore, the % conversion of ATP was less than 10% and hence initial rate conditions were maintained for all concentrations of PIK3C3 for the entire length of the assay.

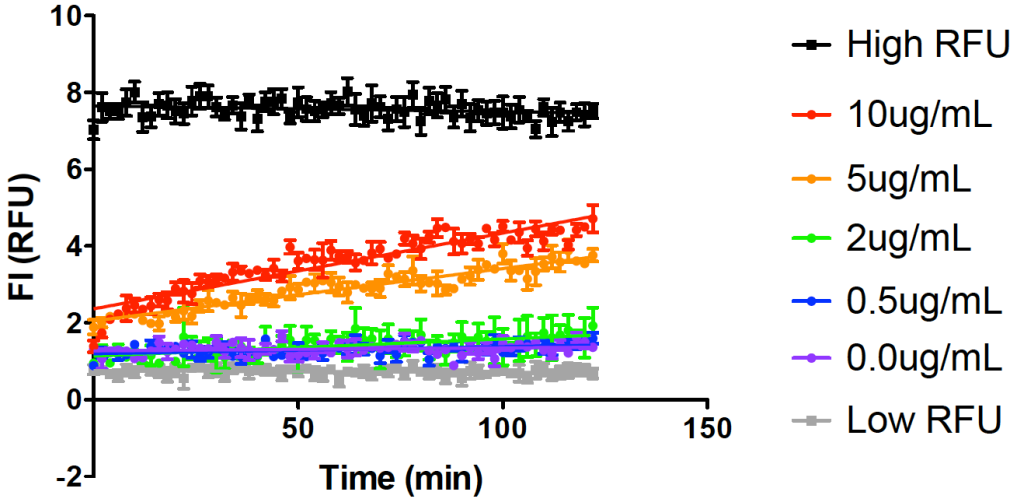

Figure 45: PIK3C3 titration for the time-Resolved assay of PIK3C3 using the Bellbrook Transcreener® ADP² FI Assay. The evolution of FI was measured over 120min for 4 different concentrations of PIK3C3. Assay conditions: 30µM ATP, 0.2mg/mL PI:3PS, 1x Lipid Dilution Buffer (25mM HEPES, 0.5mM EGTA), 28.25µg/mL ADP² Antibody-IRDye® QC-1, 4nM ADP Alexa Fluor® 594 Tracer, 1x PIK3C3 Assay Buffer (25mM HEPES, 50mM NaCl, 3mM $MgCl_2$, 0.025mg/mL BSA).

5.4.6 Controls

The lipid controls from Figure 42 were carried out when the precipitation and false signal issues were being investigated. Once Mn^{2+} had been removed, the precipitation problems solved, and the assay shown to be successful, these lipid controls were repeated, and the results are shown in Figure 46. Eliminating the precipitation issue eliminated the increase in signal over time that was observed in the PI:3PS, No PIK3C3 and the No Lipid, No PIK3C3 controls that were conducted with Mn^{2+} containing buffer. These controls also showed that the baseline for these assay conditions is around 2 RFUs.

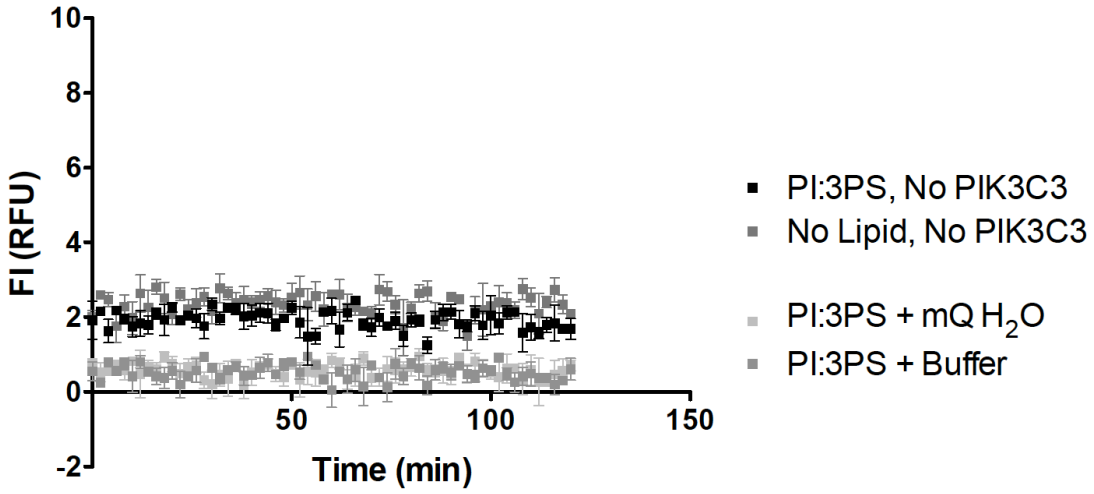

Figure 46: Lipid Controls in buffer that does not contain Mn^{2+}. PI:3PS, No PIK3C3: Assay conditions but no PIK3C3. No Lipid, No PIK3C3: 30µM ATP, 28.25µg/mL ADP[2] Antibody-IRDye® QC-1, 4nM ADP Alexa Fluor® 594 Tracer, 1x PIK3C3 Assay Buffer (25mM HEPES, 50mM NaCl, 3mM $MgCl_2$, 0.025mg/mL BSA). PI:3PS + mQH_2O: 0.2mg/mL PI:3PS, 1x Lipid Dilution Buffer (25mM HEPES, 0.5mM EGTA). PI:3PS + Buffer: 0.2mg/mL PI:3PS, 1x Lipid Dilution Buffer (25mM HEPES, 0.5mM EGTA), 1x PIK3C3 Assay Buffer (25mM HEPES, 50mM NaCl, 3mM $MgCl_2$, 0.025mg/mL BSA).

Two controls were conducted in which one of the substrates of PIK3C3, ATP or PI, were not included (Figure 47). The No ATP control gave no evolution of signal in the absence of ATP. This was the expected result and shows that the signal generated in the assays was from the hydrolysis of ATP to ADP. The enzyme titration in light of the No ATP control shows that the signal generated is from the hydrolysis of ATP to ADP by the enzyme as the signal evolution is dependent on the concentration of the PIK3C3. The PC:3PS control was the control in which PC was included instead of PI; this control was

expected to give no evolution of signal similar to the No ATP control. However, an evolution of signal was observed that overlaps with the trace for the assay at the same concentration of enzyme when PI:3PS was the substrate (Figure 45, 47, and 48). This indicates that PIK3C3 was producing ADP at approximately the same rate whether the substrate phospholipid was present or not; thus, the assay may be measuring non-productive ATP hydrolysis of the enzyme. Autophosphorylation is also possible. Autophosphorylation was observed for the yeast homolog Vps34 (40), though no autophosphorylation of PIK3C3 was observed with Mg^{2+} or Mn^{2+} by Volinia *et al*. (38). Further investigations will be required in the future to distinguish between productive phosphorylation and non-productive ATP hydrolysis.

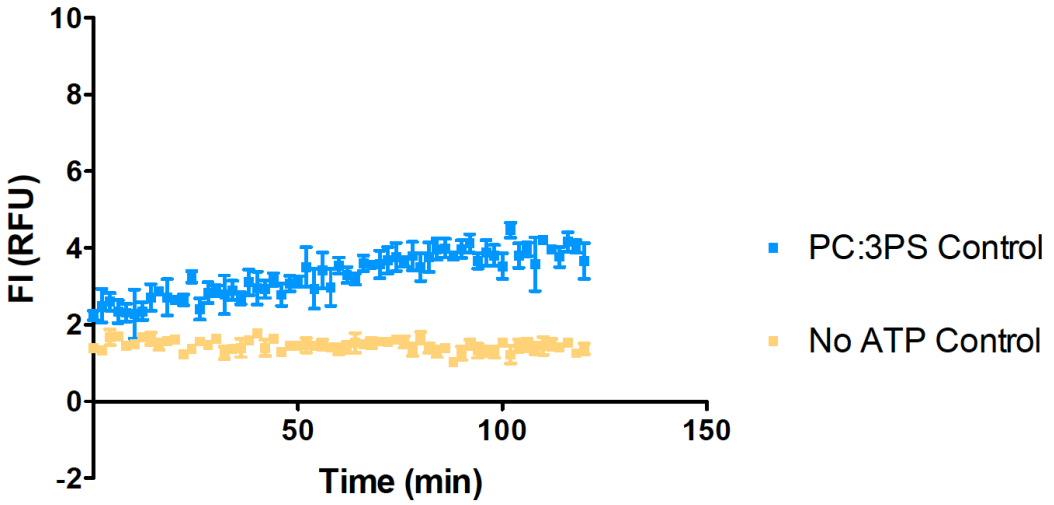

Figure 47: The PC:3PS Control (no PI) and the No ATP Controls for the time-resolved PIK3C3 assay. Both controls contained 5µg/mL PIK3C3. PC:3PS: Assay conditions but PC:3PS vesicles instead of PI:3PS vesicles. No ATP: Assay conditions but no ATP. Assay conditions: 30µM ATP, 0.2mg/mL PI:3PS, 1x Lipid Dilution Buffer (25mM HEPES, 0.5mM EGTA), 28.25µg/mL ADP^2 Antibody-IRDye® QC-1, 4nM ADP Alexa Fluor® 594 Tracer, 1x PIK3C3 Assay Buffer (25mM HEPES, 50mM NaCl, 3mM $MgCl_2$, 0.025mg/mL BSA).

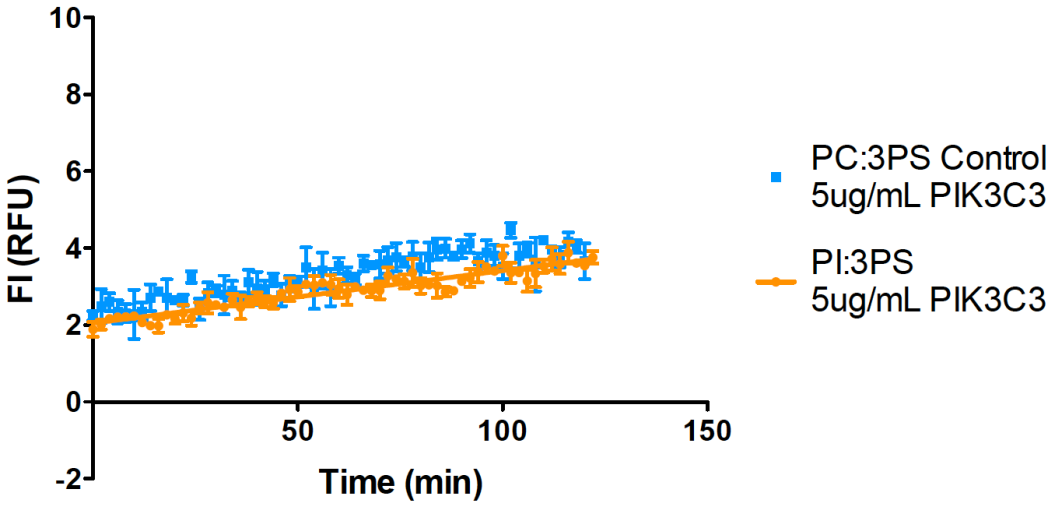

Figure 48: A comparison of the PC:3PS Control (blue trace, Figure 47) and the 5µg/mL PIK3C3 assay trace (orange trace, Figure 45) that used PI:3PS as the substrate. Both were performed at 5µg/mL PIK3C3. PC:3PS control: Assay conditions but PC:3PS vesicles instead of PI:3PS vesicles. PI:3PS 5µg/mL assay: Assay conditions. Assay conditions: 30µM ATP, 0.2mg/mL PI:3PS, 1x Lipid Dilution Buffer (25mM HEPES, 0.5mM EGTA), 28.25µg/mL ADP^2 Antibody-IRDye® QC-1, 4nM ADP Alexa Fluor® 594 Tracer, 1x PIK3C3 Assay Buffer (25mM HEPES, 50mM NaCl, 3mM $MgCl_2$, 0.025mg/mL BSA).

5.4.7 Mn^{2+} vs Mg^{2+}

In the protein kinase catalytic domain there is evidence supporting that Mg^{2+} positions the γ-phosphate for nucleophilic attack, masks charge to limit repulsion with the incoming nucleophile and stabilizes the transition state and reduces the transition state barrier by applying strong electrostatic interactions to the ADP leaving group. The presence or absence of Mg^{2+} in the active site can change the K_M of the enzyme for ATP (109). PIK3C3 is a lipid kinase and not a protein kinase, but the metal cation is still likely involved in the coordination of ATP and the catalysis of phosphate transfer. PIK3C3 is active with Mn^{2+} and only weakly active with Mg^{2+} (38). It is unclear how or why PIK3C3 is more active with Mn^{2+} than Mg^{2+} but the different metal cations may change the K_M of the enzyme for ATP.

PIK3C3 was assayed in buffer containing 50mM HEPES (pH7.5), 50mM NaCl, 3mM $MgCl_2$, 0.025mg/mL BSA, and 5mM $MnCl_2$ using the ADP-Glo® Lipid Kinase System and the apparent K_M of PIK3C3 for ATP was 40μM ATP (100). This apparent K_M was determined with both Mg^{2+} and Mn^{2+} in the buffer and thus either could be in the active site. PIK3C3 is significantly more active with Mn^{2+} than Mg^{2+} and it is only weakly active with Mg^{2+} (38). This is why a great deal of effort was spent on solving the precipitation problems and getting the assay to work in the presence of Mn^{2+}. PIK3C3 did not have an opportunity to bind Mn^{2+} in its active site as Mn^{2+} precipitated with the antibody phosphate buffer in the Assay Mix before the Enzyme Mix had a chance to come in contact with it. Thus, in a final effort to "sneak" Mn^{2+} into the assay Mn^{2+} was added to the Enzyme Mix and Mg^{2+} and Mn^{2+} were not included in the PIK3C3 Assay Buffer. Two concentrations of Mn^{2+} were attempted, 3mM and 3μM. 3μM Mn^{2+} was used in an attempt to provide PIK3C3 an opportunity to bind Mn^{2+} in its active site while reducing the amount of Mn^{2+} left in solution to precipitate when mixed with the Assay Mix. Precipitation was observed at the beginning of both assays and the data gathered from these assays is shown in Figure 49. Both concentrations of Mn^{2+} gave large signals with intensities around or above 6 RFUs for the majority of the duration of the assay. This signal was much higher than the FI that was seen for the other Mn^{2+} containing assays that had precipitated (Figure 41). This high signal could a combination of light scattering from the precipitate and signal generated from the ADP production by the enzyme. If at least some or most of this signal was from genuine ADP production by PIK3C3 it indicates that PIK3C3 was much more active with Mn^{2+} than Mg^{2+} and that the assay may have surpassed initial rate conditions by the first few minutes, as a FI of 6.55 RFUs corresponds to 10% conversion. If this is true, a lower concentration of PIK3C3 could be used in the assay. However, even if this is the case ("sneaking" Mn^{2+} into the assay this way works to increase PIK3C3 activity), the precipitate would obscure the signal and so this "sneak" method was not useful for the assay unless there was a way to remove excess Mn^{2+} from the enzyme solution after PIK3C3 has a chance to bind Mn^{2+}.

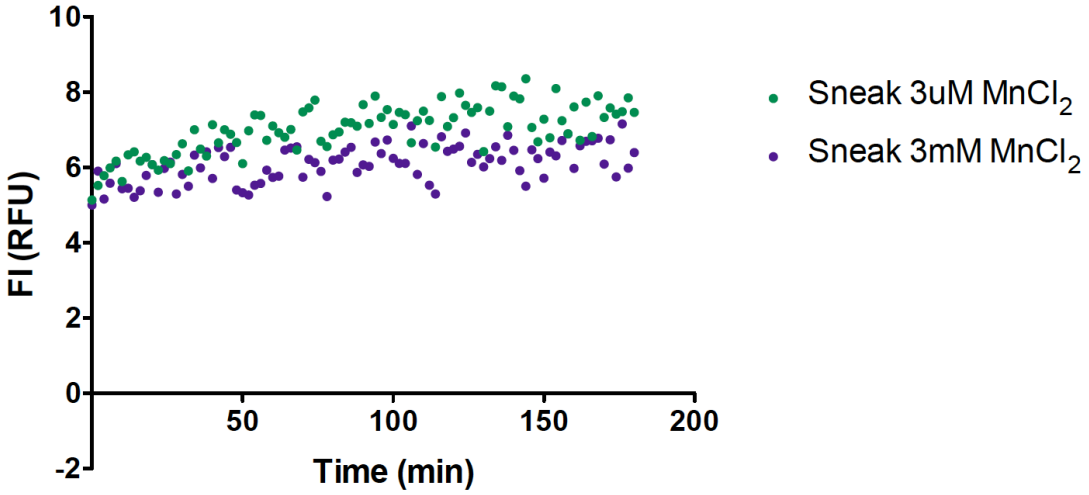

Figure 49: "Sneak" Mn^{2+} assays. PIK3C3 time-resolved assays in which Mn^{2+} was added to the Enzyme Mix such that the final assay [Mn^{2+}] was either 3µM or 3mM and Mg^{2+} and Mn^{2+} were omitted from the PIK3C3 Assay Buffer. Both were performed at 5µg/mL PIK3C3. Assay conditions: 30µM ATP, 0.2mg/mL PI:3PS, 1x Lipid Dilution Buffer (25mM HEPES, 0.5mM EGTA), 28.25µg/mL ADP^2 Antibody-IRDye® QC-1, 4nM ADP Alexa Fluor® 594 Tracer, 1x PIK3C3 Assay Buffer (25mM HEPES, 50mM NaCl, 3mM $MgCl_2$, 0.025mg/mL BSA).

6 Conclusions and Future Directions

The eventual application of this work will be to investigate the PI presentation model by which Sec14 is proposed to stimulate the activity of Pik1. Two key things were required to make a kinetic investigation into this model possible, a time-resolved assay for the activity of Pik1 and a method to express and purify the Pik1-Frq1 complex. These were the two main goals of this thesis project.

The expression of the Pik1-Frq1 complex by the BJ2168 transformants B8NA (transformed BJ2168 with clone 8 (pYEXC3H+PIK1) and clone N (pESC-Trp+FRQ1+CDC37) at the same time, colony A) and 10NE (transformed BJ2168 with clone 10 (pYEXC3H+PIK1) and clone N (pESC-Trp+FRQ1+CDC37) sequentially, colony E) was confirmed by Western blot but the purification has yet to be successful. It is possible that the transformants were expressing very little of the protein complex and so it just was not seen in the purification on a preparative scale. Next steps should thus include the optimization of the expression and purification of the complex. Next time this process is attempted, it would be logical to use YEPG to induce protein expression. The results in this thesis do not give an indication of protein expression levels, but they do show that YEPG does cause a large increase in growth, leading to a greater number of cells to extract protein from. Optimization of the purification yield was set aside for future work because it was deemed more critical for the project to move on to developing the time-resolved assay.

The Bellbrook Labs Transcreener ADP^2 FI Assay kit was successfully adapted into a time-resolved assay using the catalytic subunit of Protein Kinase A (PKA). Then it was developed further for use with PI kinases with vesicles as substrates using the human PI kinase, PIK3C3. In both the PKA and PIK3C3 assays, the signals evolved in a manner that was dependent on enzyme concentration, and as seen in PKA, there is an enzyme concentration above which the assay does not respond with a more rapid evolution of signal. This is likely a measurement of the displacement of the tracer rather than the rate of phosphorylation. Conditions that supported enzyme activity and that were also compatible with the assay kit were established for each enzyme. Mn^{2+} was found to be incompatible with the kit. Conditions were found that satisfy initial rates assumptions

(minimal decrease in substrate concentration during the time of observation), and that result in signals that increase sufficiently from the base-line, making it possible to gather reliable kinetic information from the observed data.

The goal of this work was to develop a robust, easy-to-use, time-resolved, vesicle-based assay for a PI-kinase. The assay in its current form is easy to use, time-resolved, and vesicle based, but the question of how robust the assay is still needing to be addressed. This is the next step that must be completed before the assay can be routinely applied. As more data is gathered with this assay, linear regressions of replicate measurements will have to be done and the slopes compared with a simple t-test to determine if similar traces from different conditions are statistically different. This will help establish how robust this assay is, in effect, how well it can discern two conditions that differ by only a small magnitude from each other. In addition, investigations will be required to distinguish between productive phosphorylation and non-productive ATP hydrolysis, and ATPase activity should be subtracted from all assay data. Once it is established as a reliable and robust assay it can be used to probe the model it was designed to investigate – the Pik1 and Sec14 PI presentation model.

When purified fractions of the Pik1-Frq1 complex are obtained, the first task will be to measure its activity under the normal conditions of the assay. It will be essential to ensure the activity of Pik1 can be measured with this *in vitro* assay and critical to obtain a baseline activity to which the other experiments will be compared. The assay conditions and the optimal assay concentration of Pik1 will need to be determined. PIK3C3 was chosen for the development of the assay on purpose as it is a PI kinase that is related to Pik1. The first attempt to assay the activity of Pik1 will likely be conducted at the same conditions as PIK3C3 as a starting point, then adjusted if and where necessary. An enzyme titration will be needed to determine the optimal assay concentration for Pik1. As stated previously, the goal is to find an enzyme concentration at which the signal sufficiently increases off the baseline but does not exceed 10% conversion (as determined by an ATP/ADP standard curve) during the time of the assay. The concentration of Pik1 and the time of observation are to be adjusted such that the normal assay conditions give

a trace that significantly occupies the assay window (essentially fluorescence intensity), such that any variations can be seen when the assay conditions are modified in any way.

Once the assay conditions for Pik1 have been established, there are many experiments to explore its activity and the proposed PI presentation model. The sensitivity of the Pik1-Frq1 complex to phospholipid membrane composition will be tested by conducting the assay with different phospholipid compositions. The first test of the PI presentation model will be to run the assay in the presence and absence of wild type (wt) Sec14. Further experiments will be done with mutant versions of Sec14 that are either PI or PC binding mutants. Assay experiments with Sec14 pre-incubated with PI or PC will be conducted to see how the identity of the starting lipid bound to Sec14 effects the stimulation of Pik1 activity. Members of the Atkinson research group are also synthesizing versions of PI called bola-PIs. A bola-PI has two inositol head groups and a lipid tail that spans the membrane connecting the two (blue phospholipid in Figure 50). Thus, the opposite headgroup will resist being pulled into the hydrophobic core of the membrane and will therefore prevent the bola-PI from being out of the membrane (Figure 50). Since the proposed model posits that Sec14 partially pulls PI out of the membrane to present it as a more suitable substrate to Pik1, controlling the ability of Sec14 to pull the PI out of the membrane provides a test of this hypothesis. Bola-PI analogues of different chain length will also be explored.

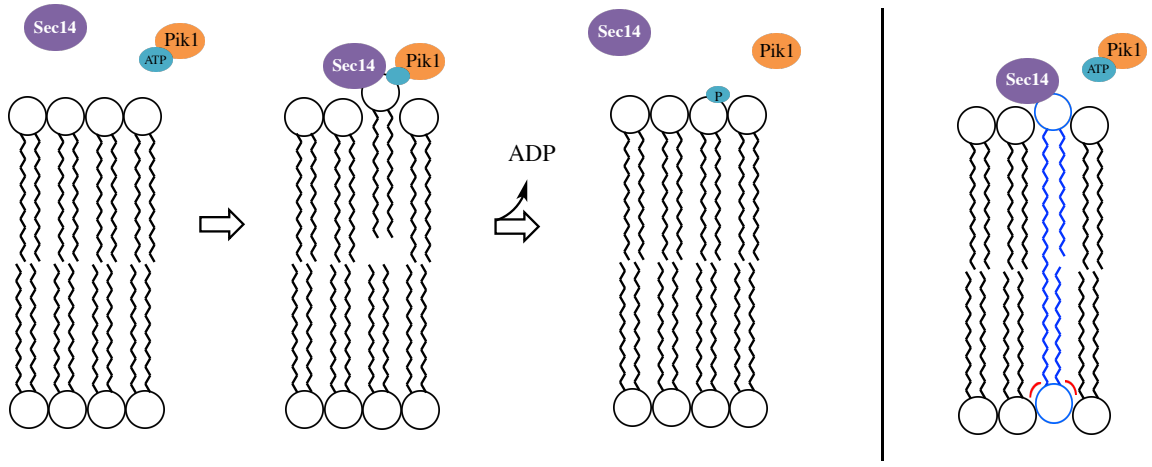

Figure 50: The proposed PI presentation model for the function of Sec14 in PIP homeostasis with natural and bola-PI. Image received with permission from Shannon Jewel.

This thesis outlines the development of a time-resolved, vesicle-based, FI assay for the activity of a lipid kinase. This assay is easy to use and can be used to measure initial rates of lipid kinases. Once it has been established as a reliable and robust assay it will be used frequently in the future work of the Atkinson research group to conduct the research outlined here. Moreover, it is not only useful in investigating Pik1 and Sec14, it can be used to investigate the activity of any lipid kinase and any lipid transfer protein, including the mammalian homologues of Sec14, principally PITPα and PITPβ (110–112). Lipid kinase assays are not only critical to gain a greater understanding of lipid transfer protein and lipid kinase function, they are also key in disease research (84) and in drug development and safety (85). This research provides an easy, time-resolved assay to investigate lipid kinase activity that can eventually be used in academic, medical, and pharmaceutical research labs.

7 References

1. Hama, H., Schnieders, E. A., Thorner, J., Takemoto, J. Y., and DeWald, D. B. (1999) Direct involvement of phosphatidylinositol 4-phosphate in secretion in the yeast Saccharomyces cerevisiae. *J. Biol. Chem.* **274**, 34294–34300
2. Walch-Solimena, C., and Novick, P. (1999) The yeast phosphatidylinositol-4-OH kinase Pik1 regulates secretion at the Golgi. *Nat. Cell Biol.* **1**, 523–525
3. Hendricks, K. B., Wang, B. Q., Schnieders, E. A., and Thorner, J. (1999) Yeast homologue of neuronal frequenin is a regulator of phosphatidylinositol-4-OH kinase. *Nat. Cell Biol.* **1**, 234–241
4. Ghosh, R., and Bankaitis, V. A. (2011) Phosphatidylinositol transfer proteins: Negotiating the regulatory interface between lipid metabolism and lipid signaling in diverse cellular processes. *BioFactors*. **37**, 290–308
5. De Craene, J. O., Bertazzi, D. L., Bär, S., and Friant, S. (2017) Phosphoinositides, major actors in membrane trafficking and lipid signaling pathways. *Int. J. Mol. Sci.* 10.3390/ijms18030634
6. Cockcroft, S., and Raghu, P. (2016) Topological organisation of the phosphatidylinositol 4,5-bisphosphate-phospholipase C resynthesis cycle: PITPs bridge the ER-PM gap. *Biochem. J.* **473**, 4289–4310
7. Tan, J., and Brill, J. A. (2014) Cinderella story: PI4P goes from precursor to key signaling molecule. *Crit. Rev. Biochem. Mol. Biol.* **49**, 33–58
8. Di Paolo, G., and De Camilli, P. (2006) Phosphoinositides in cell regulation and membrane dynamics. *Nature*. **443**, 651–657
9. Flanagan, C. A., Schnieders, E. A., Emerick, A. W., Kunisawa, R., Admon, A., and Thorner, J. (1993) Phosphatidylinositol 4-Kinase : Gene Structure and Requirement for Yeast Cell Viability. *Adv. Sci.* **262**, 1444–1448
10. Grabon, A., Bankaitis, V. A., and McDermott, M. I. (2018) The Interface Between Phosphatidylinositol Transfer Protein Function and Phosphoinositide Signaling in Higher Eukaryotes. *J. Lipid Res.*
11. Mayinger, P. (2012) Phosphoinositides and vesicular membrane traffic. *Biochim. Biophys. Acta - Mol. Cell Biol. Lipids*. **1821**, 1104–1113
12. Gericke, A., Leslie, N. R., Losche, M., and Ross, A. H. (2013) PtdIns(4,5)P2-Mediated Cell Signaling: Emerging Principles and PTEN as a Paradigm for

Regulatory Mechanism. in *Lipid-Mediated Protein Signaling*, pp. 85–104, Springer

13. Harlan, J. E., Hajduk, P. J., Yoon, H. S., and Fesik, S. W. (1994) Pleckstrin homology domains bind to PIP2. *Nature*. **371**, 168
14. Clayton, E. L., Minogue, S., and Waugh, M. G. (2013) Mammalian phosphatidylinositol 4-kinases as modulators of membrane trafficking and lipid signaling networks. *Prog. Lipid Res.* **52**, 294–304
15. Audhya, A., Foti, M., and Emr, S. D. (2000) Distinct roles for the yeast phosphatidylinositol 4-kinases, Stt4p and Pik1p, in secretion, cell growth, and organelle membrane dynamics. *Mol Biol Cell.* **11**, 2673–2689
16. Wang, Y. J., Albanesi, J. P., Wang, J., Sun, H. Q., Martinez, M., Sun, Y. X., Macia, E., Kirchhausen, T., Roth, M. G., and Yin, H. L. (2003) Phosphatidylinositol 4 phosphate regulates targeting of clathrin adaptor AP-1 complexes to the Golgi. *Cell*. **114**, 299–310
17. Godi, A., Di Campli, A., Konstantakopoulos, A., Di Tullio, G., Alessi, D. R., Kular, G. S., Daniele, T., Marra, P., Lucocq, J. M., and De Matteis, M. A. (2004) FAPPS control Golgi-to-cell-surface membrane traffic by binding to ARF and PtdIns(4)P. *Nat. Cell Biol.* **6**, 393–404
18. Dippold, H. C., Ng, M. M., Farber-Katz, S. E., Lee, S. K., Kerr, M. L., Peterman, M. C., Sim, R., Wiharto, P. A., Galbraith, K. A., Madhavarapu, S., Fuchs, G. J., Meerloo, T., Farquhar, M. G., Zhou, H., and Field, S. J. (2009) GOLPH3 Bridges Phosphatidylinositol-4- Phosphate and Actomyosin to Stretch and Shape the Golgi to Promote Budding. *Cell*. **139**, 337–351
19. Mizuno-Yamasaki, E., Medkova, M., Coleman, J., and Novick, P. (2010) Phosphatidylinositol 4-phosphate controls both membrane recruitment and a regulatory switch of the Rab GEF Sec2p. *Dev. Cell*. **18**, 828–840
20. Folch, J. (1948) Brain Diphosphoinositide, a new phosphatide having inositol metadiphosphate as a constituent. *J. Biol. Chem.* **177**, 505–520
21. Carpenter, C. L., and Cantley, L. C. (1990) Phosphoinositide kinases. *Biochemistry*. **29**, 11147–11156
22. Nishizuka, Y. (1984) Turnover of Inositol Phospholipids and Signal Transduction. *Science (80-.).* **225**, 1365–1370

23. Whitman, M., Downes, C. P., Keeler, M., Keller, T., and Cantley, L. (1988) Type I phosphatidylinositol kinase makes a novel inositol phospholipid, phosphatidylinositol-3-phosphate. *Nature*. **332**, 644–646
24. Auger, K. R., Carpenter, C. L., Cantley, L. C., and Varticovski, L. (1989) Phosphatidylinositol 3-kinase and its novel product, phosphatidylinositol 3-phosphate, are present in Saccharomyces cerevisiae. *J. Biol. Chem.* **264**, 20181–20184
25. Brown, J. R., and Auger, K. R. (2011) Phylogenomics of phosphoinositide lipid kinases: Perspectives on the evolution of second messenger signaling and drug discovery. *BMC Evol. Biol.* **11**, 4
26. Sasaki, T., Takasuga, S., Sasaki, J., Kofuji, S., Eguchi, S., Yamazaki, M., and Suzuki, A. (2009) Mammalian phosphoinositide kinases and phosphatases. *Prog. Lipid Res.* **48**, 307–343
27. Strahl, T., and Thorner, J. (2007) Synthesis and function of membrane phosphoinositides in budding yeast, Saccharomyces cerevisiae. *Biochim. Biophys. Acta - Mol. Cell Biol. Lipids*. **1771**, 353–404
28. Gehrmann, T., and Heilmeyer, L. M. G. J. (1998) Phosphatidylinositol 4-kinases. *Eur. J. Biochem.* **253**, 357–370
29. Heilmeyer, L. M. G., Vereb, G., Vereb, G., Kakuk, A., and Szivák, I. (2003) Mammalian phosphatidylinositol 4-kinases. *IUBMB Life*. **55**, 59–65
30. Kakuk, A., Friedländer, E., Vereb, G., Lisboa, D., Bagossi, P., Tóth, G., Gergely, P., and Vereb, G. (2008) Nuclear and nucleolar localization signals and their targeting function in phosphatidylinositol 4-kinase PI4K230. *Exp. Cell Res.* **314**, 2376–2388
31. Balla, A., Vereb, G., Gülkan, H., Gehrmann, T., Gergely, P., Heilmeyer, L. M. G., and Antal, M. (2000) Immunohistochemical localisation of two phosphatidylinositol 4-kinase isoforms, PI4K230 and PI4K92, in the central nervous system of rats. *Exp. Brain Res.* **134**, 279–288
32. Balla, T. (2013) Phosphoinositides: Tiny Lipids With Giant Impact on Cell Regulation. *Physiol. Rev.* **93**, 1019–1137
33. Wymann, M. P., Bulgarelli-Leva, G., Zvelebil, M. J., Pirola, L., Vanhaesebroeck, B., Waterfield, M. D., and Panayotou, G. (1996) Wortmannin inactivates

phosphoinositide 3-kinase by covalent modification of Lys-802, a residue involved in the phosphate transfer reaction. *Mol. Cell. Biol.* **16**, 1722–1733

34. XU, Y., SEET, L.-F., HANSON, B., and HONG, W. (2001) The Phox homology (PX) domain, a new player in phosphoinositide signalling. *Biochem. J.* **360**, 513–530
35. Ming, K., Yuan, W., Chen, Y., Du, H., He, M., Hu, Y., Wang, D., Wu, Y., and Liu, J. (2019) PI3KC3-dependent autophagosomes formation pathway is of crucial importance to anti-DHAV activity of Chrysanthemum indicum polysaccharide. *Carbohydr. Polym.* **208**, 22–31
36. Balla, A., and Balla, T. (2006) Phosphatidylinositol 4-kinases: old enzymes with emerging functions. *Trends Cell Biol.* **16**, 351–361
37. Boura, E., and Nencka, R. (2015) Phosphatidylinositol 4-kinases: Function, structure, and inhibition. *Exp. Cell Res.* **337**, 136–145
38. Volinia, S., Dhand, R., Vanhaesebroeck, B., MacDougall, L. K., Stein, R., Zvelebil, Marketa, J., Domin, J., Panaretou, C., and Waterfield, M. D. (1995) A human phosphatidylinositol 3-kinase complex related to the yeast Vps34p-Vps15p protein sorting system. *EMBO J.* **14**, 3339–3348
39. Takegawa, K., DeWald, D. B., and Emr, S. D. (1995) Schizosaccharomyces pombe Vps34p, a phosphatidylinositol-specific PI 3-kinase essential for normal cell growth and vacuole morphology. *J.Cell Sci.* **108 (Pt 1**, 3745–3756
40. Stack, J. H., and Emr, S. D. (1994) Vps34p is a phosphatidylinositol-specific PI 3-kinase required for vacuolar protein sorting in yeast and possesses both lipid and protein kinase activities. *J. Biol. Chem.* **269**, 31552–31562
41. UniProtKB - PIK3C3 [online] https://www.uniprot.org/uniprot/Q8NEB9 (Accessed February 12, 2019)
42. Sigma-Aldrich (2018) Certificate of Analysis: PIK3C3 (Vps34)
43. UniProtKB - Vps34 [online] https://www.uniprot.org/uniprot/P22543 (Accessed February 12, 2019)
44. Reifler, A., Li, X., Archambeau, A. J., McDade, J. R., Sabha, N., Michele, D. E., and Dowling, J. J. (2014) Conditional knockout of Pik3c3 causes a murine muscular dystrophy. *Am. J. Pathol.* **184**, 1819–1830
45. Herman, P. K., Stack, J. H., and Emr, S. D. (1992) An essential role for a protein

and lipid kinase complex in secretory protein sorting. *Trends Cell Biol.* **2**, 363–368

46. Stack, J. H., Herman, P. K., Schu, P. V., and Emr, S. D. (1993) A membrane-associated complex containing the Vps15 protein kinase and the Vps34 PI 3-kinase is essential for protein sorting to the yeast lysosome-like vacuole. *EMBO J.* **12**, 2195–204
47. Panaretou, C., Domin, J., Cockcroft, S., Waterfield, M. D., and Embo, M. D. J. (1997) Characterization of p150 , an Adaptor Protein for the Human Phosphatidylinositol (PtdIns) 3-Kinase characterized as part of a complex with a cellular pro-. *Biochemistry*. **272**, 2477–2485
48. Funderbunk, S. F., Wang, Q. J., and Yue, Z. (2010) Beclin 1-VPS34 complex - At the Crossroads of Autophagy and Beyond. *Trends Cell Biol.* **20**, 355–362
49. Meyers, R., and Cantley, L. C. (1997) Cloning and characterization of a Wortmannin-sensitive human phosphatidylinositol 4-kinase. *J. Biol. Chem.* **272**, 4384–4390
50. Flanagan, C. A., and Thorner, J. (1992) Purification and characterization of a soluble Phosphatidylinositol 4-kinase from the yeast Saccharomyces cerevisiae. *J. Biol. Chem.* **267**, 24117–24125
51. Mejdrová, I., Chalupská, D., Kögler, M., Šála, M., Plačková, P., Baumlová, A., Hřebabecký, H., Procházková, E., Dejmek, M., Guillon, R., Strunin, D., Weber, J., Lee, G., Birkus, G., Mertlíková-Kaiserová, H., Boura, E., and Nencka, R. (2015) Highly selective phosphatidylinositol 4-kinase IIIβ inhibitors and structural insight into their mode of action. *J. Med. Chem.* **58**, 3767–3793
52. McPhail, J. A., Ottosen, E. H., Jenkins, M. L., and Burke, J. E. (2017) The Molecular Basis of Aichi Virus 3A Protein Activation of Phosphatidylinositol 4 Kinase IIIβ, PI4KB, through ACBD3. *Structure*. **25**, 121–131
53. UniProtKB - PI4KB [online] https://www.uniprot.org/uniprot/Q9UBF8 (Accessed February 12, 2019)
54. Dornan, G. L., McPhail, J. A., and Burke, J. E. (2016) Type III phosphatidylinositol 4 kinases: structure, function, regulation, signalling and involvement in disease. *Biochem. Soc. Trans.* **44**, 260–266
55. UniProtKB - Pik1 [online] https://www.uniprot.org/uniprot/P39104 (Accessed February 12, 2019)

56. Ames, J. B., Hendricks, K. B., Strahl, T., Huttner, I. G., Hamasaki, N., and Thorner, J. (2000) Structure and Calcium-Binding Properties of Frq1, a Novel Calcuim Sensor in the Yeast Saccharomyces cerevisiae. *Biochemistry*. **39**, 12149–12161

57. Strahl, T., Huttner, I. G., Lusin, J. D., Osawa, M., King, D., Thorner, J., and Ames, J. B. (2007) Structural insights into activation of phosphatidylinositol 4-kinase (Pik1) by yeast frequenin (Frq1). *J. Biol. Chem.* **282**, 30949–30959

58. Huttner, I. G., Strahl, T., Osawa, M., King, D. S., Ames, J. B., and Thorner, J. (2003) Molecular interactions of yeast frequenin (Frq1) with the phosphatidylinositol 4-kinase isoform, Pik1. *J. Biol. Chem.* **278**, 4862–4874

59. Szivak, I., Lamb, N., and Heilmeyer, L. M. G. (2006) Subcellular localization and structural function of endogenous phosphorylated phosphatidylinositol 4-kinase (PI4K92). *J. Biol. Chem.* **281**, 16740–16749

60. Hsu, N. Y., Ilnytska, O., Belov, G., Santiana, M., Chen, Y. H., Takvorian, P. M., Pau, C., van der Schaar, H., Kaushik-Basu, N., Balla, T., Cameron, C. E., Ehrenfeld, E., van Kuppeveld, F. J. M., and Altan-Bonnet, N. (2010) Viral reorganization of the secretory pathway generates distinct organelles for RNA replication. *Cell*. **141**, 799–811

61. Greninger, A. L., Knudsen, G. M., Betegon, M., Burlingame, A. L., and DeRisi, J. L. (2012) The 3A Protein from Multiple Picornaviruses Utilizes the Golgi Adaptor Protein ACBD3 To Recruit PI4KIII . *J. Virol.* **86**, 3605–3616

62. Macdonald, S. (2017) Phosphatidylinositol 4-kinase III beta promotes oncogenic signaling in breast cancer by controlling endocytosis

63. Sugiura, T., Takahashi, C., Chuma, Y., Fukuda, M., Yamada, M., Yoshida, U., Nakao, H., Ikeda, K., Khan, D., Nile, A. H., Bankaitis, V. A., and Nakano, M. (2019) Biophysical Parameters of the Sec14 Phospholipid Exchange Cycle. *Biophys. J.* **116**, 92–103

64. Schaaf, G., Ortlund, E. A., Tyeryar, K. R., Mousley, C. J., Ile, K. E., Garrett, T. A., Ren, J., Woolls, M. J., Raetz, C. R. H., Redinbo, M. R., and Bankaitis, V. A. (2008) Functional Anatomy of Phospholipid Binding and Regulation of Phosphoinositide Homeostasis by Proteins of the Sec14 Superfamily. *Mol. Cell*. **29**, 191–206

65. Bankaitis, V. A., Mousley, C. J., and Schaaf, G. (2010) The Sec14-superfamily and mechanisms for crosstalk between lipid metabolism and lipid signaling. *Trends Biochem. Sci.* **35**, 150–160
66. Panagabko, C., Baptist, M., and Atkinson, J. (2019) In vitro lipid transfer assays of phosphatidylinositol transfer proteins provide insight into the in vivo mechanism of ligand transfer. *Biochim. Biophys. Acta - Biomembr.* **1861**, 619–630
67. Martin, T. F. J. (2001) PI(4,5)P2 regulation of surface membrane traffic. *Curr. Opin. Cell Biol.* 10.1016/S0955-0674(00)00241-6
68. Rivas, M. P., Kearns, B. G., Xie, Z., Guo, S., Sekar, M. C., Hosaka, K., Kagiwada, S., York, J. D., and Bankaitis, V. A. (1999) Pleiotropic Alterations in Lipid Metabolism in Yeast sac1 Mutants: Relationship to "Bypass Sec14p" and Inositol Auxotrophy. *Mol. Biol. Cell*. **10**, 2235–2250
69. Stock, S. D., Hama, H., DeWald, D. B., and Takemoto, J. Y. (2002) SEC14 - dependent Secretion in Saccharomyces cerevisiae . *J. Biol. Chem.* **274**, 12979–12983
70. Guo, S., Stolz, L. E., Lemrow, S. M., and York, J. D. (1999) SAC1-like domains of yeast SAC1, INP52, and INP53 and of human synaptojanin encode polyphosphoinositide phosphatases. *J. Biol. Chem.* **274**, 12990–12995
71. Bankaitis, V. A., Malehorn, D. E., Emr, S. D., and Greene, R. (1989) The Saccharomyces cerevisiae SEC14 gene encodes a cytosolic factor that is required for transport of secretory proteins from the yeast Golgi complex. *J. Cell Biol.* **108**, 1271–1281
72. Bankaitis, V. A., Aitken, J. R., Cleves, A. E., and Dowhan, W. (1990) An essential role for a phospholipid transfer protein in yeast Golgi function. *Nature*. **347**, 561–562
73. Skinner, H. B., Alb, J. G., Whitters, E. A., Helmkamp, G. M., and Bankaitis, V. A. (1993) Phospholipid transfer activity is relevant to but not sufficient for the essential function of the yeast SEC14 gene product. *EMBO J.* **12**, 4775–4784
74. Mcgee, T. P., Skinner, H. B., Whitters, E. A., Henry, S. A., Bankaitis, A., Mcgee, T. P., Skinner, H. B., Whitters, E. A., Henry, S. A., and Bankaitis, V. A. (1994) A Phosphatidylinositol Transfer Protein Controls the Phosphatidylcholine Content of Yeast Golgi Membranes. **124**, 273–287

75. Kearns, B. G., Mcgee, T. P., Maylngert, P., Gedvllaite, A., Phillips, S. E., Kaglwada, S., and Bankaltis, V. A. (1997) Essential role for diacylglycerol in protein transport from the yeast Golgi complex. *Nature*. **387**, 101–105
76. Salama, S. R., Clevels, A. E., Malehorn, D. E., Whitters, E. A., and Bankaitis, V. A. (1990) Cloning and characterization of Kluyveromyces lactis SEC14, a gene whose product stimulates Golgi secretory function in Saccharomyces cerevisiae. *J. Bacteriol.* **172**, 4510–4521
77. Mousley, C. J., Tyeryar, K. R., Vincent-Pope, P., and Bankaitis, V. A. (2007) The Sec14-superfamily and the regulatory interface between phospholipid metabolism and membrane trafficking. *Biochim. Biophys. Acta*. **1771**, 727–736
78. Ren, J., Pei-Chen Lin, C., Pathak, M. C., Temple, B. R. S., Nile, A. H., Mousley, C. J., Duncan, M. C., Eckert, D. M., Leiker, T. J., Ivanova, P. T., Myers, D. S., Murphy, R. C., Brown, H. A., Verdaasdonk, J., Bloom, K. S., Ortlund, E. A., Neiman, A. M., and Bankaitis, V. A. (2014) A phosphatidylinositol transfer protein integrates phosphoinositide signaling with lipid droplet metabolism to regulate a developmental program of nutrient stress-induced membrane biogenesis. *Mol. Biol. Cell*. **25**, 712–727
79. Routt, S. M., Ryan, M. M., Tyeryar, K., Rizzieri, K. E., Mousley, C., Roumanie, O., Brennwald, P. J., and Bankaitis, V. A. (2005) Nonclassical PITPs activate PLD via the Stt4p Ptdlns-4-kinase and modulate function of late stages of exocytosis in vegetative yeast. *Traffic*. **6**, 1157–1172
80. Yakir-Tamang, L., and Gerst, J. E. (2009) A Phosphatidylinositol-Transfer Protein and Phosphatidylinositol-4-phosphate 5-Kinase Control Cdc42 to Regulate the Actin Cytoskeleton and Secretory Pathway in Yeast. *Mol. Biol. Cell*. **20**, 3583–3597
81. Sha, B., Phillips, S. E., Bankaitis, V. A., and Luo, M. (1998) Crystal structure of the Saccharomyces cerevisiae phosphatidylinositol-transfer protein. *Nature*. **391**, 506
82. de Saint-Jean, M., Delfosse, V., Douguet, D., Chicanne, G., Payrastre, B., Bourguet, W., Antonny, B., and Drin, G. (2011) Osh4p exchanges sterols for phosphatidylinositol 4-phosphate between lipid bilayers. *J. Cell Biol.* **195**, 965–978

83. Stefan, C. J., Trimble, W. S., Grinstein, S., Drin, G., Reinisch, K., De Camilli, P., Cohen, S., Valm, A. M., Lippincott-Schwartz, J., Levine, T. P., Iaea, D. B., Maxfield, F. R., Futter, C. E., Eden, E. R., Judith, D., van Vliet, A. R., Agostinis, P., Tooze, S. A., Sugiura, A., and McBride, H. M. (2017) Membrane dynamics and organelle biogenesis-lipid pipelines and vesicular carriers. *BMC Biol.* **15**, 1–24

84. Kang, S., Bader, A. G., and Vogt, P. K. (2005) Phosphatidylinositol 3-kinase mutations identified in human cancer are oncogenic. *Proc. Natl. Acad. Sci.* **102**, 802–807

85. Hennek, J., Alves, J., Yao, E., Goueli, S. A., and Zegzouti, H. (2016) Bioluminescent kinase strips: A novel approach to targeted and flexible kinase inhibitor profiling. *Anal. Biochem.* **495**, 9–20

86. Zegzouti, H., Zdanovskaia, M., Hsiao, K., and Goueli, S. A. (2009) ADP-Glo: A Bioluminescent and Homogeneous ADP Monitoring Assay for Kinases. *Assay Drug Dev. Technol.* **7**, 560–572

87. Tai, A. W., and Vidugiriene, J. (2016) Kinase Screening and Profiling: Methods and Protocols. in *Methods in Molecular Biology*, pp. 75–85, **1360**, 75–85

88. Gao, T., Gu, S., Mu, C., Zhang, M., Yang, J., Liu, P., and Li, G. (2017) Electrochemical assay of lipid kinase activity facilitated by liposomes. *Electrochim. Acta*. **252**, 362–367

89. Whitman, M., Kaplan, D. R., Schaffhausen, B., Cantley, L., and Roberts, T. M. (1985) Association of phosphatidylinositol kinase activity with polyoma middle-T competent for transformation. *Nature*. **315**, 239–242

90. Garcia-Bustos, J. F., Marini, F., Stevenson, I., Frei, C., and Hall, M. N. (1994) PIK1, an essential phosphatidylinositol 4-kinase associated with the yeast nucleus. *EMBO J.* **13**, 2352–61

91. Anastassiadis, T., Deacon, S. W., Devarajan, K., Ma, H., and Peterson, J. R. (2011) Comprehensive assay of kinase catalytic activity reveals features of kinase inhibitor selectivity. *Nat. Biotechnol.* **29**, 1039–1045

92. Strahl, T., Hama, H., DeWald, D. B., and Thorner, J. (2005) Yeast phosphatidylinositol 4-kinase, Pik1, has essential roles at the Golgi and in the nucleus. *J. Cell Biol.* **171**, 967–979

93. Bellbrook Labs (2009) *Transcreener ADP 2 FI Assay Technical Manual*

94. GE Healthcare Yeast ORF Collection
95. Agilent pESC-TRP 6.5
96. Abcam (2019) Counting cells using a hemocytometer. [online] https://www.abcam.com/protocols/counting-cells-using-a-haemocytometer (Accessed September 30, 2017)
97. von der Haar, T. (2007) Optimized protein extraction for quantitative proteomics of yeasts. *PLoS One*. 10.1371/journal.pone.0001078
98. Mayer, S. E., Stull, J. T., Wastila, W. B., and Thompson, B. (1974) [9] Assay of Cyclic AMP by Protein Kinase Activation. *Methods Enzymol.* **38**, 66–73
99. Klink, T. A., Kleman-Leyer, K. M., Kopp, A., Westermeyer, T. A., and Lowery, R. G. (2008) Evaluating PI3 kinase isoforms using transcreener™ ADP assays. *J. Biomol. Screen.* **13**, 476–485
100. Promega (2015) *ADP-Glo ™ Lipid Kinase Systems Technical Manual*
101. American Type Culture Collection (2018) *Saccharomyces cerevisiae (ATCC® 208277™) Product Sheet*
102. Weinhandl, K., Winkler, M., Glieder, A., and Camattari, A. (2014) Carbon source dependent promoters in yeasts. *Microb. Cell Fact.* **13**, 1–17
103. Escalante-Chong, R., Savir, Y., Carroll, S. M., Ingraham, J. B., Wang, J., Marx, C. J., and Springer, M. (2015) Galactose metabolic genes in yeast respond to a ratio of galactose and glucose. *Proc. Natl. Acad. Sci.* **112**, 1636–1641
104. Islam, M. S., Aryasomayajula, A., and Selvaganapathy, P. R. (2017) A review on macroscale and microscale cell lysis methods. *Micromachines*. 10.3390/mi8030083
105. Nordstrom, J. W. B. and D. K. (1991) *User´s manual for WATEQ4F, with revised thermodynamic data base and test cases for calculating speciation of major, trace, and redox elements in natural waters*
106. University of Massachusetts Department of Chemistry Table of Solubility Product Constants (Ksp at 25 oC)
107. Pan, Z., Choi, S., Luo, Y., Innovation, H., and Innovation, H. (2018) Mn2+ Quenching Assay for Store-Operated Calcium Entry. *Methods Mol. Biol.* **1843**, 55–62
108. Shibuya, I., and Douglas, W. W. (1993) Indications from Mn-quenching of Fura-2

fluorescence in melanotrophs that dopamine and baclofen close Ca channels that are spontaneously open but not those opened by high [K+]o; and that Cd preferentially blocks the latter. *Cell Calcium*. 10.1016/0143-4160(93)90016-Y

109. Schwartz, P. A., and Murray, B. W. (2011) Protein kinase biochemistry and drug discovery. *Bioorg. Chem.* **39**, 192–210
110. Baptist, M., Panagabko, C., Cockcroft, S., and Atkinson, J. (2016) Ligand and membrane-binding behavior of the phosphatidylinositol transfer proteins PITPα and PITPβ. *Biochem. Cell Biol.* **94**, 528–533
111. Cockcroft, S. (2012) The Diverse Functions of Phosphatidylinositol Transfer Proteins. in *Phosphoinositides and Disease* (FALASCA, M. ed), pp. 185–208, Springer Netherlands, Dordrecht, 10.1007/978-94-007-5025-8_9
112. Cockcroft, S., and Garner, K. (2013) Potential role for phosphatidylinositol transfer protein (PITP) family in lipid transfer during phospholipase C signalling. *Adv. Biol. Regul.* **53**, 280–291